DEUTSCHES ELEKTRONEN – SYNCHROTRON DESY

DESY 88-119
FTUAM-EP-88-05
August 1988

HEAVY QUARK PHYSICS AT HERA

by

A. Ali, G. Ingelman, G.A. Schuler

Deutsches Elektronen-Synchrotron DESY, Hamburg

F. Barreiro, M.A. García, J.F. de Trocóniz

Universidad Autónoma de Madrid, Madrid, Spain

R.A. Eichler

Institute for Intermediate Energy Physics, ETH Zürich, Switzerland

Z. Kunszt

Institute for Theor. Physics, ETH Zürich, Switzerland

ISSN 0418-9833

NOTKESTRASSE 85 · 2 HAMBURG 52

To be sure that your preprints are promptly included in the
HIGH ENERGY PHYSICS INDEX,
send them to the following address (if possible by air mail):

DESY
Bibliothek
Notkestrasse 85
2 Hamburg 52
Germany

DESY 88- 119
FTUAM-EP-88-05
August 1988

ISSN 0418-9833

Heavy Quark Physics at HERA [1]

A. Ali, G. Ingelman, G.A. Schuler

DESY
Notkestrasse 85, 2000 Hamburg 52
Federal Republic of Germany

F. Barreiro[2], M.A. García[3], J. F. de Trocóniz[4]

Universidad Autónoma de Madrid
Madrid, Spain

R.A. Eichler

Institute for Intermediate Energy Physics, ETH Zürich
5234 Zürich, Switzerland

Z. Kunszt

Institute for Theoretical Physics, ETH Zürich
8093 Zürich, Switzerland

[1] To be published in the Proceedings of the DESY Workshop on HERA Physics, Hamburg, FRG(1988).
[2] Alexander von Humboldt Fellow, now at DESY.
[3] Partially supported by Cajamadrid.
[4] Partially supported by Eusko Jaurlaritza-Gobierno Vasco.

Contents

Abstract

We study some of the salient features of electroweak production of charm, bottom and top quarks at HERA for the *ep* centre of mass energy, $\sqrt{s} = 314$ GeV. The calculations described here are based on perturbative QCD followed by the usual fragmentation and weak decays of heavy hadrons. In particular, we study means of identifying top quarks at HERA and compare these methods with the ones used in corresponding searches in e^+e^- annihilation and $p\bar{p}$ collisions. Based on our studies we estimate the top quark discovery limit at HERA to be around $m_t = 70$ GeV. We find the inclusive bottom quark cross-section at HERA $\sigma(ep \rightarrow bX)$ to be $O(8\ nb)$ and hence comparable to the cross-section $\sigma(e^+e^- \rightarrow Z_0 \rightarrow bX)$ expected at $\sqrt{s} = m_Z$. This may enable experiments at HERA to undertake some precision measurements in the bottom quark sector. In particular, we investigate the prospects of measuring the mixing parameters $x_{d,s} = (\frac{\Delta M}{\Gamma})_{d,s}$ in the $B_d^0 - \bar{B}_d^0$ and $B_s^0 - \bar{B}_s^0$ sectors through the measurements of same sign and opposite sign dilepton rates, and oscillation lengths. We also discuss the possibility of measuring the Cabibbo-Kobayashi-Maskawa matrix element $|V_{bu}|$ in the inclusive leptonic and exclusive hadronic decays of B hadrons. The inclusive charm quark cross-section $\sigma(ep \rightarrow cX)$ is estimated to be $O(1\ \mu b)$ at HERA. With good particle identification and vertex reconstruction capabilities HERA may be used to search for rare decays in the charm sector, like $D^0 \rightarrow K^+\pi^-$, $D^0 \rightarrow \mu^+\mu^-, e^+e^-$ and $D^0 - \bar{D}^0$ oscillations.

1. Introduction

The study of heavy flavour physics is one of the principal areas of research at present and future high energy accelerators. The interest in e^+e^- machines such as LEP and SLC in this context has been reviewed in Ref. [1]. At hadron colliders the study of heavy quark physics is difficult due to the enormous background but clearly feasible [2,3] due to the large cross-sections and useful flavour tags. There is a world wide surge of interest in pursuing the field of heavy flavour physics with fixed target hadron machines [4,5], hadron colliders [6–8], threshold e^+e^- machines (bottom factories) presently available [9] and being planned for the future [10–12]. We also note that very high statistic results on charmed hadrons have been presented by the photoproduction experiments, in particular by the FERMILAB experiment E691 and the CERN experiment NA14 [13].

As we are going to discuss below, experiments at HERA appear to us also very promising in the study of electroweak production of heavy flavours [14–18].

To focus thinking about the kind of experimental research programme that one could envisage at HERA, we quote expected heavy quark cross-sections at $\sqrt{s} = 314$ GeV: $\sigma(ep \to cX) \sim 1\ \mu b$, $\sigma(ep \to bX) \sim 8\ nb$ and $\sigma(ep \to tX, m_t = 60\ GeV) \sim 0.3\ pb$. Thus, HERA is a broad band boson-gluon collider capable of doing broad band heavy flavour physics. This physics can be considered as ranging from being exploratory (for the top quark) to precise, enabling searches for rare processes in the charm and bottom sector. Clearly, the actual heavy quark physics programme at an experimental facility can not be judged by mere cross-sections. The quality of experimentation, namely good particle identification, vertex reconstruction, lepton momentum and charge measurements, as well as a finely segmented calorimeter are crucial prerequisites for doing qualitatively significant heavy flavour physics. We hope that this report will have some impact on optimizing the present HERA detectors for heavy flavour physics and even encourage new dedicated experimental proposals to study this subject at HERA.

In high energy ep collisions the main source of heavy flavour production is the boson-gluon fusion (BGF) mechanism. The leading order Feynman diagrams are shown in Fig. 1.1. The neutral current (NC) reaction $\gamma + g \to Q\bar{Q}$ gives the dominant contribution for $Q = c, b$ and light top quarks. For a larger top quark mass, single top production by the charged current (CC) process $W^- + g \to b + \bar{t}$ has to be taken into account. The weak production of top quark dominates over the NC process for $m_t > 55\ GeV$ at HERA energy $\sqrt{s} = 314\ GeV$. This is in contrast with the e^+e^- and $p\bar{p}$ collisions, where the heavy quark pair production process dominates. Hence the searches for a heavy top quark at HERA require new topologies and strategies. The cross-sections for the processes $ep \to QX(Q = c, b, t)$ are shown in Table 2.4, from where it is easy to see that for $m_t = 60\ GeV$ and an integrated luminosity of 100 pb^{-1} we expect 9 $t\bar{t}$ events and 13 $b\bar{t}$ events.

The problem of detecting a cross-section of $O(0.3\ pb)$ in the hard scattering background of $O(20\ \mu b)$ is by no means trivial! Clearly, the distinctive signature of a pair of isolated leptons from the process $ep \to t\bar{t} \to llX$ leaves us with practically no rate. Also, the top quark signature from the process $ep \to \nu_e tX$ with the subsequent decay $t \to bl\nu_l$ giving one isolated lepton may yield a handful of events. However, a construction of the top quark mass will not be possible due to the presence of two neutrini.

Instead, we start from the observation that the mean transverse momentum of the parton produced in the hard scattering subprocess is essentially given by its mass, $p_t = m$, leading to a broader distribution in total transverse energy $\sum E_T$ for top events as compared to the background. In addition, if light parton events have a large $\sum E_T$ then they will typically be less spherical than events coming from a heavy (slow moving) object. It is shown in [18] that just cutting in the two quantities $\sum E_T$ and sphericity can indeed result in a clean top sample, however at the expense of a too strong reduction of the top rate. The problem here is that we have to deal with the 'tails' of the distributions coming from processes involving light partons which have a much larger cross-section. In this respect top search at HERA will be closer to the corresponding search at the CERN $p\bar{p}$ collider than to the one in e^+e^- experiments [16,49]. The ratios of the top cross-section $\sigma(t\bar{t})$ to the heavy flavour background cross-sections $\sigma(b\bar{b})$ and $\sigma(c\bar{c})$ are similar in ep and the $p\bar{p}$ cases, but the contamination by light flavour events is much smaller in ep collisions due to the absence of the gg initial state. Combining the two searches based on nonleptonic and semileptonic quark decays and by using a series of topological cuts, the signal/background ratio in top quark searches at HERA can be brought down so as to enable a top quark discovery up to $m_t = 70\ GeV$.

Turning to charm and bottom quark physics, we note that not only are the charmed and bottom hadron cross-sections large at HERA but the hadrons are also rather energetic, with the heavy hadron energy-spectrum extending over hadron energy $E_H = 100\ GeV$. We have calculated the energy distributions $\frac{d\sigma}{dE(B_d)}$ and $\frac{d\sigma}{dE(D)}$ for B_d and D mesons, respectively, for a typical beam hole angle $\Theta = 100\ mrad$. This indicates that measurable cross-sections with Lorentz boost factors in excess of $\gamma_B = 15$ and $\gamma_D = 40$ for the bottom and charmed hadrons, respectively, are expected at HERA. This would lead to charmed and bottom hadron track lengths $l = c\beta\tau\gamma$ reaching up to $O(1 - 2cm)$ and $O(0.5cm)$ respectively. Thus, experiments at HERA provide a natural avenue for the use of vertex detectors.

We recall here that photoproduction experiments have already demonstrated that using silicon vertex detectors one can get charm signals which in many cases are cleaner than those in e^+e^- annihilation [13]. Clearly, the impact of such devices can be enormously enhanced if they could be combined with good particle identification $(K, \pi, p, ...)$. A good example is the possible measurement of individual bottom hadron lifetimes by vertex identification, reconstructing the bottom hadrons via the decays $B_s \to J/\Psi\phi$, $B_d \to J/\Psi(K^0, K^{*0})$ and $B_u^- \to J/\Psi(K^-, K^{*-})$ etc. Typical branching ratios in the mode $B \to J/\Psi(K, K^*, \phi)$ with the subsequent decay $J/\Psi \to l^+l^-$ are expected to be $O(10^{-3})$, thus enabling in principle such measurements at HERA, given, of course, good vertex detectors.

There is another potential use of vertex detectors at HERA experiments and this concerns measurements of the oscillation lengths for the $B_d^0 - \bar{B}_d^0$ and $B_s^0 - \bar{B}_s^0$ systems. These oscillation lengths can be expressed as $(L_{osc})_{d,s} = (\frac{2\pi}{x}\beta\gamma c\tau)_{d,s}$ where $x_{d,s} = (\frac{\Delta M}{\Gamma})_{d,s}$ are the mixing parameters for the two bottom meson systems, and β, γ are, respectively, the velocity and Lorentz boost factor for the bottom hadrons measured in the ep laboratory system. The quantity x_d has recently been measured by the ARGUS Collaboration [19] to be $x_d = 0.73^{+0.17}_{-0.19}$. Combined with the CLEO bound on x_d [20] it leads to $0.44 < x_d < 0.78(90\%\ C.L.)$. The standard model estimates for x_s may be obtained from the relationship [21,22] $x_s/x_d = |V_{ts}/V_{td}|^2(1 + \delta)$ where δ is an $SU(3)$ symmetry breaking parameter probably in the range $0 < \delta < 1$. The present bounds on $|V_{ts}/V_{td}|$ are estimated to be in the range $2.4 \leq |V_{ts}/V_{td}| \leq 6$ [22]. This suggests a value $2 < x_s < 60$ for the mixing parameter x_s. We show in Table 4.2 values of the oscillation lengths L_d and L_s for some representative values of the mixing ratios x_d and x_s and the Lorentz boost factor γ_B for bottom hadrons. For example, for

$\gamma_B = 10, x_d = 0.5$ and $x_s = 5$ we expect $L_d = 1.9\ cm$ and $L_s = 1.9\ mm$. Thus, for these values of the parameters L_d is much larger than the average B_d meson decay length, $< l >_d$, but L_s is comparable to the B_s meson average decay length, $< l >_s$, and hence it should be possible to measure the oscillation length L_s and determine x_s knowing the Lorentz factor γ_B. We note in passing that the most tricky part of these measurements would be the determination of the energy of the B_d^0 or B_s^0 meson. This would require reconstruction of bottom hadrons and their momentum measurements. The importance of projecting out bottom hadrons within definite energy intervals in the present context has also been recently emphasized in [23]. We also investigate the possibility of measuring at HERA the cross-section weighted mixing measure $\chi = \chi_s P_s + \chi_d P_d$ and find that an accuracy $\Delta\chi_s/\chi_s = 0.07$ should be possible through the dilepton rates in $ep \to b\bar{b}X \to l\bar{l}X$.

We emphasize that for larger values of x_s, say $x_s \geq 5$, it would be very difficult to extract its precise value from time integrated measurements which measure $\chi_s = \frac{x_s^2}{2(1+x_s^2)} \to \frac{1}{2}$ in the limit $x_s \gg 1$. In that case, space-dependent measurements of the type being discussed here provide, in our opinion, the only method of determining x_s.

While still on the subject of particle-antiparticle mixing, we would like to mention the present attempts in measuring $D^0 - \bar{D}^0$ mixing through the doubly suppressed Cabibbo decay modes $D^0 \to K^+\pi^-, K^+\pi^-\pi^+\pi^-$ [24]. As is well known, these final states can also be reached via $D^0 - \bar{D}^0$ mixing and hence provide information on this phenomenon. The present best limit on the quantity $r_D = \frac{P(D^0 \to \bar{D}^0)}{P(\bar{D}^0 \to D^0)} = \frac{x_d^2}{2+x_d^2}$ is due to the FERMILAB photoproduction experiment E691 [24] giving $r_d < 3.7 \times 10^{-3}(90\%\ C.L.)$ With an estimated 10^8 charmed hadrons per 100 pb^{-1} at HERA, it should be possible to investigate $D^0 - \bar{D}^0$ mixings at HERA as well, given good particle identification. The theoretical limits on the ratio r_D are quite model dependent though one expects $r_D < 10^{-3}$ [25]. Likewise, it should be possible to search for the flavour changing neutral current (FCNC) process $D^0 \to \mu^+\mu^-$. The estimated sensitivity at HERA is expected to be better than the present limit $BR(D^0 \to \mu^+\mu^-) \leq 1.1 \times 10^{-5}$ [26].

This report is organized as follows. In section 2, we describe the theoretical framework used in the study of heavy quark physics in ep collisions and define our notation and the kinematic variables used. We study various inclusive distributions for the charm, bottom and top hadrons and estimate backgrounds from the light quark NC and CC processes. Section 3 is devoted to the search for top quark signals at HERA using semileptonic and nonleptonic decays $t \to bl\nu_l, bq\bar{q}$. In particular, we study the topological configuration with an isolated lepton and more than two jets, used for top quark searches at the $Sp\bar{p}S$ collider. In addition, we also study nonleptonic decays from the CC process $ep \to \nu b\bar{t}$ and the NC process $ep \to et\bar{t}$, involving multijets in the final state. The problem of the top mass reconstruction from these topologies is studied quantitatively, taking into account the background from the light quark CC and NC processes. In section 4, we discuss some of the salient features of the bottom and charm physics, which can be studied at HERA. We present various techniques to separate charm and bottom events and also estimate the time integrated mixing measure χ from dilepton rates. We address the question of measuring oscillation lengths in the $B_d^0 - \bar{B}_d^0$ and $B_s^0 - \bar{B}_s^0$ complexes. Attempts at measuring the matrix element $|V_{bu}|$ at HERA are also reported here. We present theoretical estimates of various inclusive distributions involving lepton, dilepton and J/Ψ production. These measurements will provide quantitative tests of perturbative QCD at HERA, and because of the dominance of the BGF mechanism will also provide means to determine the gluon structure function, particularly at lower values of x. The subject of heavy quark contribution to the proton structure functions is covered in a separate report [14]. Section 5 contains a summary and conclusions.

2. Heavy Quark Production in ep Collision

2.1 *Quark Parton Model contribution*

In the Quark Parton Model (QPM), heavy quark production in lepton-nucleon collisions occurs via the charged current (CC) process

$$e + q \to \nu_e + Q \tag{2.1}$$

shown in Fig. 2.1. The cross-section can be estimated by multiplying the deep inelastic scattering (DIS) cross-section from a quark of flavour q in the proton, σ_q, and the appropriate Cabibbo-Kobayashi-Maskawa (CKM) matrix element squared, V_{Qq}^2

$$\sigma(Q) = \sum_q V_{Qq}^2 \sigma_q \tag{2.2}$$

The CKM matrix element V_{ub} is at most of $O(1\%)$ [27] giving,

$$\frac{\sigma(e^- + u \to \nu_e + b)}{\sigma(e^- + u \to \nu_e + d)} = O(10^{-4}) \tag{2.3}$$

and hence entirely negligible. Likewise, V_{td} is expected to be of the same order as V_{bu}. Hence,

$$\frac{\sigma(e^+ + d \to \nu_e + t)}{\sigma(e^+ + d \to \nu_e + u)} = O(10^{-4}) \tag{2.4}$$

which is also negligible.

The process $e^- + \bar{d} \to \nu_e + \bar{t}$ has the additional suppression due to the scattering off the $\bar{d}(sea)$ quark in the proton. Thus, only the process $e^+ + d \to \bar{\nu}_e + c$, $e^+ + s \to \bar{\nu}_e + c$, and their charge conjugates $e^- + \bar{d} \to \nu_e + \bar{c}$, $e^- + \bar{s} \to \nu_e + \bar{c}$ are expected to have measurable cross-sections, with the scattering off the s and $\bar{s}$ dominating. The cross-sections $\sigma(e^+p \to \bar{\nu}_e cX)$ and $\sigma(e^-p \to \nu_e \bar{c}X)$ are of $O(4\ pb)$ at HERA energies assumming $m_c = 1.5$ GeV [17,18] (See Tables 2.2–2.4) However, as we are going to discuss below the inclusive NC charm quark pair production cross-section $\sigma(e^-p \to e^-c\bar{c}X)$ is of order 1 μb and hence completely dominates over the CC cross-section [15–18]. Thus, it appears that the prospects of measuring the CKM matrix elements of interest V_{cd}, V_{cs}, V_{td}, V_{ts}, V_{tb}, V_{cb}, V_{ub} at HERA through the CC processes are exceedingly dim.

2.2 *Boson gluon fusion contribution*

In Quantum Chromodynamics (QCD), the leading order contribution to heavy quark production is due to the boson-gluon fusion (BGF) mechanism shown in Fig. 1.1

$$CC : W^+ + g \to Q + \bar{Q}' \tag{2.5}$$

$$NC : \gamma/Z^0 + g \rightarrow Q + \bar{Q} \tag{2.6}$$

They occur as $O(\alpha_s\alpha^2)$ parton level subprocesses in the corresponding CC and NC ep scatterings

$$e(l_e) + p(P) \rightarrow \nu_e(l') + Q_f(p_f) + \bar{Q}'_f(p'_f) + X \tag{2.7}$$

$$e(l_e) + p(P) \rightarrow e(l') + Q_f(p_f) + \bar{Q}_f(p'_f) + X \tag{2.8}$$

where we have indicated the corresponding 4-momenta of the particles. The gluon entering the subprocesses (2.5) and (2.6) carries a fraction x_g of the proton momentum i.e. $p = x_g P$. Thus, as opposed to the QPM subprocess (2.1), the BGF processes need the gluon density in a proton as input. Conversely, experimental measurements of heavy quark distributions can be used to determine the gluon density in a proton.

The BGF processes have been discussed extensively in the literature [14–18,28,29]. We shall restrict ourselves here to those features which are relevant for the calculations we are going to present below. We start by defining the variables needed for the processes (2.7) and (2.8)

$$\hat{s} = (p_f + p'_f)^2 \tag{2.9}$$

$$Q^2 = -q^2 = -(l_e - l')^2 \tag{2.10}$$

$$W^2 = (P + q)^2 \tag{2.11}$$

$$x = \frac{Q^2}{2P.q} \tag{2.12}$$

and

$$y = \frac{P.q}{P.l_e} \tag{2.13}$$

These variables are related to each other, for example,

$$Q^2 = xys \tag{2.14}$$

$$W^2 = Q^2\frac{1-x}{x} + m_p^2 \tag{2.15}$$

$$\hat{s} = Q^2\frac{x_g - x}{x} \tag{2.16}$$

and hence only three of them are independent, given $\sqrt{s}$. In addition, two more variables are needed in order to specify the event completely. For these we take

$$z = \frac{P.p_f}{P.q} \tag{2.17}$$

and the azimuthal angle Φ between the lepton and hadron planes

$$cos\Phi = \frac{(\vec{p} \times \vec{l_e}).(\vec{p} \times \vec{p_f})}{|\vec{p} \times \vec{l_e}||\vec{p} \times \vec{p_f}|} \tag{2.18}$$

measured in the boson-gluon CM frame i.e. $\vec{p_f} + \vec{p_{f'}} = 0$. The variable z is related to the angle of the $Q\bar{Q}$-axis with respect to the boson-gluon axis in the CM frame. It can be related to the heavy quark transverse momentum in this frame through the relation

$$p_T^2 = \hat{s}z(1-z) + z(m_f^2 - m_{f'}^2) - m_f^2 \tag{2.19}$$

The cross-section for the process (2.5) can now be expressed as

$$\sigma(ep \rightarrow Q\bar{Q}X) = \int dy \int dQ^2 \int dx_g \int dz \int d\Phi\, g(x_g, M_g^2)\, \hat{\sigma}(y, Q^2, x_g, z, \Phi) \tag{2.20}$$

which is a convolution of the gluon density $g(x_g, M_g^2)$ evaluated at the mass scale M_g^2 and the QCD parton level cross-section $\hat{\sigma}$ for the process shown in Fig. 1.1. The cross-section $\hat{\sigma}$ has been calculated taking into account the heavy quark mass, the electroweak structure for both the NC and CC processes, and for arbitrary longitudinal polarization of the incoming electron or positron. The cross-section in Eq. (2.20) is usually evaluated by performing the 5-dimensional integration using Monte Carlo techniques, given the boundaries of the variables. They are defined as follows

$$y_{max,min} = \frac{s + W_1^2 \pm \sqrt{(s - W_1^2)^2 - 4m_e^2W_1^2}}{2(s + m_e^2)} \tag{2.21}$$

$$W_1^2 = W_0^2 - m_p^2 \tag{2.22}$$

$$W_0^2 = (m_f + m_{f'} + m_p)^2 \tag{2.23}$$

$$Q^2_{min} = m_e^2\frac{y^2}{1-y} \tag{2.24}$$

$$Q^2_{max} = ys - W_1^2 \tag{2.25}$$

$$(x_g)_{min} = \frac{(m_f + m_{f'})^2 + Q^2}{ys} \tag{2.26}$$

$$(x_g)_{max} = 1 \tag{2.27}$$

$$z_{max,min} = \frac{\gamma^2 \pm \sqrt{\lambda}}{2\hat{s}} \tag{2.28}$$

$$\gamma^2 = \hat{s} + m_f^2 - m_{f'}^2 \tag{2.29}$$

$$\lambda = (\hat{s} - m_f^2 - m_{f'}^2)^2 - 4m_f^2m_{f'}^2 \tag{2.30}$$

and $0 < \Phi \leq 2\pi$.

Monte Carlo techniques can also be used to simulate the fully differential cross-section, which provides the four-momenta of the final partons and thereby generates parton level events [16,30,31]. This can be further complemented with parton fragmentation and weak decays of the heavy hadrons in order to simulate the complete final state of observable particles. We will in the following mainly use the program AROMA [30] unless otherwise stated, since it contains the complete electroweak structure of the BGF heavy flavour cross-section for an arbitrary Q^2. It takes higher order QCD corrections approximately into account and performes fragmentation and particle decays.

2.3 *The Weiszäcker-Williams approximation*

Before we present the numerical results for various cross-sections and related distributions, it is perhaps useful to discuss the Weiszäcker-Williams approximation (WWA) often used in the evaluation of the NC processes (2.8), which are dominated by the photon exchange. The WWA method factorizes the cross-section for the NC process (2.8) into the probability of

emitting a photon from the lepton vertex and the BGF cross-section $\gamma g \to Q\bar{Q}$ involving real photons, giving

$$\sigma(ep \to eQ\bar{Q}X) = \int_{y_{min}}^{1} dy P_\gamma(y) \int_{x_{g_{min}}}^{1} dx_g g(x_g, M_g^2) \hat{\sigma_\gamma}(\hat{s} = y x_g s) \tag{2.31}$$

where $P_\gamma(y)$ is related to the probability of finding a photon in the electron

$$P_\gamma(y) = \frac{\alpha}{2\pi} \frac{1+(1-y)^2}{y} ln \frac{Q_2^2}{Q_1^2} \tag{2.32}$$

where Q_2^2, Q_1^2 can be identified with Q_{min}^2 and Q_{max}^2, defined earlier. The cross-section $\hat{\sigma_\gamma}$ for the process $\gamma + g \to Q\bar{Q}$ can be essentially obtained (modulo colour factors) from the QED process $\gamma + \gamma \to e^+e^-$ and is given by

$$\hat{\sigma_\gamma} = \frac{\pi Q_f^2 \alpha \alpha_s}{\hat{s}} ((2 + 2\omega - \omega^2) ln \frac{1+\chi}{1-\chi} - 2\chi(1+\omega)) \tag{2.33}$$

where χ is the velocity of the Q (or $\bar{Q}$) in the γg CM frame, $\chi = \sqrt{(1-\omega)}$ and $\omega = \frac{4m_f^2}{\hat{s}}$. In what follows we shall see that the WWA and the exact cross-sections obtained from Eqs. (2-31) and (2.20), respectively, are very close to each other at HERA energies [14,17].

It is obvious from Eq. (2.20) that the BGF cross-sections for the processes (2.7) depend on the gluon density function $g(x_g, M_g^2)$, and the QCD scale parameter Λ, which enters both in the evolution of $g(x_g, M_g^2)$ from an input value at $M_{g_0}^2$ and in the cross-section $\hat{\sigma}$. In addition, there is some dependence on the precise values of the heavy quark masses m_c and m_b. We shall comment on these uncertainties later.

2.4 *Inclusive heavy quark rates at HERA*

We present in this section the inclusive cross-sections at HERA for the process

$$e + p \to Q + X \tag{2.34}$$

The inclusive cross-section is defined as

$$\sigma(ep \to QX) = \sigma(ep \to \nu QX) + \sigma(ep \to \nu Q\bar{Q}'X) + 2\sigma(ep \to eQ\bar{Q}X) \tag{2.35}$$

where the first term on the r.h.s. of Eq. (2.35) is the QPM contribution , the second term is the BGF cross-section (CC processes) and the third term the cross-section for the NC processes. It is obvious from our definition that we are not distinguishing between a Q and $\bar{Q}$. Unless otherwise stated the BGF cross-sections are evaluated in the leading order, $O(\alpha_s \alpha^2)$. The parameters of the standard model used in our numerical calculations are shown in Table 2.1. All results are given for an unpolarized electron beam with $E_e = 30$ GeV and $E_p = 820$ GeV, resulting in a center of mass energy $\sqrt{s} = 314$ GeV. We use the parametrization of the gluon density $g(x_g, M_g^2)$ due to Eichten, Hinchliffe, Lane and Quigg (set 1) [32], if not otherwise stated.

The inclusive cross-sections for the charm, bottom and top quarks are given in Tables (2.2)-(2.4), where we have also shown the QPM contributions. As discussed above, the heavy quark contribution from the QPM are several orders of magnitude smaller than the

Table 2.1: Assumed values of the standard model parameters used in the estimates of cross-sections

Quantities	*Values*
CKM matrix elements	$V_{ud}^2 = 0.95$ $V_{us}^2 = 0.05$ $V_{ub}^2 = 10^{-4}$ $V_{cd}^2 = 0.05$ $V_{cs}^2 = 0.948$ $V_{cb}^2 = 0.002$ $V_{td}^2 < 4.10^{-4}$ $V_{ts}^2 = 0.002$ $V_{tb}^2 = 0.998$
Quark masses	$m_s = 0.5\ GeV$ $m_c = 1.5\ GeV$ $m_b = 5.0\ GeV$
Weak boson masses and angle	$m_W = m_z cos\theta_W = \frac{38.68 GeV}{sin\theta_W}$ $sin^2\theta_W = 0.226$
Mass scales	$M_s^2 = M_g^2 = \hat{s}$
QCD scale	$\Lambda_{QCD} = 0.2$ GeV
No. of flavours in $\alpha_S(Q^2)$	$n_f = 3$

Table 2.2: Charm cross sections at HERA

$\sigma(ep \to cX)$ [pb] at HERA ($m_c = 1.5$ GeV)								
	CC			NC $c\bar{c}$				inclusive
e^-p	$\bar{c}d$	$\bar{c}s$	$\bar{c}b$	NC	γ	Z	γ-Z	$c + \bar{c}$
BGF	0.46	8.2	0.012	5.1×10^5	5.1×10^5	0.60	4.7	1.0×10^6
e^-p	$\bar{d} \to \bar{c}$	$\bar{s} \to \bar{c}$						
QPM	0.26	3.3						3.6
e^+p	$d \to c$	$s \to c$						
QPM	0.75	3.3						4.1

Table 2.3: Bottom cross sections at HERA

$\sigma(ep \to bX)$ [pb] at HERA ($m_b = 5\,\text{GeV}$)								
	CC			NC $b\bar{b}$				inclusive
e^-p	$\bar{u}b$	$\bar{c}b$	$\bar{t}b$	total	γ	Z	γ-Z	$b+\bar{b}$
BGF	$\leq 0.96 \times 10^{-3}$	0.012	0.13	4.2×10^3	4.2×10^3	0.35	0.59	8.4×10^3
e^-p	$u \to b$							
QPM	$\leq 0.56 \times 10^{-2}$							$\leq 0.56 \times 10^{-2}$
e^+p	$\bar{u} \to \bar{b}$							
QPM	$\leq 0.12 \times 10^{-2}$							$\leq 0.12 \times 10^{-2}$

Table 2.4: Top cross sections at HERA for $m_t = 60\,\text{GeV}$

$\sigma(ep \to tX)$ [pb] at HERA ($m_t = 60\,\text{GeV}$)								
	CC			NC $t\bar{t}$				inclusive
e^-p	$\bar{t}d$	$\bar{t}s$	$\bar{t}b$	total	γ	Z	γ-Z	$t+\bar{t}$
BGF	$\leq 0.14 \times 10^{-3}$	$\leq 0.62 \times 10^{-3}$	0.13	0.09	0.09	0.4×10^{-3}	0.6×10^{-4}	0.31
e^-p	$\bar{d} \to \bar{t}$	$\bar{s} \to \bar{t}$						
QPM	2×10^{-3}	8×10^{-3}						1×10^{-2}
e^+p	$d \to t$	$s \to t$						
QPM	4×10^{-3} QPM	8×10^{-3}						1.2×10^{-2}

corresponding cross-sections based on the BGF mechanism. For the BGF processes, the NC cross-sections for charm and bottom quarks are much larger than the CC ones and they are dominated by the γ exchange term. Thus, the characteristics of the electroproduction of these quarks at HERA are essentially those of real photoproduction. However, contrary to the charm and bottom quarks, top quark production via the CC process can not be neglected and this process actually dominates over the NC production for $m_t > 55$ GeV due to the reduced threshold energy for the former as shown in Fig. 2.2. For top quark mass larger than 80 GeV, the cross-section is expected to fall below the threshold of observability at HERA, i.e. less than 10 events per 200 pb^{-1}.

Several comments about the cross-section estimates are in order, since they contain theoretical uncertainties. The scales M^2, M_s^2, M_g^2 needed in the definition of the QED running coupling constant $\alpha(M^2)$, the corresponding QCD coupling constant $\alpha_s(M_s^2)$, and the gluon density $g(x_g, M_g^2)$, respectively, are ill defined in $O(\alpha_s{}^2\alpha)$ that we are using for the calculation. Clearly, the ususal DIS choice of $Q^2 = -q^2$ is not appropriate since as we discussed above, the cross-sections are dominated by $Q^2 = 0$. Instead, $\hat{s}$, the invariant squared mass of the $Q\bar{Q}$ system, is, in our opinion, more appropriate for the mass scales M_s^2 and M_g^2. Reasonable variations of these scales lead to uncertainties of order 10%. For α, the scale $M^2 = 0$ is used and we note that varying it between $M^2 = 0$ and $M^2 = s$ changes the cross-section by at most 12%. These uncertainties can, in principle, be eliminated if the complete next to leading order corrections in the electroweak and QCD processes are known. Very recently, the $O(\alpha^2\alpha_s{}^2)$ corrections to the heavy quark photoproduction cross-section have been reported in [68]. The corrections to the double differential distribution $\frac{d^2\sigma}{dE_\perp d\eta_Q}$ in this order have yet to be calculated. A part of this contribution from the Born diagrams in $O(\alpha^2\alpha_s{}^2)$ was previously obtained in [29] and we shall discuss them below.

Continuing our discussion of the cross-section estimates, we note that the heavy quark cross-sections are uncertain also due to the input gluon density. Using different parametrizations of the gluon structure function [32,33] of a conventional type give variations less than 25% for bottom and top production and less than 40% for charm production. A parametrization [34] with a $xg(x) \sim 1/\sqrt{x}$ behaviour at small x increases the charm cross-section by a factor two, but modifies only slightly the bottom and top results since the range in x_g in these latter two cases does not extend to as small values. In addition, the charm and bottom cross-sections depend on the precise values of the quark masses used. Taking an uncertainty of $\Delta m_{c,b} = 0.3$ GeV, we estimate

$$\sigma(ep \to cX) = 1.0^{+0.68}_{-0.36}\ \mu b\ for\ m_c = 1.5 \mp 0.3\ GeV \tag{2.36}$$

and

$$\sigma(ep \to bX) = 8.4^{+1.85}_{-1.43}\ nb\ for\ m_b = 5.0 \mp 0.3 GeV \tag{2.37}$$

We remark that the charm cross-section estimate (2.36) should be taken as a lower limit, since there are indications from low energy photoproduction experiments that the BGF model estimates may turn out to be lower than data [35], though the experimental situation at present is not completely equivocal on this point. We expect that experiments at HERA will help clarify this point. These cross-sections are to be compared with the corresponding cross-sections at LEP-I/SLC, for which one expects [36]

$$\sigma(e^+e^- \to Z_0 \to cX) = 6.5\ nb \tag{2.38}$$

$$\sigma(e^+e^- \to Z_0 \to bX) = 9.0\ nb \tag{2.39}$$

Thus, the bottom pair production cross-sections at LEP-I/SLC ($\sqrt{s} = m_Z$) and HERA ($\sqrt{s} = 314$ GeV) are comparable but the charm cross-section at HERA is at least a factor 100 higher than the cross-section estimates for LEP. On the other hand, the ratios $\frac{\sigma(c\bar{c})}{\sigma_{tot}}$ and $\frac{\sigma(b\bar{b})}{\sigma_{tot}}$ are much more favourable at LEP/SLC than at HERA.

For an integrated luminosity of 1 fb^{-1}, say with five years of data taking, one will have $O(10^9)$ charmed hadron events and $O(10^7)$ bottom hadron events, making HERA powerful charm and bottom factories. We should probably hasten to add that the corresponding cross-sections at the existing photoproduction and hadroproduction experiments are also not small. As we have already noted, the average charm cross-section at the FERMILAB photoproduction experiment [24] with 145 GeV photon beams is estimated to be $3.17 \pm 0.22 \pm 0.80$ $\mu b/Be$ nucleus, assuming $\sigma_N = A^{0.92}\sigma$ and $\sigma(\gamma p \to cX) = 0.42 \pm 0.03 \pm 0.10$ μb [13]. The cross-sections at the $Sp\bar{p}S$ collider are estimated to be [3]

$$\sigma(p\bar{p} \to cX) = O(0.1 - 0.2)\ mb \tag{2.40}$$

$$\sigma(p\bar{p} \to bX) = O(20)\ \mu b \tag{2.41}$$

and they are consistent with the measured cross-sections by the UA1 Collaboration [2].

Thus, it is obvious that the progress in heavy quark physics that will eventually be made at HERA depends very sensitively on the tailoring of the detectors to the topology of events. We remark en passant that as far as the characteristics of the charmed hadron events at HERA are concerned, an appropriately energy boosted version of the fixed target E691 photoproduction events is probably not a bad first guess. The most important difference between the two lies in the much more energetic nature of the HERA events. In our opinion, this can be advantageously exploited at HERA. It is therefore expected that the success of the low energy charm photoproduction experiments will be set forth at HERA, despite the obvious observation that the proton at HERA does not provide an active target in the sense of fixed target collisions at CERN and FERMILAB.

Before discussing the detailed topological features of heavy quark production processes at HERA, we would like to comment on the stability of the so-called $2 \to 2$ QCD processes used in the estimates of the heavy quark production cross-sections above.

2.5 $2 \to 3$ *Processes involving heavy quarks*

It is interesting to recall here that in e^+e^-annihilation, where both the $O(\alpha^2\alpha_s)$ and $O(\alpha^2{\alpha_s}^2)$ corrections have been calculated, these turn out to be numerically unimportant. In hadron-hadron collisisons the situation is, however, quite different. The leading diagrams in $O({\alpha_s}^2)$ and $O({\alpha_s}^3)$ are shown in Fig. 2.3. It is well known [37] that the $O({\alpha_s}^3)$ process $g + g \to g + Q + \bar{Q}$ overwhelms the $O({\alpha_s}^2)$ processes for charm quark production at the CERN $Sp\bar{p}S$ collider energies ($\sqrt{s} = 540 - 630$ GeV). The corresponding corrections for $p\bar{p} \to bX$ are also substantial [38] but are not expected to be very large for a top quark of mass ≥ 40 GeV. The reason for this is easily understood in terms of the helpful colour factors in $g + g \to g + Q + \bar{Q}$ and the fact that $p\bar{p}$ and pp collisions are dominated by the gg initiated processes. As $\sqrt{s}$ increases, heavy quark multiplicity in pp and $p\bar{p}$ collisions is expected to rise rather fast, in particular for the charm quark, as shown in Fig. 2.4. The higher order QCD corrections for $ep \to QX$ are expected to lie somewhere in between the $e^+e^-$and $p\bar{p}$ cases, since the probability of finding a gluon in the electron at HERA energies is not very high. This has been recently verified by Ellis and Nason [68]. One can judge

the importance of the $O(\alpha^2{\alpha_s}^2)$ corrections to the heavy quark cross-section at HERA by comparing the estimates presented in Eqs. (2.36) and (2.37) with the corresponding $O(\alpha^2{\alpha_s}^2)$ results [68]: $\sigma(ep \to cX) = 1.36 \pm 0.5\ \mu b$ for $m_c = 1.5\ GeV$ and $\sigma(ep \to bX) = 12.0 \pm 2.2\ nb$ for $m_b = 4.5 - -5.0\ GeV$. These results indicate that the K-factors in the heavy quark production cross-section at HERA are not very large. This reduces one source of theoretical uncertainty.

Returning to the discussion of $2 \to 3$ processes we recall that the parton-parton luminosity functions can be defined as

$$\frac{dL}{dM} = \frac{2M}{s}\int_\tau^1 \frac{dx}{x} F_{a/A}(x, M^2) F_{b/B}(\frac{\tau}{x}, M^2) \tag{2.42}$$

where the function $F_{a/A}(x, M^2)$ denotes the number density of parton a in particle A, $\tau = \frac{M^2}{s}$, M is the parton-parton collision energy, and $\sqrt{s}$ has been defined earlier. For the NC process $ep \to QX$, the following cases have been calculated in ref. [29]

$$\begin{aligned} ep &\to \gamma g X \\ ep &\to \gamma q X \end{aligned} \tag{2.43}$$

$$\begin{aligned} ep &\to qgX \\ ep &\to gqX \\ ep &\to ggX \\ ep &\to \bar{q}qX \\ ep &\to q\bar{q}X \end{aligned} \tag{2.44}$$

The results for $\sqrt{s} = 314$ GeV using the EHLQ [32] parametrizations, for $F_{q/p}(x, Q^2)$ and $F_{g/p}(x, Q^2)$, and the Q^2 evolution of the gluon and quark number densities within the electron $F_{g/e}(x, Q^2)$ and $F_{q/e}(x, Q^2)$ of Ref. [39] are shown in Figs. 2.5 and 2.6. Of these only the γg case contributes to $ep \to QX$ at $O(\alpha^2\alpha_s)$. This is quite different in hadron-hadron collisions where the corresponding luminosity function, $\frac{dL}{dM}(pp(\bar{p}) \to ggX)$, dominates over the others for low values of τ. Thus, whereas the final partons in Eq. (2.44) can scatter in ep collisions in the same manner as in hadronic collisions, the actual contribution of all the processes shown in Eq. (2.44) are suppressed in the former case, since the hadronic wave functions of the electron are suppresed.

The only non-negligible contribution in the NC processes is then expected due to the perturbative correction from $\gamma g \to gQ\bar{Q}$. This is shown in Fig. 2.7 for the b quark, where the total cross-sections $\sigma(ep \to e\ b\ X)$ are plotted from the subprocesses

$$\begin{aligned} \gamma g &\to Q\bar{Q} \\ \gamma g &\to Q\bar{Q}g \\ \gamma q &\to Q\bar{Q}q \\ q\bar{q} &\to Q\bar{Q} \\ gg &\to Q\bar{Q} \end{aligned} \tag{2.45}$$

Since the exact $O(\alpha^2\alpha_s{}^2)$ calculations for the double differential distribution $\frac{d^2\sigma}{dE_\perp d\eta_Q}$ are not yet available, we have regulated the $2 \to 3$ processes by a cut-off $p_T^Q = 5$ GeV. We note that with this choice of the p_T^Q cut-off, the sum of the $2 \to 2$ and $2 \to 3$ cross-sections is in approximate agreement with the complete $O(\alpha^2\alpha_s{}^2)$ result obtained in [68]. Also, judging from the $O(\alpha_s{}^3)$ K-factor calculations for $p\bar{p} \to QX$ [38], it is expected that this choice of p_T^Q is reasonable and the remaining corrections are probably not very important numerically [40]. It would be nice to check this point by an exact $O(\alpha^2\alpha_s{}^2)$ calculation for the double differential distribution $\frac{d^2\sigma}{dE_\perp d\eta_Q}$.

The differential cross-section in rapidity $\frac{d\sigma}{d\eta^b}$ and transverse momentum $\frac{d\sigma}{dp_T^b}$ for the process $ep \to e\ b\ X$ are shown in Figs. 2.8 and 2.9, respectively. They have been generated with a cut $p_T^b > 5$ GeV for the $2 \to 3$ processes , as explained above. In the forward direction (with respect to the proton) the dominant correction to $\frac{d\sigma}{d\eta^b}(ep \to e\ b\ X)$ is due to the subprocess $g + g \to Q + \bar{Q} + g$. On the other hand, this contribution dominates over the other $O(\alpha_s{}^2)$ corrections only at low p_T. For high p_T the process $\gamma + g \to Q + \bar{Q} + g$ dominates over the other corrections in this order.

The relative importance of the $2 \to 3$ processes over the $2 \to 2$ in the Weiszäcker-Williams approximation involving light (u, d, s), charm and bottom quarks can also be seen in Fig. 2.10, showing the transverse energy distributions corresponding to the heavy quark processes $\gamma g \to Q\bar{Q}, Q\bar{Q}g$ and $\gamma q \to Q\bar{Q}q$ $(Q = c, b)$, and the light quark pair production processes

$$\begin{aligned} \gamma + g &\to q + \bar{q} \\ \gamma + q &\to g + q \\ \gamma + g &\to q + \bar{q} + g \\ \gamma + q &\to q' + \bar{q}' + q \\ \gamma + q &\to g + g + q \end{aligned} \tag{2.46}$$

The distributions shown have been obtained by constraining the jet multiplicity to be greater than 2. This in turn demands that for all parton (jet) pairs i, j, one must satisfy the kinematic constraint

$$\Delta R_{ij} > 1.0,\ E_{Tj} > 5\ GeV;\ i, j = 1, 2, 3 \tag{2.47}$$

where ΔR_{ij} is the longitudinal boost invariant quantity defined as

$$\Delta R_{ij} = \sqrt{(\eta_i - \eta_j)^2 + (\Phi_i - \Phi_j)^2} \tag{2.48}$$

with η_i, Φ_i being the pseudorapidities and azimuthal angles of the final state partons.

Very much like the hadroproduction of heavy flavours, one expects the next to leading order QCD corrections to depend on the quark mass, with the corrections being numerically important for charm and to a lesser extent for bottom (in particular for large E_T) at HERA energies. The light jet background is, however, much larger making it difficult to use jet spectroscopy alone to separate charm and bottom jets from the background of light quark and gluons jets. Also, demanding more jets does not help (see Fig. 2.11). It will, therefore, be necessary to demand a lepton in the final state and missing transverse momentum, $\not{p}_T$, with the additional requirement that the lepton be isolated and $\not{p}_T$ be large for the top quark separation (more on this in next section).

Table 2.5: Percentages of $t\bar{t}$ pairs from boson gluon fusion relative to total $t\bar{t}$ cross section

	$Q^2 \leq 1$	$1 \leq Q^2 \leq 10$	$10 \leq Q^2 \leq 10^2$	$10^2 \leq Q^2 \leq 10^3$	$10^3 \leq Q^2 \leq 10^4$
$x \leq 10^{-3}$	66.16	10.21	8.55	–	–
$10^{-3} \leq x \leq 10^{-2}$	0.0	0.0	2.20	7.59	–
$10^{-2} \leq x \leq 5.10^{-2}$	0.0	0.0	0.0	1.68	2.80
$5.10^{-2} \leq x \leq 10^{-1}$	0.0	0.0	0.0	0.0	0.60
$10^{-1} \leq x \leq 2.10^{-1}$	0.0	0.0	0.0	0.0	0.15
$2.10^{-1} \leq x \leq 5.10^{-1}$	0.0	0.0	0.0	0.0	0.0
$5.10^{-1} \leq x \leq 1$	0.0	0.0	0.0	0.0	0.0

Table 2.6: Percentages of $t\bar{b}$ pairs from boson gluon fusion relative to total $t\bar{b}$ cross section

	$Q^2 \leq 10$	$10 \leq Q^2 \leq 10^2$	$10^2 \leq Q^2 \leq 10^3$	$10^3 \leq Q^2 \leq 10^4$	$10^4 \leq Q^2 \leq 4.10^4$
$x \leq 10^{-3}$	0.40	1.41	–	–	–
$10^{-3} \leq x \leq 10^{-2}$	0.01	2.59	13.93	–	–
$10^{-2} \leq x \leq 5.10^{-2}$	0.0	0.05	15.58	32.08	–
$5.10^{-2} \leq x \leq 10^{-1}$	0.0	0.0	0.51	21.38	–
$10^{-1} \leq x \leq 2.10^{-1}$	0.0	0.0	0.04	8.30	1.20
$2.10^{-1} \leq x \leq 5.10^{-1}$	0.0	0.0	0.0	0.75	0.99
$5.10^{-1} \leq x \leq 1$	0.0	0.0	0.0	0.0	0.0

2.6 *General characteristics of heavy flavour production at HERA: parton level results*

Having discussed the cross-sections for heavy flavour production at HERA, we would now like to study the various distributions which are characteristic of these processes. We start with the inclusive distributions in the variables introduced in Eqs. (2.9)-(2.18), once again recalling that not all of these variables are independent. We show in Tables 2.5-2.9 the normalized distributions

$$\frac{1}{\sigma}\frac{d^2\sigma}{dxdQ^2} \tag{2.49}$$

for NC processes $ep \to eqX$ for light ($q = u, d, s$) flavours and $ep \to eQ\bar{Q}X$ for heavy ($Q = c, b, t$) flavours, together with the CC process $ep \to \nu_e t\bar{b}X$ involving single top quark production. The heavy quark distributions are based on $2 \to 2$ processes (in the BGF sense) for an assumed top quark mass $m_t = 60$ GeV. The light quark production was implemented using the DIS process with $Q^2 \geq 1\ GeV^2$. It is obvious from these tables that all the NC processes involving heavy quarks are dominated by low Q^2. This, however, is not true for the CC process shown, which has important contributions at large Q^2 due to the exchange of the massive W-boson. This gives a distribution spread out both in x and Q^2. For $m_t = 60$ GeV, we note that in the region defined by $10^{-2} < x < 1$ and $0.4 < y < 1$, $t\bar{b}$ production is actually close to $\sim 1\%$ of the total CC deep inelastic cross-section. The inclusive distributions $\frac{d\sigma}{dlnQ^2} = Q^2\frac{d\sigma}{dQ^2}$ are shown in Fig. 2.12 for the NC processes giving $c\bar{c}$, $b\bar{b}$, $t\bar{t}$ and the CC process giving $t\bar{b}$. The dependence on Q^2 is reflected in the angle of the scattered lepton as shown in Fig. 2.13. Thus, for the NC processes shown, the scattered electron is dominantly at very small angles so that its detection would require a very forward detector which is integrated with the machine magnet elements to bend the (lower energy) scattered electron out of the beam. On the other hand, there is no overriding interest in tagging the scattered electron in the NC processes as far as heavy flavour studies are concerned, except perhaps for top quark searches. This, however, for the range of current interest for the top quark mass would involve the CC process $ep \to \nu_e t\bar{b}$ which does not give rise to any scattered electron in the final state.

The distributions in the invariant mass, $\sqrt{\hat{s}}$, of the $Q\bar{Q}$ pair $\frac{d\sigma}{d\sqrt{\hat{s}}}$, which can be measured if both the quark and antiquark are reconstructed in the detector, are shown in Fig. 2.14. The cross-section peaks close to the threshold and falls steeply for large values of $\sqrt{\hat{s}}$. The invariant mass W of the complete hadronic system has a rather different distribution, shown in Fig. 2.15, due to the addition of the target remnant. We note that a cut in W is not effective in separating the bottom and top from the dominant charm production. In contrast a cut in $\hat{s}$ would be better, though the W_{vis} distribution (incorporating the beam pipe cut) may also be useful.

2.7 *Hadronization and weak decays*

The formalism presented so far has been applied to those aspects of heavy quark production which can presumably be calculated at the parton level. However, it is obvious that for a complete description of final states, the hadronization of quarks and gluons and weak decays of heavy quarks must be included. To incorporate these features we have used the Monte

Table 2.7: Percentages of $b\bar{b}$ pairs from boson gluon fusion relative to total $b\bar{b}$ cross section

	$Q^2 \leq 1$	$1 \leq Q^2 \leq 10$	$10 \leq Q^2 \leq 10^2$	$10^2 \leq Q^2 \leq 10^3$	$10^3 \leq Q^2 \leq 10^4$
$x \leq 10^{-3}$	81.154	8.978	3.065	–	–
$10^{-3} \leq x \leq 10^{-2}$	0.019	0.999	3.399	1.037	–
$10^{-2} \leq x \leq 5.10^{-2}$	0.0	0.014	0.517	0.638	0.031
$5.10^{-2} \leq x \leq 10^{-1}$	0.0	0.0	0.018	0.086	0.014
$10^{-1} \leq x \leq 2.10^{-1}$	0.0	0.0	0.003	0.023	0.006
$2.10^{-1} \leq x \leq 5.10^{-1}$	0.0	0.0	0.001	0.0	0.001
$5.10^{-1} \leq x \leq 1$	0.0	0.0	0.0	0.0	0.0

Table 2.8: Percentages of $c\bar{c}$ pairs from boson gluon fusion relative to total $c\bar{c}$ cross-section

	$Q^2 \leq 1$	$1 \leq Q^2 \leq 10$	$10 \leq Q^2 \leq 10^2$	$10^2 \leq Q^2 \leq 10^3$	$10^3 \leq Q^2 \leq 10^4$
$x \leq 10^{-3}$	89.210	5.457	0.233	–	–
$10^{-3} \leq x \leq 10^{-2}$	0.649	1.662	1.149	0.108	–
$10^{-2} \leq x \leq 5.10^{-2}$	0.021	0.313	0.363	0.059	0.006
$5.10^{-2} \leq x \leq 10^{-1}$	0.0	0.028	0.040	0.009	0.0
$10^{-1} \leq x \leq 2.10^{-1}$	0.0	0.003	0.037	0.006	0.000
$2.10^{-1} \leq x \leq 5.10^{-1}$	0.0	0.0	0.006	0.0	0.0
$5.10^{-1} \leq x \leq 1$	0.00	0.00	0.00	0.00	0.00

Table 2.9: NC production of light flavours for $Q^2 \geq 1GeV^2$

	$Q^2 \leq 10$	$10 \leq Q^2 \leq 10^2$	$10^2 \leq Q^2 \leq 10^3$	$10^3 \leq Q^2 \leq 10^4$
$x \leq 10^{-3}$	22.76	1.66	–	–
$10^{-3} \leq x \leq 10^{-2}$	27.79	3.56	0.25	–
$10^{-2} \leq x \leq 5.10^{-2}$	23.07	2.75	0.31	0.01
$5.10^{-2} \leq x \leq 10^{-1}$	8.92	1.10	0.12	0.01
$10^{-1} \leq x \leq 2.10^{-1}$	3.64	1.04	0.10	0.10
$2.10^{-1} \leq x \leq 5.10^{-1}$	0.71	0.89	0.09	0.01
$5.10^{-1} \leq x \leq 1.$	0.00	0.04	0.01	0.01

Carlo simulation model AROMA [30] to generate all heavy flavour samples. This program is based on the following main ingredients:

- The complete $O(\alpha^2\alpha_S)$ matrix elements for the BGF processes as discussed earlier. This includes the quark mass effects and takes into account the full electroweak structure of the interaction.
- Gluon emission from the $Q\bar{Q}'$ system in a parton cascade approach [41]. This leads to a better description of the internal structure of jets and also gives rise to multijet events.
- Hadronization of the quarks and gluons using the LUND string model [42].
- Weak decays of the charm, bottom and top quarks according to the standard V-A matrix elements.

The parton shower gluon emission is important for a realistic estimate of the background in the top search based on multijet requirements. In particular, the $b\bar{b}g$ final state is expected to be an important background for the signature based on an isolated lepton plus a jet. We note, however, that the leading logarithm approximation used in the parton cascade formalism may not be quite adequate for hard gluon emission at large angles and the multijet rates obtained should, therefore, be taken with some caution. A comparison with the available $O(\alpha^2\alpha_s^2)$ exact matrix elements would be important for this reason, but such a study has not yet been performed.

The fragmentation function for the charmed and bottom hadrons are experimentally found to be considerably harder than for light quarks [43]. The available data from e^+e^- are often parametrized by the Peterson et al. function [44]

$$f(z) = N\frac{1}{zF(z)^2},\ F(z) = 1 - \frac{1}{z} - \frac{\epsilon}{1-z} \tag{2.50}$$

where N is a normalization factor, $z = P_{hadron}/P_{quark}$ and ϵ is a fitted parameter depending on m_Q with $\epsilon = 0.3$ for charm and $\epsilon = 0.02$ for bottom. The data can equally well be described by the Lund symmetric fragmentation function [45]

$$f(z) = \frac{(1-z)^a}{z}\exp\left\{\frac{-bm_\perp^2}{z}\right\} \tag{2.51}$$

which is used in AROMA. This gives an increasingly harder spectrum for heavier hadrons, asymptotically $<1-z>=(a+1)/bm^2$. Although we have not explicitly estimated the sensitivity of our results to the uncertainties in the heavy quark fragmentation function, we expect it to be quite small.

The standard V–A matrix elements for the processes

$$t \to bl^+\nu_l \tag{2.52}$$
$$c \to sl^+\nu_l$$

$$b \to cl^-\bar{\nu}_l \tag{2.53}$$

are given by the expressions [46]

$$|M|^2 = \begin{cases} Cp_{14}p_{23} & \text{(for 2.52)} \\ Cp_{13}p_{24} & \text{(for 2.53)} \end{cases} \tag{2.54}$$

where $p_{ij} = p_i.p_j$, and the momenta are defined by $p_1 \rightarrow p_2 p_3 p_4$. We note that for heavier top ($m_t > 70$ GeV), the W-propagator effects become important. In that case the $|M|^2$ shown in (2.54) should be modified as follows:

$$|M|^2 \rightarrow \frac{|M|^2}{\{(2p_{34} - m_W^2)^2 + (\Gamma_W m_W)^2\}} \tag{2.55}$$

The background to heavy flavour production from processes involving light quarks only has also been investigated by Monte Carlo methods. Here, we treat the low-Q^2 and high-Q^2 regions separately since they correspond to somewhat different processes, photoproduction and deep inelastic scattering, respectively. The former is treated in AROMA by introducing the two $O(\alpha\alpha_s)$ processes of photon-gluon fusion into a light quark-antiquark pair and the QCD Compton process $\gamma + q \rightarrow q + g$. In both cases, a cutoff $p_\perp^q > 1$ GeV on the final quark transverse momentum is introduced in order to avoid divergences and obtain realistic cross-sections. The deep inelastic region (which we define by $Q^2 \geq 4\ GeV^2$, $x \geq 10^{-3}$ and $W^2 \geq 5\ GeV^2$) is simulated using the standard DIS Monte Carlo LEPTO 5.2 [47], which is based on the electroweak cross-sections for DIS scattering and takes QCD corrections into account via parton cascades.

In Fig. 2.16 we show the transverse momentum distributions $\frac{d\sigma}{dp_\perp}$ for the heavy quarks and hadrons and in Fig. 2.17 the distributions for the rapidity of the heavy quarks and hadrons $\frac{d\sigma}{dy_{lab}}$, where $y_{lab} < 0$ defines the proton beam hemisphere in the HERA laboratory frame. It is obvious from these distributions that most of the cross-sections involving heavy hadrons are concentrated at rather central rapidities and thus most of the heavy flavours emerge in a region covered by HERA detectors, i.e. $-3.5 \leq y_{lab} \leq 2$. Only for charmed hadrons does one find that there is a substantial fraction of events boosted down the beam pipe in the proton direction. On the other hand a simple cut in rapidity is no great help in enhancing bottom and top samples at the expense of charm events. The transverse momentum distributions are strongly suppressed only for values above the corresponding quark mass, thus one has increasingly large mean transverse momenta in the sequence charm-bottom-top hadrons.

Next, we would like to show a number of inclusive distributions from heavy quark production and decays, which should help in separating the charm, bottom and top events at HERA experiments (for top, these searches are meaningful only if $m_t \leq 70$ GeV). In Fig. 2.18 we show the distributions in the total transverse energy $\sum E_\perp$ from the NC production of $c\bar{c}$, $b\bar{b}$ and $t\bar{t}$ quarks and the CC process involving $\bar{t}b$. Also shown are the distributions corresponding to the NC DIS process (with $Q^2 \geq 10\ GeV^2$) and the light $q\bar{q}$ and qg (with $Q^2 \leq 10\ \mathrm{GeV}^2$). From the transverse momenta increasing with m_Q in the production process and the corresponding larger energy release in the decays, one expects an increasing transverse energy for heavier flavours in low Q^2 processes. This expected behaviour can be quantitatively seen in Fig. 2.18, where all stable (charged and neutral) particles outside a beam pipe cut of 100 $mrad$ are included as in a straightforward measurement of total transverse energy in a calorimeter. A large cut in $\sum E_\perp$ can help in enriching the bottom and top quark samples. Transverse sphericity, or circularity, is also a useful variable for top quark searches at HERA. We shall discuss both of these points in the next section.

The variable sphericity has been used historically to find quark jets in e^+e^- annihilation. It is defined as [48]

$$S = \frac{3}{2} \frac{(\sum_i p_{T_i}^2)_{min.}}{\sum_i \vec{p_i}^2} \tag{2.56}$$

where the p_{T_i} are measured w.r.t. the sphericity axis, which minimizes it. It has also been used in the search for heavy quarks, since near threshold they are expected to give rise to

spherical events ($S \rightarrow 1$). In Fig. 2.19(a) we show the distribution $\frac{d\sigma}{dS}$ for the NC production $c\bar{c}$, $b\bar{b}$, $t\bar{t}$ processes and the CC process $t\bar{b}$, evaluated at HERA energy $\sqrt{s} = 314$ GeV. One can make use of the much broader $\sum E_\perp$ distributions for the $t\bar{t}$ and $t\bar{b}$ events (see Fig. 2.18) and study the sphericity distribution $\frac{d\sigma}{dS}$ by imposing a cut on $\sum E_\perp$. The results are shown in Fig. 2.19(b-d), for $\sum E_\perp > 20, 60, 80$ GeV, respectively. For $\sum E_\perp \geq 60$ GeV, the tail in $\frac{d\sigma}{dS}$ for the events containing a t quark emerges over the $c\bar{c}$, $b\bar{b}$ backgrounds, giving the result that large $\sum E_\perp$ and large S events are suitable candidates for top quark searches.

A separation of the charm, bottom and top quarks can, in principle, also be done using the p_T of the $l^\pm$ from the semileptonic decays of these quarks. A better separation is obtained if the p_T^l can be measured w.r.t. the heavy quark direction. To quantify this, we use the sphericity axis of the visible hadronic system in its centre of mass. The results for the processes $ep \rightarrow l^\pm X$ at HERA are shown in Fig. 2.20, where the distribution $\frac{d\sigma}{dp_T^l}$ measured w.r.t. the sphericity axis as well as the beam axis are shown. Again, a large cut in the variable $\sum E_\perp$ can be used to enhance the bottom and top content in the inclusive final states, $ep \rightarrow l^\pm X$. Thus, events containing large-p_T leptons, having large $\sum E_\perp$ are expected to arise from top quarks at HERA, (again assuming $m_t < 70$ GeV, beyond which the inclusive top quark cross-section becomes very small).

Finally, we remark that the same sign dilepton final states $ep \rightarrow l^\pm l^\pm X$ with large p_T^l for both the leptons are also expected to be dominantly produced by the bottom and top quarks. Again, the $c|b|t$ separation can be improved with cuts in $\sum E_\perp$. The price one has to pay is obviously in rates due to $(BR)_l^2$ which may reduce the cross-section to be prohibitively small for events containing a top quark.

3. Top Quark Search at HERA

In this section we describe in detail top quark search strategies at HERA [16,49]. In the discussion below we follow closely the analysis of [49]. We use the Monte Carlo simulation described earlier in section 2.7. The total cross sections for the signal and background processes are summarized in Table 3.1. We find that the background is typically about seven orders of magnitude larger than the top quark cross section. In order to reduce the background we first search for characteristics of top production. Table 3.1 also gives the mean values of the summed visible tranverse energy, $\sum E_\perp$, circularity, C, and the charged particle multiplicity, n_{ch}. The circularity (transverse sphericity) is defined by $C = 2\lambda_2$ in terms of the smaller eigenvalue, λ_2, of the two dimensional sphericity tensor ($S_{\alpha\beta} = \sum_i p_{i\alpha} p_{i\beta} / \sum_i p_i^2$ where α, β are Cartesian components and i runs over the particles in the event). We find that neither the circularity nor the number of charged particles provides a clean top signature. It is $\sum E_\perp$ which provides us with a first inclusive quantity to reduce the background, as already remarked in the previous section. In the following we shall present two different analyses based on the semileptonic and nonleptonic top quark decays, which suggest a number of selective cuts to bring down the background.

We have already shown in Fig. 2.18 the distributions in $\sum E_\perp$ for the top signal and the various background processes, and have commented on the broad $\sum E_\perp$ distribution for top events due to the large value of m_t. One notices, however, the long tail in the $\sum E_\perp$ distributions of the light quark events, reflecting the large $p_\perp$ and Q^2 reachable in ep processes at HERA. In CC reactions Q^2 is typically large resulting in the wide $\sum E_\perp$ distribution of Fig. 2.18, but also the NC reactions extend to large values of $\sum E_\perp$. Recalling the tiny signal to background ratio it is clear that the high Q^2 events although of the order of a percent will dominate the high $\sum E_\perp$ range and become an even more important background than the low Q^2 part. A first step in reducing the background will be a lower cut in $\sum E_\perp$ which will typically be chosen as 20, 40 or 60 GeV.

3.1 *Semileptonic analysis*

In this section we study the top quark signatures arising from its semileptonic decays:

$$e^- + g \to \nu_e + \bar{t} + b \qquad \text{with} \quad \bar{t} \to \bar{b} + l^- + \nu_l \tag{3.1}$$
$$e^- + g \to e^- + t + \bar{t} \qquad \text{with} \quad \bar{t} \to \bar{b} + l^- + \nu_l \ + c.c.$$

The signatures are an isolated lepton and missing transverse momentum from the (decay) neutrino, possibly with a number of jets. In order to take the beam pipe into account we disregard all particles with an angle less than 100 *mrad.* to the beam directions:

$$\theta_{beam} = 100\,\text{mrad}. \tag{3.2}$$

We also apply a lower cut in the total visible transverse energy

$$\sum E_\perp \geq 20\,\text{GeV} \tag{3.3}$$

This cut suppresses the background substantially while the top quark signal remains practically unchanged.

Table 3.1: Characteristics of heavy quark production at HERA

general cut: beam hole angle $\theta = 0.1$ rad				
for DIS events: $Q \geq 2\,\text{GeV}$, $x \geq 0.001$, $W^2 \geq 5\,\text{GeV}^2$				
for light quark events: $p_\perp^q \geq 1\,\text{GeV}$				
process	σ[pb]	$\langle \sum E_\perp \rangle$[GeV]	$\langle C \rangle$	$\langle n_{ch} \rangle$
NC				
$b\bar{b}$	4.2×10^3	14.	0.44	16
$c\bar{c}$	5.1×10^5	7.2	0.51	12
DIS	1.3×10^5	8.6	0.12	5
qG	7.3×10^5	3.4	0.42	5
$q\bar{q}$	7.8×10^5	6.2	0.50	10
CC				
$\bar{c}s$	8.3	25.	0.18	13
light quarks	71.	42.	0.14	15
$\bar{t}b$ $m_t =$				
40 GeV	0.36	48.	0.30	21
60 GeV	0.13	58.	0.28	21
80 GeV	0.05	70.	0.26	22
$t\bar{t}$ $m_t =$				
40 GeV	1.9	66.	0.36	26
60 GeV	0.09	93.	0.37	28
80 GeV	4.3×10^{-3}	117.	0.38	29

Single lepton spectra

The basic idea to separate the top quark signal from the background is to use the lepton (electron or muon) from the semileptonic top quark decay as a tag. Ideally, one would like to measure the lepton momentum transverse to the emitting quark direction. This strategy has been suggested for top searches in e^+e^- annihilation [1,50]. On the other hand, in $p\bar{p}$ collisions such searches turned out to be difficult since it is not easy to reconstruct the quark direction. Therefore one might think of measuring the lepton momentum transverse to the beam direction [51–54]. Again, the lepton from top quark decay is expected to be the hardest one since the $p_\perp$ of the hard scattering process increases with the quark mass resulting in a corresponding higher mean transverse momentum of the quark and thereby of its decay lepton. The larger energy release in top quark decays will also contribute to a higher lepton $p_\perp$.

In $p\bar{p}$ collisions the initial state at the parton level consists (to a good approximation) of collinear partons. The $p_\perp$ of the final state is thus governed by the hard scattering process:

$$p_\perp \approx p_\perp^{QCD} \tag{3.4}$$

In contrast, there are two sources of $p_\perp$ in ep collsions: One originating from the QCD process, $p_\perp^{QCD}$, and the other $p_\perp$ arising from the scattered lepton (electron or neutrino) given by

$$p_\perp^{DIS} = Q\sqrt{1-y} \tag{3.5}$$

Note that the latter $p_\perp$ is essentially independent of the quark mass.

There is, however, the true DIS (i.e. high Q^2) events of light partons which will also lead to high $p_\perp$ (w.r.t. the beam axis) leptons. The NC DIS events can experimentally be discriminated by the clean signature of a high $p_\perp$ isolated electron (the scattered electron) on one side of the detector and the hadronic event on the other side, where in addition the values of Q^2 and y measured from the scattered lepton and hadron flow match. We therefore introduce an upper cutoff in Q^2 for all NC events:

$$Q^2 \leq 10\,\mathrm{GeV}^2 \qquad \text{for NC events} \tag{3.6}$$

This cut leaves the top quark signal almost unchanged but diminishes substantially the NC background. On the other hand, for the CC DIS background there is no corresponding simple criterion. Although the total CC cross section is much smaller than the NC one, the former can become increasingly important in the tail of high $p_\perp$ leptons.

Fig. 3.1 shows the cross sections for producing leptons (electrons and muons) versus the lower cut off in the lepton tranverse momentum $p_\perp(l)$ (for events containing more than one lepton the highest $p_\perp$ lepton is taken). We find that not only are the cross sections for charm and bottom quark production large, but also the background from the light quarks, in particular the CC background, is above the top signal. The background can only be reduced by selecting very high $p_\perp$ events which, however, also diminishes the top signal very much. From Fig. 3.1 we see that a lower cut of

$$p_\perp^{cut}(l) = 10\,\mathrm{GeV} \tag{3.7}$$

is a reasonable compromise to improve the signal to background ratio on the one hand and not to loose too much signal on the other.

Lepton isolation

An additional lepton isolation criterion is needed to suppress the backgrounds. Lepton isolation is defined by introducing a cone around the lepton momentum in the space of pseudorapidity η and azimuthal angle ϕ around the beam axis:

$$\Delta R \equiv \sqrt{(\Delta\eta)^2 + (\Delta\phi)^2} \leq R_c \tag{3.8}$$

A lepton is said to be isolated if its accompanying energy, E_{acc}, i.e. the total transverse energy within this cone, is less than a given minimum value E_{acc}^{cut}. We have checked that the isolation criterion is rather insensitive to variations in R_c and have chosen

$$R_c = 0.4 \tag{3.9}$$

Fig. 3.2 compares the cross sections of produced leptons with $p_\perp \geq 8\,\mathrm{GeV}$ versus the cut in accompanying energy E_{acc}^{cut}. Very little of the light quark and charm background has $E_{acc} \leq 1$ GeV, whereas practically all of the top signal (both $t\bar{t}$ and $\bar{t}b$ events) falls in this range. The main background comes from $b\bar{b}$-production. These events are considerably reduced by cutting in E_{acc} but are still around two orders of magnitude larger than the top signal. From Fig. 3.2 we define the isolation criterion:

$$E_{acc} \leq 1\,\mathrm{GeV} \tag{3.10}$$

Missing transverse momentum

Besides the isolated lepton the missing transverse momentum, $\not{p}_\perp$, carried away by the neutrino is a signature of a semileptonic heavy quark decay. The missing transverse momentum, $\not{p}_\perp$, is measured by overall momentum conservation. It consists of contributions from the neutrino accompanying the isolated trigger lepton, from the neutrini of other semileptonic decays that may be present, and from the particles lost in the beam pipe. There are various other experimental uncertainties. These depend on the specific detector setup and are not included in our analysis. There is yet another important contribution coming from the scattered (DIS) lepton. For NC events a low Q^2 electron can not be identified. This, however, is small since in this case $\not{p}_\perp \equiv p_\perp^{DIS} = Q\sqrt{1-y}$.

For CC events on the other hand, where Q^2 is typically large, the missing $p_\perp$ from the scattered (DIS) neutrino can become large and exceed the missing transverse momentum from a semileptonic heavy quark decay. This has two consequences: Firstly, the top quark mass in $\bar{t}b$ events cannot be reconstructed because of the presence of two neutrini which yield two uncorrelated, large contributions to $\not{p}_\perp$. Secondly, a cut in $\not{p}_\perp$ is inefficient to suppress CC backgrounds. From Fig. 3.2 we notice that the CC background can be suppressed by the lepton isolation criterion. Yet there is an $O(\alpha_s^2)$ CC contribution to heavy quark production (in particular for charm production) which has not yet been calculated and included:

$$e^- + q \to \nu_e + q' + Q + \bar{Q} \qquad \text{with} \quad Q \to q + l^- + \nu_l \tag{3.11}$$

Simulating these events via parton showers indicates that this could become a severe background. Thus, our distributions in $\not{p}_\perp$ and $\sum E_\perp$ below should be taken with some care. The result of top quark reconstruction in the $\bar{t}t$ case is unaffected since there additional cuts are applied (see below). Also the nonleptonic analysis (see next subsection) is independent of this subtlety.

Table 3.2: Number of t quark events passing the cuts of the semileptonic analysis for $\int L\,dt = 1\,\mathrm{fb}^{-1}$. The cuts are: $\sum E_\perp \geq 20\,\mathrm{GeV}$, event contains isolated lepton (with $p^l_\perp \geq 8\,\mathrm{GeV}$, $E_{acc} \leq 1\,\mathrm{GeV}$), $\not{p}_\perp \geq 10\,\mathrm{GeV}$, $\theta_{\mathrm{beam}} = 100\,\mathrm{mrad}$, and $Q^2 \leq 10\,\mathrm{GeV}^2$ for NC events.

m_t[GeV]	40	60	80
$t\bar{t}$	220	16	0.9
$\bar{t}b$	40	21	9

Table 3.3: Mean values of $\sum E_\perp$ in t quark production for various t quark masses. Cuts as in Table 3.2.

m_t[GeV]	40	60	80
$t\bar{t}$	60	82	104
$\bar{t}b$	44	50	58

Fig. 3.3 shows the cross sections versus the lower cutoff $\not{p}_\perp^{cut}$ in the missing transverse momentum for events containing an isolated lepton. We find that the dominant $b\bar{b}$ background is completely suppressed by a cut of about 10 GeV. From the complete analysis we obtain a clean top quark sample at the expense of a signal reduction by a factor 5–9, depending on the top quark mass. Assuming an integrated luminosity of 1 fb^{-1} corresponing to five years HERA running, the expected number of top events are given in Table 3.2. With the above mentioned caveat (i.e. omission of the process (3.11)) the background is estimated to be about one event! We conclude that a clean top sample up to about 70 GeV seems possible at HERA.

t quark mass determination

The simplest hint for the top quark mass is the number of top events which clearly depends on its mass. Several distributions sensitive to m_t can also be investigated. Fig. 3.4 shows the differential distributions in missing transverse momentum for the total background and the top signal for three different top quark masses where all events are required to contain an isolated lepton. Similarly, Fig. 3.5 gives the differential cross sections in the total transverse energy where in addition $\not{p}_\perp \geq 10\,\mathrm{GeV}$ is required. The mean values clearly increase with the top quark mass, and in particular the distribution $d\sigma/d\sum E_\perp$ will lead to a top quark mass estimate as can be seen from the mean values of $\sum E_\perp$ given in Table 3.3.

The final aim, of course, will be to reconstruct the top quark event and hence measure the top quark mass. As already mentioned, this will be impossible for $\bar{t}b$ events in the semileptonic channel due to the presence of two neutrini. In the $t\bar{t}$ case we expect the following topology

for semileptonic decay of one of the top quarks:

$$t \to b + l^+ + \nu_l \to l^+ + \not{p}_\perp + \mathrm{jet} \qquad (3.12)$$
$$\bar{t} \to \bar{b} + q + \bar{q} \to \mathrm{jet} + \mathrm{jet} + \mathrm{jet}$$

Thus, the top quark mass could be reconstructed from both decay channels: One channel uses the information from three jets:

$$m_t \approx m_h \equiv m(3j) \qquad (3.13)$$

The other top quark mass can only partially be reconstructed since the information on the neutrino momentum is lost:

$$(m_t)_l \approx m_l \equiv m_l(l, \not{p}_\perp, j) \qquad (3.14)$$

Here $m_l(l, \not{p}_\perp, j)$ denotes the minimum mass constructed from the lepton, jet and the missing transverse momentum. The minimum mass is defined similar to the transverse mass [55]. It is the minimum invariant mass which can be constructed for the jet-l-ν_l system (and is identical to the cluster transverse mass defined in ref. [67].

The jet finding algorithm applied is of the UA1 type with the following specifications: the cone in the (η,ϕ)-plane is given by $\Delta R = 0.7$, the minimum jet transverse energy is 7 GeV, the allowed rapidity range is $|\eta| \leq 3$. The granularity of the bins used in the analysis is $\Delta\eta\Delta\phi = (0.24) \times (12°)$. The resulting jet multiplicity disributions are shown in Fig. 3.6 for the total background and the top quark signal ($m_t = 60\,\mathrm{GeV}$) after applying the following cuts: $\sum E_\perp \geq 60\,\mathrm{GeV}$, isolated lepton, $\not{p}_\perp \geq 10\,\mathrm{GeV}$. We find that there are many three-jet configurations for the $t\bar{t}$ signal which means that one of the four expected jets was unresolved or lost. (There are also configurations with more than four jets). In order to obtain as much statistics as possible we introduce a lower cutoff in the number of jets, $N(jets) \geq 3$, and apply a jet finding algorithm which forced the number of jets to be four. With four-jet configurations we now calculate the top quark mass using the hadronic mass, m_h, and the leptonic (minimum) mass, m_l, defined above. Unfortunately there are several combinatoric possibilities since it is not clear which jet to associate with the top quark decaying semileptonically.

Fig. 3.7 shows the differential cross section in the reconstructed minimum (leptonic) mass (3.7a) and hadronic mass (3.7b). Shown is the sum of all four combinations of $\bar{t}b$ events ($m_t = 60\,\mathrm{GeV}$), the sum of the three wrong combinations and the right combination of $\bar{t}t$ events. The background is too small to appear in the plot. In the case of the hadronic mass we find a nice peak of the right combination out of the combinatoric background, whereas in the case of reconstructing the top quark mass from lepton, missing transverse momentum and one jet, the signal is below the combinatoric background. To improve the ratio of signal to combinatoric background we show in Fig. 3.8 the distributions in m_h and m_l again, but now after a selection of a window in both quantities simultaneously: $m_l \in [50, 65]\,\mathrm{GeV}$ and $m_h \in [40, 65]\,\mathrm{GeV}$. This suggests that a top quark in the mass range of 60 GeV can be reconstructed at HERA. Here, we expect a total signal (all combinations) of about 15 events for an integrated luminosity of 1 fb^{-1}.

3.2 *Nonleptonic analysis*

If one wants to use the $\bar{t}b$ sample to reconstruct the top quark mass one must consider the nonleptonic top decays. To be close to the experimental situation we define the nonleptonic

sample as consisting of those events which do not contain an isolated lepton. We have checked that the top event sample which we obtained in this way almost coincides with the actual Monte Carlo top quark sample which decayed hadronically. The cuts in the beam hole angle and Q^2 are as in the semileptonic case. The cut in $\sum E_\perp$ is increased to 40 GeV.

Circularity analysis

We start from the expectation that light parton events which have a large $\sum E_\perp$ will typically be less spherical, or circular, than events coming from the decay of a heavy (slow moving) object. The circularity distributions for the top quark signal and the NC and CC backgrounds are shown in Fig. 3.9. We find that the background is indeed much less circular than the signal. There are, however, tails in the background to high circularity values which still overwhelm the signal. Note that here a cut $\sum E_\perp \geq 40$ GeV has already been introduced. Taking a cut in circularity of

$$C \geq 0.25 \tag{3.15}$$

the background is reduced by roughly a factor 10, while we loose about one third of the signal.

Jet activity

Top events are expected to produce four (six) jet final states in $\bar{t}b$ ($t\bar{t}$) events via nonleptonic the weak decays

$$\begin{aligned} e^- + g &\to \nu_e + \bar{t} + b \quad \text{with} \quad \bar{t} \to \bar{b} + q + \bar{q}' \\ e^- + g &\to e^- + t + \bar{t} \quad \text{with} \quad \bar{t}(t) \to \bar{b}(b) + q + \bar{q}' \end{aligned} \tag{3.16}$$

Due to the jet resolvability and fluctuations the actual number of observed jets may be different. For the background the jet multiplicity is determined by the amount of gluon radiation. The latter in turn depends on the scale in the parton shower treatment, which is not designed for hard parton emission at wide angles. However, it is precisely this emission which results in well separated jets. The uncertainty in the multijet rate is "multiplied", and increases powerlike with the number of branchings. Let us finally mention that there is a damping factor for parton radiation in ep collisions. This factor is given by a ratio of parton densities and affects both initial and final state radiation. Currently available Monte Carlo generator programs do not apply this factor to final state radiation. Hence, the Monte Carlo predictions with parton showers must be interpreted with some caution for the high jet multiplicity events.

Fig. 3.10 shows the jet multiplicities for the top signal ($m_t = 60$ GeV) and the total NC and CC backgrounds. The jet algorithm is of the UA1 type as described in the semileptonic analysis above. Top events have typically one to two jets unresolved, resulting in a mean value of 3.0 (4.2) for $\bar{t}b$ ($t\bar{t}$) events. For the background the mean jet multiplicity is between two and three. To effectively suppress the background one has to require high jet multiplicties and even then one does not obtain a clean top signal. In particular $\bar{t}b$ events cannot be isolated via a cut in the number of jets. To improve the signal to background ratio we take:

$$n_{jet} \geq 3 \tag{3.17}$$

With this cut we still retain most of the $\bar{t}b$ signal.

Missing transverse momentum

To enhance the $\bar{t}b$ sample we can make use of the fact that even in nonleptonic decays there is typically a large $\not{p}_\perp$ due to their CC production mechanism. All NC events, on the other hand, should be substantially suppressed. Fig. 3.11 a) shows the differential cross section $d\sigma/d\not{p}_\perp$ in missing transverse momentum for the total NC and CC background and the top signal for three different top quark masses. The applied cuts are: $\sum E_\perp \geq 40$ GeV, $C \geq 0.25$ and $n_{jet} > 2$. We find that a cut in $\not{p}_\perp$ which we choose as

$$\not{p}_\perp \geq 15\,\text{GeV} \tag{3.18}$$

is well suited to separate NC and CC events. In particular we obtain a $\bar{t}b$ sample whose only background is given by the light parton CC events. This background, however, is still larger than the signal. In particular at high $\not{p}_\perp$ values the CC background is much larger than the signal. This can be understood as follows: Via the cut in number of jets we have already selected light quark CC events with a high jet activity, i.e. events having high values of W^2 and thereby of Q^2. Through the relation $\not{p}_\perp = Q\sqrt{1-y}$ this in turn favours high $\not{p}_\perp$ values. Thus, in principle one could improve the signal to background ratio by selecting a window in $\not{p}_\perp$ rather than a lower cut only. Due to imperfections of the detectors the actual $\not{p}_\perp$-distributions may be shifted to higher $\not{p}_\perp$ values. We therefore do not pursue this strategy. With the cut $\not{p}_\perp \geq 15$ GeV we obtain a $\bar{t}b$ ($t\bar{t}$) sample of 30 fb (7.5 fb) while the total background is about a factor 20 larger.

One could think of improving the signal to background ratio by requiring a higher number of jets. Fig. 3.11 b) shows the distributions in missing $p_\perp$ for the total NC and CC background and the top signal ($m_t = 60$ GeV) for $n_{jet} > 3$. The shapes of the curves are the same as in the $n_{jet} > 2$ case. The distributions are scaled down by an essentially constant factor, thus the higher cut in the jet multiplicity essentially results in a lower signal rate and a similar signal to background ratio.

t-quark mass reconstruction

The background can be further reduced by considering the distributions in the invariant masses of the relevant jets. At the same time we might hope to reconstruct the top quark mass. To this end we consider the events containing three and four jets. For our $\bar{t}b$ sample we make the following assumptions which we have checked with the Monte Carlo: If the number of jets equals three we assume that all three jets originate from the top quark, since the bottom quark is often not energetic enough to give a reconstructed jet. If there are four-jets, one of them is assigned to the fragmentation of the bottom quark. In the latter case we have to consider all possible combinations.

The distributions in the assumed reconstructed top quark mass, $m(jjj)$, is shown in Figs. 3.12 a) and b) for the top signal and the total background. Fig. 3.12 a) gives the mass distributions for three-jet events. Fig. 3.12 b) shows the resulting mass distributions for events containing four-jets. Here, for the top signal ($\bar{t}b$ events) we show separately the mass distribution of the right combination (denoted by $\bar{t}b_R$) and the sum of the wrong combinations (denoted by $\bar{t}b_W$). The right combination is defined to be the distribution of three jet invariant mass where all three jets originate from the $\bar{t}$ decay. For the background we show the sum of all (four) possible combinations in the four-jet case.

We find that the signal peaks at the input mass of 60 GeV, the background is flat but always larger than the signal. Selecting a window in the reconstructed mass we might hope

to improve the signal to background ratio. Taking the window to be $m \in [52, 60]$ GeV the expected total top signal (adding the three- and four-jet cases) is now about 0.02 pb. However, the background still is roughly a factor 10 larger. As discussed earlier, the background is probably overestimated. Also additional cuts might be applied to reduce the background so that the above described method of reconstructing the top quark could be improved. We have explicitly checked that a cut in the total visible hadronic energy squared, W^2_{vis}, does not improve the signal to background ratio. Here W^2_{vis} is defined as the squared hadronic invariant mass as calculated from all neutral and charged particles outside the beam hole.

We emphasize, however, that HERA offers a "simple trick" to substantially reduce the background by switching to positron scattering. The positron probes different quarks in the proton. This not only results in a smaller overall DIS cross section, but also a softer Q^2 distribution, which in turn leads to less gluon radiation. To illustrate what one could gain we show in Figs. 3.12 also the resulting reconstructed mass distribution using a positron beam. Here we have also used Q^2 instead of W^2 as mass scale for the parton radiation. The combined effect reflects mostly the reduction of the DIS cross-section in switching from e^- to e^+ beams, but also the result of changing the scale in the parton shower. We thus conclude that it should be possible to reconstruct the top quark also in its nonleptonic decays allowing the exploration of the $\bar{t}b$ production mechanism. Again, top quark search at HERA will be limited to $m_t < 70$ GeV, unless the machine luminosity and/or energy increases significantly.

4. Charm and Bottom Physics at HERA

We have presented in section 2 the production cross-sections for charm and bottom quarks at HERA, together with some inclusive distributions. In this section we take a closer look at the possible bottom and charm physics that one may expect from experiments at HERA.

4.1 *Energy-angle profiles of charm and bottom jets*

The cross section for charm and bottom quark production at HERA is dominated by the NC process $\gamma g \to Q\bar{Q}$ at $Q^2 = 0$ (real photoproduction). As a consequence the scattered electron in $ep \to eQ\bar{Q}X$ is usually lost in the beam pipe. The scatter plots $\frac{d^2\sigma}{dE_Q d\theta_Q}$ (θ_Q measured w.r.t. beam axis) for the heavy mesons produced in the processes $ep \to ecX \to eDX$ and $ep \to ebX \to eBX$ are shown in Fig. 4.1, from where it is easy to see that the most energetic heavy hadrons are in the proton direction ($\theta_Q = \pi$ ($Q = c, b$)) due to the obviously larger Lorentz boost in this direction. Despite this, there is also a peak near $\theta_Q = 0$, i.e. when the heavy hadron is close to the electron beam direction (Fig. 4.2). This is a consequence of the u-channel contribution in the $\gamma g \to Q\bar{Q}$ process (the peak near $\theta_Q \simeq 180°$ is due to the t-channel contribution in the γg fusion process). Thus, it will pay off if the detectors at HERA are instrumented for heavy flavour physics also in the electron hemisphere. The inclusive energy distributions $\frac{d\sigma}{dE_M}(ep \to eMX)$ for $M = D, B$ mesons at $\sqrt{s} = 314$ GeV are shown in Fig. 4.3. The energy-angle profiles of the charmed meson (D^+), the decay lepton from the semileptonic process $c \to sl^+\nu_l$, and the kaon from both the semileptonic and nonleptonic processes at HERA are shown in Figs. 4.4. The corresponding profiles for the bottom mesons are shown in Figs. 4.5. In order to illustrate the effect of the losses through the beam pipe, we also show the energy distributions with a beam pipe cut of 100 mrad. The resulting energy distributions are shown as shaded areas in Figs. 4.4. and 4.5. Note that the effect of the beam pipe cut is rather drastic. Comparing the distributions in Figs. 4.2-4.5, one sees that the heavy mesons and their decay leptons and kaons have very similar distributions as their parent quark. The effect of large c.m. energy $\sqrt{s} = 314$ GeV and the asymmetric HERA beams are also obvious from these figures. We emphasize in particular the energetic nature of the charmed and bottom hadrons in Figs. 4.4 and 4.5, which show that measurable cross-sections at HERA are expected for charmed and beauty hadrons having Lorentz boosts up to $\gamma_B = 15$, $\gamma_D = 40$ respectively. Consequently, with a good vertex resolution detector one can make use of these characteristics. We assume that such vertex detectors will be available at HERA and study a number of experimental measurements involving heavy hadron track lengths.

4.2 *Charm/bottom separation*

For a variety of experimental measurements, it is necessary to separate charm and bottom events. For exclusive final states, this can be achieved by charm and bottom hadron

Table 4.1: Charm and bottom quark separation using decay leptons and J/Ψ tags

Number of events at $\int L\,dt = 100\,\mathrm{pb}^{-1}$		
signal	$\#c$	$\#b$
muons: $p_\perp \geq 3.0\,\mathrm{GeV}$	8.1×10^3	9.8×10^3
$p_\perp \geq 7.0\,\mathrm{GeV}$	180	420
dileptons: $p_\perp(l_1) \geq 0.8\,\mathrm{GeV}$	4.5×10^5	7.9×10^4
$p_\perp(l_1) \geq 3.0\,\mathrm{GeV}$	4.7×10^3	1.1×10^4
isolated l: $p_\perp \geq 1.0\,\mathrm{GeV}$	9.0×10^5	1.3×10^5
$(E_{acc} \leq 2\,\mathrm{GeV})$ $p_\perp \geq 3.6\,\mathrm{GeV}$	1.2×10^3	9.0×10^3
J/Ψ with $p_\perp(J/\Psi) \geq 5\,\mathrm{GeV}$	-	55

reconstruction. However for the bottom hadrons, experience at e^+e^-machines limits the efficiency of such reconstruction to $O(10^{-3})$ [56]. Hence, more inclusive measures have to be employed. Obvious tags are available for bottom hadrons namely large-p_T leptons from the semileptonic decays $b \to cl\nu_l$ and the decays $B \to J/\Psi X$, which are experimentally found to have a branching ratio $\sim 1.5\%$ [56]. Clearly, the backgrounds in the former method from the much larger charm cross section at HERA and the subsequent semileptonic decay $c \to sl\nu_l$ have to be studied carefully. Also, the direct J/Ψ production from the process $\gamma g \to J/\Psi g$ in the latter case has to be separated. We have already shown the distribution $\frac{d\sigma}{dp_T^l}$ (measured w.r.t. the sphericity and beam axis) from the heavy quark processes $ep \to QX$ in section 2. Here we would like to study the charm/bottom separation in more detail.

The integrated cross-sections for the reaction $ep \to (e,\nu_e)l^\pm X$ as a function of a cut on the p_T of the hardest lepton in the event are displayed in Fig. 4.6, where apart from the NC $b\bar{b}$ and $c\bar{c}$ cases we have also shown the contributions from the NC DIS processes, from the light quarks and gluons (labelled as $q\bar{q} + qg$), the CC process and the $W^-g \to \bar{c}\ s$ final states. It is easy to see that the light-quark background falls off very steeply and is negligible above $p_T^{cut} = 2$ GeV on the lepton. The $b\bar{b}/c\bar{c}$ cross-over occurs at around $p_T^{cut} = 3$ GeV. The suppression of the background as well as $b\bar{b}/c\bar{c}$ separation can be improved by imposing isolation on the hadronic energy accompanying the trigger lepton. The integrated cross-sections $\sigma(ep \to (e,\nu_e)l^\pm X$ with $p_T^l > p_T^{cut}$ and $E_{acc} < 2$ GeV) are shown in Fig. 4.7, from where it is easy to see that the background becomes negligible for $p_T^{cut} > 1$ GeV and the $b\bar{b}/c\bar{c}$ cross-over now occurs at around $p_T^{cut} \simeq 2$ GeV. The expected number of events from the $b\bar{b}$ and $c\bar{c}$ production processes for various p_T^{cut} and E_{acc} values are displayed in Table 4.1 for an integrated luminosity $\int Ldt = 100\ pb^{-1}$. We remark that for $p_T^{cut} = 1$ GeV and $E_{acc} < 2.0$ GeV (isolated large-p_T^l sample) one expects $\sim 10^6\ ep \to ec\bar{c}X \to el^\pm X$ events/($100\ pb^{-1}$). A clean sample of b events is obtained by increasing p_T^{cut} to 3.5 GeV, for which we estimate $\sim O(10^4)\ ep \to eb\bar{b}X \to el^\pm X$ events/$(100\ pb^{-1})$. The dependence of the integrated cross-sections $\sigma(E_{acc} > E_{acc}^{cut})$ on E_{acc}^{cut} for an assumed cut on p_T^l is shown in Fig. 4.8.

Judging from the large observable inclusive lepton cross sections for the charm and bottom

quarks at HERA, we think that these cross sections can be used to test both QCD quantitatively as well as determine the gluon structure function particularly in the low x ($x < 10^{-3}$) region. The estimated $O(10^4)$ tagged bottom events (for $p_T^{cut} > 3.5$ GeV) per $100\ pb^{-1}$ yield a sizeable sample to tag the other bottom meson in the process $ep \to b\bar{b}X$ for detailed b-physics studies like $B - \bar{B}$ oscillations.

There is considerable theoretical interest in the measurements of dileptons cross sections and distributions at HERA. What we have in mind are processes of the variety,

$$\begin{aligned} ep \to\ & e + \underbrace{Q\bar{Q}}\ X \\ & \to\ l^\pm l^\mp X, l^\pm l^\pm X \\ & \quad (Q = c,b,t; l = e,\mu) \end{aligned} \tag{4.1}$$

which, though formally give rise to trileptons in the final state but since the scattered e will be lost in most of the cases, will be measured as dilepton final states. We recall that both the UA1 [2] and ARGUS [19] collaborations were able to measure $B^0 - \bar{B}^0$ mixing in the dilepton final states $p\bar{p} \to l^\pm l^\pm X, l^\pm l^\mp X$ and $e^+e^- \to \Upsilon(4s) \to l^\pm l^\pm X, l^\pm l^\mp X$, respectively. Since $\sigma(ll) = 4\sigma(\mu\mu)$, it will be very important to be able to measure both electrons and muons.

In Fig. 4.9, we plot the cross sections for the dilepton events (4.1) from the charm and bottom quarks as well as from the NC (light quarks) and CC processes, and the $W^\pm g \to \bar{c}s, \bar{c} \to l^- X$. Actually what is shown is $\sigma(p_T^l > p_T^{cut})$ where the cut-off p_T^{cut} refers to the p_T of the hardest lepton. It can be easily seen that the dominant background for the NC (light quarks) is already below the $c\bar{c}$ cross section for $p_T^{cut} > 0.4$ GeV and it falls below the $b\bar{b}$ cross section for $p_T^{cut} > 0.8$ GeV. The $b\bar{b}/c\bar{c}$ cross-over occurs at around $p_T^{cut} = 1.2$ GeV. The expected number of dilepton events for assumed p_T^{cut} values are also given in Table 4.1. We remark that even with a stringent cut-off $p_T^{cut} = 3$ GeV, one expects an inclusive dilepton sample of $\sim 1.5 \times 10^4$ events (with $b\bar{b}/c\bar{c}$ approximately in the ratio 2 : 1). Though this number will definitely go down by the hardware cut on the second lepton, we expect that it will still leave a sizeable number of dilepton events. To get an estimate of this cut, the integrated dilepton cross section $\sigma(p_T^l > p_T^{cut})$ is plotted in Fig. 4.10 against the p_T^{cut} of the second hardest lepton with a cut of $p_T^l > 3$ GeV on the hardest lepton. Thus, for example for $p_T^{l_1} \geq 3$ GeV, $p_T^{l_2} \geq 1$ GeV, one has ~ 10 pb and ~ 30 pb for the dilepton cross section from charm and bottom , respectively. This would give about ~ 1000 dileptons from the $c\bar{c}$ and ~ 3000 dileptons from the $b\bar{b}$ sample for an integrated luminosity of $100\ pb^{-1}$. The inclusive dilepton sample can be enriched in the prompt leptons ($b \to cl\nu_l$) from the $b\bar{b}$ production and decays by imposing an stringent cutoff p_T^{cut} on both leptons, the choice of which will be determined by the experimental conditions. The azimuthal angle distribution $\frac{1}{\sigma}\frac{d\sigma}{d\Phi}(ep \to eb\bar{b}X)$, measured in the transverse plane of the $b\bar{b}$ event, is shown in Fig. 4.11, from where it is obvious that the $b\bar{b}$ (as well as $c\bar{c}$) are produced almost back to back in this plane. Since we have shown that the heavy hadrons (B,D,..) and their decay products have very similar distributions, the azimuthal angle cut can be used on the flavour tags ($l^\pm, K, ...$) themselves.

Another method to tag the B mesons is due to the decay $B \to J/\Psi X$ [56]. Due to their good experimental signatures, J/Ψ tagging has already been used in $p\bar{p}$ collisions successfully [57]. In fact, there is considerable theoretical interest in the decays $B_d \to J/\Psi K_s$, $B_s \to J/\Psi\Phi$ etc. since these exclusive modes are suspected of showing measurable CP violation effects in the asymetry $\frac{\Gamma(B\to J/\Psi K_s)-\Gamma(\bar{B}\to J/\Psi K_s)}{\Gamma(B\to J/\Psi K_s)+\Gamma(\bar{B}\to J/\Psi K_s)}$ [58]

The J/Ψ's, however, can also be produced directly in the process

$$g(p_1) + \gamma(p_2) \rightarrow J/\Psi(p_3) + g(p_4) \tag{4.2}$$

The competing mechanism, which one would like to use for B tagging, is of course

$$\begin{array}{rlll} g(p_1) + \gamma(p_2) \rightarrow & b & \bar{b}X \\ & \rightarrow & J/\Psi X \end{array} \tag{4.3}$$

In Fig. 4.12 we plot the transverse momentum distribution of J/Ψ via the processes (4.2) and (4.3), assuming $BR(B \rightarrow J/\Psi + X) \simeq 1.1\%$ and $\Gamma(J/\Psi \rightarrow e^+e^-) = 4.7$ keV. We see that the direct J/Ψproduction (4.2) overwhelms the B decay mechanism (4.3) for $p_T^{J/\Psi} < 5$ GeV. The total integrated cross sections from the two processes are estimated to be [16,69]

$$\sigma(ep \rightarrow J/\Psi + X) \simeq 3\ nb,\ \sigma(ep \rightarrow B + \bar{B} + X \rightarrow J/\Psi + X) \simeq 90\ pb \tag{4.4}$$

Requiring $p_T^{J/\Psi} > 5$ GeV with 14% branching ratio of $J/\Psi \rightarrow$ leptons we get

$$\sigma(ep \rightarrow B + \bar{B} + X \rightarrow J/\Psi + X,\ p_T^{J/\Psi} > 5GeV).BR(J/\Psi \rightarrow l^+l^-) \simeq 0.55\ pb \tag{4.5}$$

This would then give ~ 55 tagged J/Ψ events for an integrated luminosity of 100 pb^{-1}, which is much lower compared to the rates in Table 4.1 obtained for the jet(s) plus hard lepton and dilepton signals. The separation of the J/Ψ due to B-decays can be improved by requiring the production of non-isolated J/Ψ, which discriminates against the (mostly isolated) J/Ψ from the QCD process (4.2).In that case the cut on the transverse momentum of the J/Ψ can be lowered, by increasing the number of $B \rightarrow J/\Psi\ X$ events by a factor of two or more. The rapidity distributions of the two processes are plotted in Fig. 4.13, which show that a cut on the rapidity will not be very helpful in enriching the $B \rightarrow J/\Psi\ X$ sample. In the case of Υ production the cross section for the process

$$\gamma + g \rightarrow \Upsilon + g \tag{4.6}$$

is estimated to be $\simeq 6.3$ pb [16,69]. With $BR(\Upsilon \rightarrow e^+e^-/\mu^+\mu^-) = 0.056$, one obtains

$$\sigma(ep \rightarrow \Upsilon + X)BR(\Upsilon \rightarrow e^+e^-/\mu^+\mu^-) \simeq 0.35\ pb \tag{4.7}$$

Thus, one expects $\simeq 35\Upsilon$ events with a luminosity of 100 pb^{-1}. In Fig. 4.14 we show the dilepton invariant mass distribution $\frac{d\sigma}{dm_{\mu\mu}}(ep \rightarrow e(\mu^+\mu^-)X)$ at HERA for $\sqrt{s} = 314$ GeV, based on the processes (4.1), (4.2) and (4.6). The distribution for J/Ψ and Υ shown in Fig. 4.14 are obtained by folding a Gaussian experimental resolution of $\Delta m_{\mu\mu} = 50$ MeV.

We conclude that by combining the three methods described here and using intelligent cuts, a sample of several thousand $B\bar{B}$ events can be isolated at HERA for an integrated luminosity of 100 pb^{-1}. In particular, we emphasize that $b\bar{b}$ production but not $c\bar{c}$ production yield same sign dileptons. For the $l^{\pm}l^{\pm}X$ case the p_T^{cut} on the leptons can be lowered to a value below 1 GeV, for which the number of dileptons from the light quark background can be practically eliminated. The information on the bottom sector from these measurements at HERA is therefore expected to be comparable and somewhat complementary to the one obtained from the existing $p\bar{p}$ data. However, heavy flavour tagging can be enormously improved combining vertex detection and particle identification, a feature which has not yet been exploited by the collider experiments. In fact, time dependent measurements of the B decays have not yet been studied anywhere so far. This, in principle, is possible at HERA.

4.3 *Measuring the Cabibbo-Kobayashi-Maskawa angles at HERA*

At first sight the CC processes offer a natural means to measure the CKM matrix elements. The lowest order CC process is shown in Fig. 2.1. The CC cross-sections are usually written in the form [14,15]

$$\frac{d\sigma}{dxdy}(ep \rightarrow \nu_e QX) = \frac{G_F^2 s}{\pi} \frac{1}{(1 + \frac{Q^2}{m_W^2})^2} x \sum_{i,j} \{q_i(x)|V_{ij}|^2 + (1-y)^2 \bar{q}_i(x)|V_{ij}|^2\} \tag{4.8}$$

where the sum i is over the charge $+\frac{2}{3}$ quarks and $+\frac{1}{3}$ antiquarks, with q_i and $\bar{q}_i$ being the corresponding quark and antiquark densities, respectively, inside the proton. Since, only heavy quarks $Q = c, b, t$ have a useful tag, we shall concentrate only on those final states which have a heavy quark. It is then trivial to see that the only non-zero transitions in (4.8) (in the Born approximation) are as follows:

$$\begin{aligned} \sigma(e^-p \rightarrow \nu_e \bar{c}X) &\propto \bar{b}(x)|V_{cb}|^2 + \bar{s}(x)|V_{cs}|^2 + \bar{d}(x)|V_{cd}|^2 \\ \sigma(e^-p \rightarrow \nu_e \bar{t}X) &\propto \bar{b}(x)|V_{tb}|^2 + \bar{s}(x)|V_{ts}|^2 + \bar{d}(x)|V_{td}|^2 \\ \sigma(e^-p \rightarrow \nu_e \bar{b}X) &\propto u(x)|V_{bu}|^2 + c(x)|V_{bc}|^2 + t(x)|V_{bt}|^2 \end{aligned} \tag{4.9}$$

The CKM matrix elements $|V_{ij}|$ appearing in (4.9) are only partly known. The matrix elements involving top quark V_{ti} $(i = b, s, d)$ and V_{bu} are the main objects of interest in future experiments. The inclusive CC cross section at HERA by itself is very small as can be seen in Fig. 4.6 (see also Table 3.1). Judging from the orders of magnitude larger cross-sections for the BGF process $\gamma g \rightarrow Q\bar{Q}$ $(Q = c, b, t)$ we find that the prospects for extracting quantitatively new information on the matrix elements V_{ij} from CC processes at HERA are rather dim. We shall, therefore, investigate below whether detailed studies of the final states in the heavy flavour NC processes $\gamma g \rightarrow Q\bar{Q}X$ could provide new information on V_{ij}.

There are two ways in which information on the matrix elements of interest namely V_{ti} $(i = b, s, d)$and V_{bu} may be obtained from experiments at HERA. They can be categorized as direct and indirect measurements. The direct measurements of the charmless final states in B decays, namely $b \rightarrow u\bar{u}d$ and $b \rightarrow ul^-\bar{\nu}_l$, are observable as specific final states $B \rightarrow \pi\pi$, $\rho\pi$, $p\bar{p}\pi$,... and through the larger tail in the inclusive measurements of the lepton transverse energy spectrum, measured with respect to the b-jet axis. The possibility of similar direct measurements of the matrix elements V_{ti} can already be ruled out for experiments at HERA, in view of the tiny inclusive top quark cross section presented in previous sections. Indirect measurements of these matrix elements V_{ti} are, however, possible if one is able to measure experimentally the quantities $x_d(= \frac{\Delta M}{\Gamma})_{B_d}$ and $x_s(= \frac{\Delta M}{\Gamma})_{B_s}$ relevant for $B^0 - \bar{B}^0$ mixings. We shall discuss the present status of x_d and x_s and possible measurements of these quantities at HERA in the next subsection. Here we would like to briefly review the present status and the prospects of the measurements of the ratio $\frac{V_{bu}}{V_{bc}}$ and hence of V_{bu} at HERA.

The present information on the matrix element V_{bc} and V_{bu} are summarized below. One set of constraints on these matrix elements is obtained from the average lifetime measurement of the bottom hadrons and the average B-hadron semileptonic branching ratios. The present world average of $< \tau_B >$and $< BR(B \rightarrow lX) >$ are [27]

$$\begin{aligned} < \tau_B > &= (1.11 \pm 0.16) \times 10^{-12} sec \\ < BR(B \rightarrow lX) > &= (10.5 \pm 0.6 \pm 0.6)\% \end{aligned} \tag{4.10}$$

These two measurements can be combined to yield weighted average of $|V_{bu}|^2$ and $|V_{bc}|^2$. For example, in the free quark decay model one gets [36]

$$\Gamma_{SL}(B \to lX) = \frac{BR(B \to lX)}{\tau_B} = \frac{G_F^2 m_b^5}{192\pi^3}(0.86|V_{bu}|^2 + 0.48|V_{cb}|^2) \tag{4.11}$$

Eqs. 4.10 and 4.11 then give

$$(0.86|V_{bu}|^2 + 0.48|V_{cb}|^2) = 0.0010 \pm 0.0003 \tag{4.12}$$

where the error also includes uncertainties due to the b-quark mass. The other piece of information comes from the experimental upper limit on the ratio $\bar{R} \equiv \frac{\Gamma(b\to ul\nu_l)}{\Gamma(b\to cl\nu_l)}$ which can be expressed as (again using the free quark model)

$$\left|\frac{V_{bu}}{V_{bc}}\right|^2 = 0.55\bar{R} \tag{4.13}$$

Present experimental bounds on $\bar{R}$ (though somewhat model dependent) give [27]

$$\left|\frac{V_{bu}}{V_{bc}}\right| < 0.17 \tag{4.14}$$

Eqs. (4.12) and (4.14) give the constraints on V_{ub} (upper bound) and V_{cb} . The lower bound on V_{ub} shown in Fig. 4.15 is from the recent measurements of the charmless B decays by the ARGUS collaboration [59]:

$$BR(B_u^{\pm} \to p\bar{p}\pi^{\pm}) = (5.2 \pm 1.4 \pm 1.9) \times 10^{-4}$$

$$BR(B_d^0 \to p\bar{p}\pi^+\pi^-) = (6.0 \pm 2.0 \pm 2.2) \times 10^{-4} \tag{4.15}$$

These branching ratios can in principle be converted into measurements of the CKM ratio $\frac{V_{bu}}{V_{bc}}$. In practice, the model dependence is considerable. A plausible (though by no means conclusive) lower bound can be obtained from the phase space arguments and the usually quoted bound is [27,56]:

$$|\frac{V_{bu}}{V_{bc}}| > 0.07 \tag{4.16}$$

This would then give

$$V_{bc} = 0.045 \pm 0.07, \quad 0.004 < |V_{ub}| < 0.008 \tag{4.17}$$

The bounds in Eq. (4.17) can also be expressed in terms of the experimental quantity of interest $\bar{R}$. One expects (using Eq. (4.13) and $0.07 < |\frac{V_{bu}}{V_{bc}}| < 0.17$) that in the free quark decay model $\bar{R}$ is bounded by the present data in the range

$$0.01 < \bar{R} < 0.05 \tag{4.18}$$

Taking into account various B decay models en vogue a reasonably reliable range for $\bar{R}$ is [27,56]

$$0.01 < \bar{R} < 0.08 \tag{4.19}$$

So, the question is if $\bar{R}$ in the range (4.19) can be measured at HERA given the b-jet profile and rates discussed earlier.

We discuss below the attempts at measuring $\bar{R}$ at HERA. Clearly, the lepton energy spectrum is not the appropriate quantity due to its dependence on the structure functions in the process $ep \to ebX \to el^{\pm}X$. Instead, one should concentrate on the distribution $\frac{d\sigma}{dp_T^l}$, where e.g. the p_T^l is measured w.r.t. the jet axis. The normalized distribution $\frac{1}{\sigma}\frac{d\sigma}{dp_T^l}$ for the process $ep \to eb\bar{b}X$ with $b \to cl\nu_l$ and $ep \to eb\bar{b}X$ with $b \to ul\nu_l$ are shown in Fig. 4.16, where the complete chain of production, fragmentation and decays were generated using the Monte Carlo programme AROMA [30]. The relative normalization of the two curves is given by $\bar{R}$ (see (4.19) for the present bounds). The considerably longer tail of the p_T^l distribution is due to the transverse momentum of bottom hadrons but more importantly from gluon bremsstrahlung giving rise to $ep \to b\bar{b} + ng + X$, thereby making the determination of the jet axis more difficult. The much larger tail in the p_T^l distributions can be reduced by a more stringent selection of events, for example by selecting back to back jets in the transverse plane. Thus, it seems to us that unless $\bar{R} \geq 0.05$, and the jet profiles are well understood, this method may not give a very definitive result on $|\frac{V_{bu}}{V_{bc}}|$.

We hasten to add that measuring $\bar{R}$ is very probably not the only possibility of measuring $|\frac{V_{bu}}{V_{bc}}|$. In fact, if the ratio $|\frac{V_{bu}}{V_{bc}}|$ lies in the range (4.19) then a lot of two-body and quasi two-body decays of the B mesons should have branching ratios in the vicinity of their present upper bounds [56]. Thus, for any channel X with $BR(B \to X) \simeq 10^{-4}$ one expects $\approx 2 \times 4 \times 10^5 \times 100 \times 10^{-4} \simeq 80$ events for an integrated luminosity of 100 pb^{-1}. We have investigated the case of $B \to \pi\pi$, for which, however, the combinatoric background from the usual processes at HERA is so large that a straight forward search for the bump in the dipion invariant mass is not likely to detect the $B \to \pi\pi$ contribution. The background can be reduced by selective cuts. We exemplify the differences in the topologies of the b-quark jet in which the B-meson is decaying into a two-body mode, like $B_d \to \pi^+\pi^-$, and of the process $ep \to eQ\bar{Q}X$ (Q=c,b) followed by the usual decays of the b and c quarks. The $p_\perp(\pi^+\pi^-)$ distribution of the $\pi^+\pi^-$ pair from $b \to BX$ with $B \to \pi\pi$ and the background are shown in Fig. 4.17. Note the considerable softer nature of the background as compared to the $p_\perp$ distribution from the $B \to \pi\pi$ decay sample. The latter follows the $p_\perp$ distribution of the B meson in the process $ep \to eBX$, as expected. Thus, using a cut $p_\perp \geq 10$ GeV brings down the background to the level of the $B \to \pi^+\pi^-$ sample.

Another difference is expected to show up in the energy distribution of the hadrons accompanying the $\pi^+\pi^-$ pair. Note that because of the harder $b \to B$ fragmentation, one expects the $\pi^+\pi^-$ pair to be relatively isolated in the decay $B \to \pi^+\pi^-$, as compared to the one from background processes. Conversely, the $\pi^+\pi^-$ pair from the decay $B \to \pi^+\pi^-$ is expected to follow the b quark fragmentation, as opposed to the pair from jet fragments and the dominant weak decays of the charmed and bottom hadrons. Selecting the $\pi^+\pi^-$ pair in a jet, we show the resulting distributions in the scaled variable $z = \frac{E(\pi^+\pi^-)}{E_{jet}}$ in Fig. 4.18. This shows that a cut on z, say $z > 0.8$, would bring the background below the $B \to \pi^+\pi^-$ sample. One should stress here that a rejection of the dominant background due to the CKM allowed decay $b \to c \to (s,d)$ can also be improved by combining the cuts mentioned above with the information from the vertex reconstruction. We recall that the $b \to u$ transition will involve just one decay vertex as opposed to the $b \to c \to (s,d)$ transition, which will involve two decay vertices due to the bottom and subsequent charm decays.

The background can also be reduced by restricting the data sample to jets containing a large p_T lepton, for which one has only to consider the background from the NC processes $ep \to ec\bar{c}X \to el^{\pm} + jet + X$, and $ep \to eb\bar{b}X \to el^{\pm} + jet + X$ with $b \to cX$. However, in

this case the $B \to \pi\pi$ event sample is reduced also; one expects only $\sim 5B \to \pi\pi$ events for $L = 100\ pb^{-1}$, $BR(B \to \pi\pi) = 10^{-4}$ and an assumed efficiency of 5% for tagging the lepton from the decay $b \to l^{\pm}X$. The signal can be enhanced by summing over a large number of two-body (or quasi two-body) decay modes. Thus, it seems to us that measuring the matrix element $|\frac{V_{ub}}{V_{bc}}|$ from the exclusive B decay mode $B \to \pi\pi$ at HERA is feasible but requires more work. We have not investigated other exclusive channels in B decays. We conclude that whereas the inclusive branching ratio $BR(b \to uX)$ may eventually turn out to be as large as $(5-8)\%$, the prospects of measuring $|\frac{V_{ub}}{V_{bc}}|$ in a "clean mode" at HERA depend on particle identification and vertex reconstruction. It is conceivable that there are other decay modes like (4.15), with large branching ratios and moderate background. It is difficult to be specific here but the rather large number of B events expected at HERA demands a broad search. We hope to report on this in a future publication [60].

4.4 $B^0 - \bar{B}^0$ Mixings : present status

In this section we take up the question of measuring the quantities x_d and x_s related to $B^0 - \bar{B}^0$ mixings in the $B_d^0 - \bar{B}_d^0$ and $B_s^0 - \bar{B}_s^0$ sector, respectively. These quantities are usually calculated in the standard model by the box diagrams [22]

$$x_d = \frac{\Delta M}{\Gamma}(B_d^{(1)} - B_d^{(2)}) = C_d \frac{m_t^2}{m_W^2} F(\frac{m_t^2}{m_W^2})|V_{td}^* V_{tb}|^2 \tag{4.20}$$

$$x_s = \frac{\Delta M}{\Gamma}(B_s^{(1)} - B_s^{(2)}) = C_s \frac{m_t^2}{m_W^2} F(\frac{m_t^2}{m_W^2})|V_{ts}^* V_{tb}|^2 \tag{4.21}$$

where the various quantities C_d, C_s and $F(x)$ are defined as follows

$$C_d = \frac{G_F^2 m_{B_d}}{6\pi^2} m_W^2 (B_d f_{B_d}^2) \eta_{QCD} \tau_{B_d} \tag{4.22}$$

$$C_s = \frac{G_F^2 m_{B_s}}{6\pi^2} m_W^2 (B_s f_{B_s}^2) \eta_{QCD} \tau_{B_s} \tag{4.23}$$

$$F(x) = \frac{1}{4} + \frac{9}{4(1-x)} - \frac{3}{2}\frac{1}{(1-x)^2} - \frac{3}{2}\frac{x^2 ln x}{(1-x)} \tag{4.24}$$

with the QCD correction factor $\eta_{QCD} \simeq 0.85$ (calculated in the approximation $m_t < m_W$) and the coupling constant products $B_d f_{B_d}^2$ and $B_s f_{B_s}^2$ expected to lie in the range $(0.1-0.2)\ GeV^2$.

Knowing x_d, x_s and m_t experimentally, one can determine the matrix elements $|V_{td}^* V_{tb}|$ and $|V_{ts}^* V_{tb}|$ assuming $B f_B^2$. An m_t-independent, and otherwise also less model dependent, quantity is the ratio[21]

$$\frac{x_s}{x_d} = |\frac{V_{ts}}{V_{td}}|^2 (1+\delta) \tag{4.25}$$

where

$$\delta = (\frac{m_{B_s} f_{B_s}^2}{m_{B_d} f_{B_d}^2} - 1) \geq 0 \tag{4.26}$$

Measurement of $\frac{x_s}{x_d}$ is then essentially equivalent to the measurement of the V_{CKM} ratio $|\frac{V_{ts}}{V_{td}}|^2$.

Estimates of C_d and C_s abound in the literature [61]. For $B f_{B_d}^2 = 0.15 \pm 0.05 GeV^2$ one obtains [22]

$$C_d = (0.24^{+0.33}_{-0.17}) \times 10^4 \tag{4.27}$$

with C_s somewhat larger. The lifetime difference $y_d = \frac{\Delta\Gamma}{\Gamma}(B_d^{(1)} - B_d^{(2)})$ and $y_s = \frac{\Delta\Gamma}{\Gamma}(B_s^{(1)} - B_s^{(2)})$ are expected to be very small [62] and hence we shall neglect them in subsequent discussions.

Turning to the discussion of the present status of $B^0 - \bar{B}^0$ mixings in e^+e^- and $p\bar{p}$ collisions, we recall that there are essentially two methods that have been employed in the experimental measurements undertaken so far. The first depends on the measurement of the cross sections at $\Upsilon(4S)$

$$\Upsilon(4S) \to B_d^0 B_d^0, \bar{B}_d^0 \bar{B}_d^0, B_d^0 \bar{B}_d^0 \tag{4.28}$$

The ratio of the cross sections

$$Y_d \equiv \frac{\sigma(B_d^0 B_d^0) + \sigma(\bar{B}_d^0 \bar{B}_d^0)}{\sigma(B_d^0 \bar{B}_d^0)} \tag{4.29}$$

can be expressed as (on the $\Upsilon(4S)$ alone)

$$Y_d = r_d = \frac{x_d^2 + y_d^2}{2 + x_d^2 - y_d^2} \simeq \frac{x_d^2}{2 + x_d^2} \tag{4.30}$$

where $r_d = \frac{P(B \to \bar{B})}{P(B \to B)}$ is the ratio of the time integrated probabilities.

What has actually been measured are the same-sign and opposite-sign dilepton cross-sections from the process $\Upsilon \to (B\bar{B}, BB, \bar{B}\bar{B}) \to l^+l^-X, l^{\pm}l^{\pm}X$. The ARGUS Collaboration has measured r_d to be [19]

$$r_d = 0.21 \pm 0.08 \tag{4.31}$$

which corresponds to

$$x_d = 0.74^{+0.17}_{-0.19} \tag{4.32}$$

The present 90% $C.L.$ upper limit on r_d from CLEO is [20]

$$r_d \leq 0.24 \tag{4.33}$$

giving $x_d \leq 0.78$. Thus, the present 90% $C.L.$ bounds on r_d and x_d are

$$0.09 \leq r_d \leq 0.24 \tag{4.34}$$

$$0.44 \leq x_d \leq 0.78 \tag{4.35}$$

The measurements of $B - \bar{B}$ mixings have also been done in e^+e^- and $p\bar{p}$ collisions above the Υ-resonance region. Here, the relationship between Y_d and r_d is more complicated. A particularly useful quantity to use in such measurements is [63]

$$\chi = \chi_d P_d + \chi_s P_s \tag{4.36}$$

where

$$\chi_{d,s} = \frac{Prob(B_{d,s}^0 \to \bar{B}_{d,s}^0)}{Prob(B_{d,s}^0 \to all)} = \frac{r_{d,s}}{1 + r_{d,s}} \tag{4.37}$$

with P_d (P_s) being the probability of finding a B_d (B_s) meson in the decay of a b quark. In the continuum where the B and $\bar{B}$ are produced incoherently, it is easy to show that for the lepton pairs from $b\bar{b}$ production and primary semileptonic decays the following relation holds,

$$\frac{\sigma(l^+l^+) + \sigma(l^-l^-)}{\sigma(l^+l^-)} = \frac{2\chi(1-\chi)}{\chi^2 + (1-\chi)^2} \tag{4.38}$$

The present experimental status of the UA1 and MARK II results can be summarized in terms of χ as follows

$$\chi = 0.121 \pm 0.047 \tag{4.39}$$

$$\chi \geq 0.065(90\%\ C.L.) \tag{4.40}$$

from the UA1 results at the CERN $p\bar{p}$ collider at $\sqrt{s} = 546$ GeV [2] and

$$\chi \leq 0.12(90\%\ C.L.) \tag{4.41}$$

from the MARK II data on e^+e^- annihilations at $\sqrt{s} = 29$ GeV [63].

The present experimental 90% $C.L.$ upper and lower bounds on χ_d and χ_s (equivalently r_d and r_s) following from Eqs. (4.35), (4.36), (4.40) and (4.41) are shown in Fig. 4.19a) for the choice $P_d = 0.375$ and $P_s = 0.15$. It shows that χ_s (or r_s) is essentially unconstrained from the present experimental data. On the other hand a lower bound on x_s can be obtained from the experimental determination of x_d and the unitarity relation (4.25) obtained in the standard three-family model. We recall that in the standard three-family model one expects

$$|V_{ts}| \simeq |V_{tb}| \simeq 0.045 \pm 0.007 \tag{4.42}$$

The matrix element $|V_{td}|$ is bounded from above by unitarity $|V_{td}| \leq 0.024$ and from below by the measurement of x_d. This latter constraint can be seen from Fig. 4.20 where the 90% $C.L.$ lower bound ($x_d \geq 0.44$) is used to constrain $|V_{td}|$ as a function of m_t, given $Bf_{B_d}^2$. This gives (for $m_t \leq 180$ GeV, and $f_B f_{B_d}^2 \leq 0.2\ GeV^2$)

$$|V_{td}| \geq 0.006 \tag{4.43}$$

Thus, in the standard CKM model one finds [22]

$$0.006 \leq |V_{td}| \leq 0.024$$

$$2 \leq |\frac{V_{ts}}{V_{td}}| \leq 8 \tag{4.44}$$

Combining (4.25), (4.35) and (4.44) one expects x_s to lie in the range

$$2 \leq x_s \leq 60 \tag{4.45}$$

The unitarity constraint in the CKM model on χ_s are shown in Fig. 4.19b) [22], giving $0.4 \leq \chi_s \leq 0.5$. Since

$$\chi_s = \frac{x_s^2}{2(1+x_s^2)} \to 0.5\ when\ x_s \gg 1 \tag{4.46}$$

the sensitivity of χ_s on x_s is very quickly lost as x_s increases above 2. Thus, it may become essential to determine x_s from time dependent measurements, where the experimental measures depend linearly on x_s (in contrast to the time integrated measure χ). We turn to the investigation of this point in the next subsection.

4.5 *Measuring x_d and x_s at HERA*

We briefly recall here the formalism for time dependent oscillations. Defining the definite flavour meson states produced at $t = 0$ by

$$|M^0> \equiv |M^0(t=0)> \tag{4.47}$$

$$|\bar{M}^0> \equiv |\bar{M}^0(t=0)> \tag{4.48}$$

the time evolution equations in the presence of mixing are given by

$$|M^0(t)> = f_+(t)|M^0> + \eta_{CP} f_-(t)|\bar{M}^0> \tag{4.49}$$

$$|\bar{M}^0(t)> = f_+(t)|\bar{M}^0> + \eta_{CP}^{-1} f_-(t)|M^0> \tag{4.50}$$

with the amplitudes $f_\pm(t)$ given by

$$f_\pm = \frac{1}{2} e^{-imt}\{e^{-\frac{1}{2}(\Gamma_1 + i\Delta m)t} \pm e^{-\frac{1}{2}(\Gamma_2 - i\Delta m)t}\} \tag{4.51}$$

which in the approximation $\Gamma_1 \sim \Gamma_2 = \Gamma$ become

$$f_+(t) = e^{-imt} e^{-\frac{t\Gamma}{2}} cos(\frac{\Delta m t}{2}) \tag{4.52}$$

$$f_-(t) = e^{-imt} e^{-\frac{t\Gamma}{2}} sin(\frac{\Delta m t}{2}) \tag{4.53}$$

Expressions (4.52) and (4.53) are supposed to be valid for $B^0 - \bar{B}^0$ mixings. It is straightforward to calculate the following differential (in time) probabilities

$$N\frac{dP}{dt}(M^0 \to M^0) = \bar{N}\frac{dP}{dt}(\bar{M}^0 \to \bar{M}^0) = |f_+(t)|^2 \tag{4.54}$$

$$N\frac{dP}{dt}(M^0 \to \bar{M}^0) = |\eta^{CP}|^2 |f_-(t)|^2 \tag{4.55}$$

$$\bar{N}\frac{dP}{dt}(\bar{M}^0 \to M^0) = |\eta^{CP}|^{-2} |f_-(t)|^2 \tag{4.56}$$

where

$$|f_+(t)|^2 = e^{-t\Gamma} cos^2 \frac{\Delta m t}{2} \tag{4.57}$$

$$|f_-(t)|^2 = e^{-t\Gamma} sin^2 \frac{\Delta m t}{2} \tag{4.58}$$

N and $\bar{N}$ are normalization constants to ensure conservation of probability. Integrating over (4.54)-(4.56) one obtains the usual relations [64]

$$r_M = \frac{P(M^0 \to \bar{M}^0)}{P(M^0 \to M^0)} = |\eta_{CP}|^2 \frac{x^2 + y^2}{2 + x^2 - y^2} \sim |\eta_{CP}|^2 \frac{x^2}{2 + x^2} \tag{4.59}$$

with

$$\frac{\bar{r}_M}{r_M} = |\eta_{CP}|^{-4} \tag{4.60}$$

In what follows we shall ignore CP violation (i.e. set $\eta_{CP} = 1$). Eqs. (4.54-4.56) then reduce to the simple form

$$\tau\frac{dP}{dt}(M^0 \to M^0) = \tau\frac{dP}{dt}(\bar{M}^0 \to \bar{M}^0) = e^{-\frac{t}{\tau}}cos^2\omega t \tag{4.61}$$

$$\tau\frac{dP}{dt}(M^0 \to \bar{M}^0) = \tau\frac{dP}{dt}(\bar{M}^0 \to M^0) = e^{-\frac{t}{\tau}}sin^2\omega t \tag{4.62}$$

where $\omega = \frac{x}{2\tau}$ and $x = \frac{\Delta M}{\Gamma}$. The oscillation period is then given by

$$T_{osc} = \frac{\pi}{\omega} = \frac{2\pi\tau}{x} \tag{4.63}$$

The oscillation length, λ_{osc}, depends on the Lorentzt boost factors β and γ

$$\lambda_{osc} = \beta\gamma c T_{osc} = \beta\gamma\frac{2\pi}{x}. < \lambda >\simeq \frac{2\pi}{x}\beta\gamma(0.3mm) \tag{4.64}$$

where we have indicated the expected average mean free path for B mesons $< \lambda >= c\tau$. The oscillation time and length are inversely proportional to x (as opposed to the quadratic dependence of χ on x) and hence their measurements provide, at least in principle, a more sensitive method of measuring x_d and x_s. In Figs. 4.21 and 4.22 we plot the functions $|f_+(t)|^2$ and $|f_-(t)|^2$, respectively, for $x = 0.5$ (relevant for mixing in the B_d sector) and $x = 5, 10$ as illustration for x_s. Also shown is the exponential decay of a particle, $e^{-\frac{t}{\tau}}$, which does not mix, for example $B_u^{\pm}$.

It is evident from Figs. 4.21 and 4.22 that measuring the departure of $|f_+(t)|^2$ for the B_d^0 system from an exponential will require a very large number of bottom events, though the buildup of $|f_-(t)|^2$ from zero should be measurable. On the other hand, the oscillation period for B_s is much smaller. As an example, for $x_s \simeq 2\pi$, $T_{osc} \simeq 1ps$. Thus, the two oscillation times are very different and, in principle, they can be extracted from data in a model independent way. This is to be contrasted with the time integrated measure χ from which χ_d and χ_s can only be extracted if the parameters P_s and P_d are known. On the other hand, measuring the oscillation time of $O(1Ps)$ directly is not possible. What actually will be measured are oscillation lengths. Knowing the momentum of the B-hadron, this however, can be converted into the time distribution to be compared with the theoretical expectations, shown in Figs. 4.21 and 4.22.

The oscillation lengths themselves can be obtained by convoluting the functions $|f_\pm|^2$ with the energy distribution of the B hadrons. We have calculated them for the process $ep \to eb\bar{b}X$ using the Monte Carlo programme AROMA [30] at $\sqrt{s} = 314$ GeV. The decay length distributions $\frac{d\sigma}{dl}(ep \to eb\bar{b}X \to B_iX)$ are shown in Fig. 4.23 ($B_d^0 \to B_d^0, x_d = 0.5$), Fig. 4.24 ($B_d^0 \to \bar{B}_d^0, x_d = 0.5$), Fig. 4.25 ($B_s^0 \to B_s^0, x_s = 5.0$), Fig. 4.26 ($B_s^0 \to \bar{B}_s^0, x_s = 5.0$), Fig. 4.27 ($B_s^0 \to B_s^0, x_s = 10.0$), and Fig. 4.28 ($B_s^0 \to \bar{B}_s^0, x_s = 10.0$). They have been obtained by fixing the flavour of the other $\bar{b}$ quark in the Monte Carlo event generator. This, for example, can be done in an experiment by demanding $\bar{b} \to l^+X$ in the jet recoiling against the B hadron whose track lengths are being measured. In order to avoid confusion we state here that the cross-sections shown in Figs. 4.23–4.28 do not take into account any tagging efficiencies. The oscillation lengths are obtained by projecting out the B-hadrons in the energy bins indicated on the figures. This projection is essential, since otherwise the oscillations (which linearly depend on E_B) are smeared by E_B distributions and are not discernible from

Table 4.2: Oscillation lengths for the indicated values of the Lorentz factor γ and the mixing parameter $x = \frac{\Delta M}{\Gamma}$

γ	$x = 0.5$	$x = 5.0$	$x = 10.0$	$x = 20$
$\gamma = 2$	$7.5mm$	$0.75mm$	$0.376mm$	$0.188mm$
$\gamma = 5$	$18.8mm$	$1.88mm$	$0.942mm$	$0.471mm$
$\gamma = 10$	$37.6mm$	$3.76mm$	$1.88mm$	$0.942mm$

the background which is exemplified by the distribution $\frac{d\sigma}{dl}(ep \to eb\bar{b}X \to B^{\pm}X)$ in Fig. 4.29. The resulting oscillation lengths are shown in Table 4.2.

A number of remarks are in order about Figs. 4.22-4.29. As already pointed out earlier, the deviation of $\frac{d\sigma}{dl}(ep \to B_dX)$ from an exponential for the "right-sign meson" $B_d \to B_d$ case is probably difficult to measure at HERA. The eagle shape structure in Fig. 4.23 shows itself at too low a cross-section to be measurable, particularly if one takes into account the necessary condition that the other B hadron be definitely flavour tagged, for which the efficiency is not going to be much larger than a few per cent. The yield $\frac{d\sigma}{dl}(ep \to \bar{B}_dX)$ with "wrong-sign meson" $B_d \to \bar{B}_d$ shown in Fig. 4.24 may, however be measurable at HERA. The oscillation structure of the B_s meson in both the "right-sign meson" distribution $\frac{d\sigma}{dl}(ep \to B_sX)$ with $B_s \to B_s$ and the "wrong-sign meson" distribution $\frac{d\sigma}{dl}(ep \to \bar{B}_sX)$ with $B_s \to \bar{B}_s$ is clearly visible as shown in Figs. 4.25 and 4.26 ,respectively, for $x_s = 5$. The oscillation length decreases linearly in going from $x_s = 5$ to $x_s = 10$, which can be seen by comparing Figs. 4.27 and 4.28.

It is suggestive from these results that as far as the "right-sign" distributions $\frac{d\sigma}{dl}(ep \to BX)$ with $B \to B$ are concerned, all of them, except for the $B_s \to B_s$ case, are almost exponential in the visible cross-section region. Thus, one could parametrize the background in the limit case $x = 0$ and subtract it from the inclusive distribution $\frac{d\sigma}{dl}(ep \to BX)$ for the "right-sign" transition $B \to B$. The resulting signals showing clear oscillations for the $B_s \to B_s$ case are given in Figs. 4.30 and 4.31 for $x_s = 5$ and $x_s = 10$ respectively. That these oscillations are not washed out if one convolutes the decay length distribution with a vertex detector resolution of say $\sigma_V \sim 100\mu m$ and furthermore takes into account beam pipe acceptance cut of 100 mrad is shown in Fig. 4.32. Thus, it seems to us that experiments at HERA which have a good vertex resolution and are capable of hadron momentum measurements are well suited for measuring x_s.

Finally we show in Fig. 4.33 the time integrated dilepton ratio

$$R(\frac{\pm\pm}{+-}) = \frac{\sigma(l^+l^+) + \sigma(l^-l^-)}{\sigma(l^+l^-)} \tag{4.65}$$

at HERA as a function of χ_s. The contributions to $R(\frac{\pm\pm}{+-})$ arise from the heavy quark processes shown in Eq. 4.1. The analysis was performed as follows [65]. We started by selecting 2-jet events using the standard cluster algorithm, satisfying $E_T > 20$ GeV. We then selected those

2-jet events with dileptons in them, having $p_T^l > 1.2$ GeV, measured with respect to the jet axis and in the back-to-back configuration in the azimuthal plane $\pi > \phi_{JJ} > \pi - 10°$. The acceptance was taken into account by demanding a 100 mrad beam pipe cut. The cuts reduced the background from light quarks and gluons and from the DIS NC processes, as well as from $c\bar{c}$ and $c\bar{s}$ production. Mixing in the $B_d - \bar{B}_d$ sector was incorporated using $\chi_d = 0.15$, consistent with present measurements. In addition, we assumed $P_d = 0.375$ and $P_s = 0.15$, which are the expected values for these parameters.

We have calculated the statistical accuracy $\Delta\chi_s/\chi_s$ at HERA for an integrated luminosity of 200 pb^{-1} and find it to be 7%. The theoretical uncertainty on χ_s is, however, bigger since as we have pointed out earlier, the ratio $R(\frac{\pm\pm}{+-})$ is a measure of $\chi = P_d\chi_d + P_s\chi_s$. Extracting χ_s from a measurement of χ needs P_d and P_s (assuming that χ_d will have been determined by that time). The uncertainty on P_s is at least 25%. So, the error on χ_s will be dominated by theoretical uncertainty on P_s.

In any case, it should be possible for HERA experiments to measure the ratio R in Eq. (4.65) with a higher accuracy than the present $p\bar{p}$ and e^+e^- experiments. We have discussed this already in the section on charm and bottom separation and will not elaborate on this point again.

5. Summary and Conclusions

We have discussed some aspects of heavy flavour production at HERA. The cross-sections and relevant distributions were all based on perturbative QCD, including the BGF mechanism. We recall that the comparisons of present data for low energy charm photoproduction with the predictions of the BGF mechanism are not conclusive [13,35]. Experiments at HERA will be able to measure this cross-section well. It may turn out that at HERA energies the inclusive charm cross-section is somewhat underestimated by the boson gluon fusion mechanism. The charmed hadron yield at large p_T ($p_T^c > a\ few\ GeV$) should be reliably calculable in the framework discussed here, though we do expect additional higher twist contributions at small p_T and large x_F for charm production which we have not quantified. However, since these contributions are essentially power corrections, their importance for bottom and top quark production is not expected to be significant and hence the estimates based on the BGF mechanism for bottom and top quark production at HERA presented here should be reliable, for all values of p_T and x_F.

The BGF mechanism predicts $O(10^8), O(10^6)$ and $O(30)$ events for inclusive charm, bottom and top quark ($m_t = 60\ GeV$) production at HERA, respectively, for an integrated luminosity of 100 pb^{-1} expected per year. Taking into account the experimental acceptance of HERA detectors, a substantial fraction of these events will be measurable. The interest in heavy flavour studies at HERA is manifold. The large charm and bottom cross-section should enable quantitative tests of QCD and provide precise measurements of the gluon structure function through the measurement of inclusive lepton, dilepton, D^*X and $J/\Psi X$ cross-sections and distributions. These measurements have already been done in hadronic collisions. However, because of the relatively large uncertainty in the parton densities and large perturbative corrections, hadroproduction heavy flavour data do not yet provide completely quantitative tests of QCD. Such tests should be relatively cleaner in ep collisions. We hope that the required theoretical work needed for such precise QCD tests at HERA will be forthcoming.

One of the primary interests in all present high energy experiments lies in the discovery of the top quark. Based on the present direct and indirect top quark searches one expects its mass to lie in the range $40GeV \leq m_t \leq 180\ GeV$. Experiments at LEP I are sensitive to the top quark mass up to $m_t \sim 55$ GeV. The sensitivity at the Fermilab Tevatron Collider is much larger due to the large cross-section for $p\bar{p} \to t\bar{t}X$. However, for $m_t > m_W$ the background process $p\bar{p} \to W + jet + jet + X$ with $W \to l\nu_l$ and the dijet invariant mass $m_{JJ} \sim m_W$ is effectively very similar to the top signal $p\bar{p} \to t\bar{t}X \to WWX$ with $W^\pm \to l^\pm\nu_l$ and $W^\mp \to jet + jet$ [66]. The sensitivity to the top quark mass at HERA is limited essentially by the smaller cross-section. We have presented here a rather detailed analysis of the top quark events and backgrounds. Based on this study, we feel that the background for top searches at HERA can be brought down to an acceptable level. This should enable top searches up to $m_t \sim 70\ GeV$, though this sensitivity increases somewhat if the center of mass energy and/or luminosity exceed the numbers that we have assumed here. Thus, it is conceivable that experiments at HERA may get a shot at the top quark.

The other interest in heavy flavour studies at HERA lies in searching for rare decays of the charmed and bottom hadrons. The cross-sections for charm and bottom hadrons are large

enough to warrant such searches both in B and D decays. We have concentrated here on B physics. Experiments at HERA may be able to measure the CKM suppressed transition $|V_{bu}|$ through the NC process $ep \to eb\bar{b}X$, with subsequent two-body or quasi two-body decays of the B meson, $B \to \pi\pi, \rho\pi$ etc. The chances of measuring the CKM angles in the charged current processes at HERA are small. The phenomenon of $B^0 - \bar{B}^0$ mixing is observable at HERA, for example via the measurement of $\chi = \chi_d P_d + \chi_s P_s$ through the same sign and opposite sign dilepton rates. In addition, due to the fact that the B hadrons are boosted it may be possible to use the vertex detectors to measure time dependent oscillations. This would enable measurement of x_d and in particular x_s through oscillation lengths.

Likewise, the large cross-section for charm can be used to search for rare decays, $D^0 \to \mu^+\mu^-, e^+e^-$ and $D^0 - \bar{D}^0$ oscillations. Many of these searches have clear experimental signatures and we believe that at HERA the background can be brought down so as to expect improved sensitivity for $BR(D^0 \to l^+l^-, l = e, \mu)$ and $r_D = \frac{Prob(D^0 \to \bar{D}^0)}{\bar{D}^0 \to \bar{D}^0)}$.

It is evident that heavy quark physics is going to be an exciting aspect of HERA physics and hence, in our opinion, it deserves a lot more attention.

Acknowledgments

We expresss our thanks to our colleagues who showed interest in this study and participated at various stages. In particular, we acknowledge with thanks the participation of U. Baur, J.J. van der Bij, R. Godbole and R. Marshall in this study. We also thank S. Brodsky, R. Peccei, R. Rückl, W. Schmidt-Parzefall and G. Wolf for useful discussions, and H. Schröder for allowing us to use Fig. 4.15 from his Erice talk. We thank G. Wolf also for a critical reading of the manuscript.

One of us (F.B.) would like to thank the Alexander von Humboldt Stiftung for supporting his stay at DESY during the summer of 1988, when this report was written.

Bibliography

[1] Physics at LEP, CERN Report 86/02(1986), Vols. 1 and 2, Editors: J. Ellis and R. Peccei.

[2] C. Albajar et al., UA1 Collaboration, Phys. Lett. 186B (1987) 237, 186B (1987) 247, and (Err.) 197B (1987) 565.

[3] A. Ali, B. van Eijk and I. ten Have, Nucl. Phys. B292 (1987) 1; see also B. van Eijk (Ph. D. Thesis), Amsterdam 1986.

[4] B. Cox et al., Fermilab Proposal E771 (1987); N.W. Reay, Letter of Intent of a Tevatron Collider Beauty Factory, (1987); N.S. Lockyer et al., Proposal for a Bottom Collider Detector at Fermilab (1987); R. Dixon, Invited talk at the 6Th INFN ELOISATRON Project Workshop on Heavy Flavour Physics, Erice-Trapani, Italy (1988).

[5] A. Vorobyov, in Proceedings of the Workshop on the Experimental Programme at UNK, Serpukhov, USSR (1988); J.D. Bjorken, in Proceedings of the Workshop on High Sensitivity Beauty Physics at Fermilab, Editors: A. Slaughter, N. Lockyer and M. Schmidt.

[6] B. Cox, F.J. Gilman and T.D. Gottschalk, in Proceedings of the 1986 Summer Study on the Physics of the Superconducting Super Collider, Editors: R. Donaldson and J. Marx, (American Physical Society, New York 1986).

[7] A. Ali et al., in Proceedings of the ECFA-CERN Workshop on a Large Hadron Collider in the LEP tunnel, Lausane and CERN 1984, ECFA 84/85, CERN 84-10, Geneva 1984, Editor: M. Jacob.

[8] B. Cox, in Proceedings of the 4th. INFN ELOISATRON Project Workshop, Erice-Trapani, Italy (1987).

[9] D. L. Rubin, CESR Luminosity Upgrade, in [10]; W. Schmidt-Parzefall, DESY Internal Report (1988); R. Aleksan et al., SLAC Report (to be published).

[10] Proceedings of the UCLA Workshop, Linear Collider $B\bar{B}$ factory, Conceptual Design Los Angeles, U.S.A., Editor: D. Stark.

[11] Proceedings of the Workshop on Heavy Quark Factory and Nuclear Physics Facility with Superconducting Linacs, Courmayeur, Italy, Editors: E.D. Santis, M. Greco, M. Piccolo and S. Tazzari (Italian Physical Society, Bologna, Italy, 1988).

[12] R. Eichler et al., Motivation and Design Study for a B-meson Factory with High Luminosity, SIN Report PR-86-13 (1986); K. Wille, The SIN Project, Proceedings of the 2nd. Inter. Symposium on the Production and Decay of Heavy Flavours, SLAC, Stanford, U.S.A. (1987).

[13] For a recent review on high energy photoproduction experiments see M.S. Witherall, in Proceedings of the 1987 Int. Symposium on Lepton and Photon Interactions, Hamburg, FRG, Editors: W. Bartel and R. Rückl (North Holland, Amsterdam, 1988).

[14] U. Baur, J.J. van der Bij, CERN-TH.4875/87 (1987) and these Proceedings.

[15] M. Glück, R.M. Godbole, E. Reya, Dortmund Univ. preprint, DO-TH-87/17 (1987).

[16] R.A. Eichler, Z. Kunszt, ETHZ-IMP P/88-1 (1988), to be published in Nucl. Phys. B

[17] G.A. Schuler, Nucl. Phys. B299 (1988) 21.

[18] G. Ingelman, G.A. Schuler, DESY preprint, DESY 88-020 (1988).

[19] H. Albrecht et al., ARGUS Collaboration, Phys. Lett. 192B (1987) 245.

[20] A. Bean et al., CLEO Collaboration, Phys. Rev. Lett. 58 (1987) 183.

[21] A. Ali and Z. Z. Aydin, Nucl. Phys. B148 (1979) 165.

[22] A. Ali, DESY Report 87-083 (1987), published in the Proceedings of the UCLA Workshop in [10].

[23] R. D. Peccei, DESY Report 87-134 (1987), published in the Proceedings of the Workshop on the Experimental Programme at UNK, Serpukhov, USSR (1988).

[24] J. C. Anjos et al., Phys. Rev. Lett. 60 (1988) 1239.

[25] L. L. Chau, Phys. Rep. 95C (1983) 1; L. Wolfenstein, Carnegie Mellon University Report CMU-HEP 85-10 (1985); A. Dutta and P. Kumbhakar, Zeit. f. Physik C27 (1985) 515; G. Ecker and W. Grimus, Universität Wien Preprint UWThPh-1985-14 (1985).

[26] For a recent compilation of limits on rare D decays see D. Hitlin in Proceedings of the 1987 Int. Symposium on Lepton and Photon Interactions, Hamburg, FRG, Editors: W. Bartel and R. Rückl (North Holland, Amsterdam, 1988).

[27] For a recent update on B meson semileptonic branching ratios and V_{bu} measurements, see H. Schröder, Invited talk at the 6th INFN ELOISATRON Project Workshop, Erice-Trapani, Italy, June 1988.

[28] F. Halzen, in Proceedings of the 21st. International Conference on High Energy Physics, Paris, France (1982).

[29] R.K. Ellis and Z. Kunszt, Nucl. Phys. B303 (1988) 633

[30] G. Ingelman, G.A. Schuler, AROMA 1.2 - A Generator of Heavy Flavour Events in *ep* Collisions, DESY preprint in preparation.

[31] J. Engelen, S. de Jong and J. Vermaseren, private communication.

[32] E. Eichten, I. Hinchliffe, K. Lane, C. Quigg, Rev. Mod. Phys. 56 (1984) 579, ibid., 58 (1986) 1047.

[33] D.W. Duke, J.F. Owens, Phys. Rev. D30 (1984) 49
M. Glück, E. Hoffman, E. Reya, Z. Phys. C13 (1982) 119.

[34] A.D. Martin, R.G. Roberts, W.J. Stirling, Rutherford preprint RAL-87-052 (1987).

[35] E. Hoffmann and R. Moore, Z. Phys. C20 (1983) 71. See also S. Brodsky, Invited talk at the 6th INFN ELOISATRON Project Workshop on heavy flavour physics, Erice-Trapani, Italy, 1988.

[36] See for example A. Ali in [1].

[37] F. Halzen and P. Hoyer, Phys. Lett. 154B (1985) 324; V. Barger and R.J.N. Phillips, Phys. Rev. D31 (1985) 215; G. Köpp, J.H. Kühn and P.M. Zerwas, Phys. Lett. 153B (1985) 315; A. Ali and G. Ingelman, Phys. Lett. 156B (1985) 111; E.W.N. Glover, K. Hagiwara and A.D. Martin, Phys. Lett. 168B (1986) 289; A. H. Müller and P. Nason, Phys. Lett. 157B (1985) 226.

[38] G. Altarelli, M. Diemoz, G. Martinelli, P. Nason, CERN-TH.4978/88.

[39] M. Drees and K. Grassie, Zeit. f. Phys. C28 (1985) 451.

[40] This, for example, can be seen by comparing the cross-sections obtained in [3] for $p\bar{p} \to QX$ (with a cut-off $p_T^Q \geq 5$ GeV in $O(\alpha_s^3)$ QCD processes) with the $O(\alpha_s^3)$ results obtained in [38].

[41] M. Bengtsson, T. Sjöstrand, Comput. Phys. Common. 43 (1987) 367.

[42] B. Andersson, G. Gustafson, G. Ingelman, T. Sjöstrand, Phys. Rep. 97 (1983) 31.

[43] S. Bethke, Zeit. f. Phys. C29 (1985) 175.

[44] C. Peterson, D. Schlatter, I. Schmitt and P.M. Zerwas, Phys. Rev. D27 (1983) 105.

[45] B. Andersson, G. Gustafson, B. Söderberg, Z. Phys. C20 (1983) 317
For a comparison with data see
G. Ingelman, proc. XV International Symposium on Multiparticle Dynamics, Lund, Sweden, Editors: G. Gustafson, C. Peterson (World Scientific, Singapore, 1984.)

[46] A. Ali, Zeit. f. Phys. C1 (1979) 25.

[47] G. Ingelman, LEPTO 5.2, DESY preprint in preparation.

[48] J. D. Bjorken and S. J. Brodsky, Phys. Rev. D1 (1970) 1416.

[49] G. Ingelman, G.A. Schuler, J.F. de Troconiz, DESY preprint in preparation.

[50] G.G. Hanson, Invited talk presented at the International Symposium on the Production and Decay of Heavy Flavors, Stanford, 1987, SLAC-Pub-4487 (1987).

[51] C. Albajar et al., UA1 collaboration, CERN-EP/87-190.

[52] H. Baer, V. Barger, H. Goldberg, R.J.N. Phillips, MAD/PH/367 and FSU-HEP 87/116 (1987).

[53] R. Kleiss, A.D Martin, W.J. Stirling, University of Durham preprint, DTP/87/44 (1987).

[54] F. Halzen, Invited talk at Physics in Collisions, Tsukuba, Japan, University of Wisconsin-Madison Report, MAD/PH/372 (1987).

[55] E.L. Berger, D. Dibitonto, M. Jacob, W.J. Stirling, Phys. Lett. 140B (1984) 259.

[56] For a recent survey of B physics see W. Schmidt-Parzefall, in Proceedings of the 1987 Int. Symp. on Lepton Photon Interactions, Hamburg, FRG, Editors: W. Bartel and R. Rückl (North Holland, Amsterdam, 1988).

[57] C. Albajar et al., UA1 Collaboration, Phys. Lett. 200B (1988) 380.

[58] For a theoretical discussion of CP violation in exclusive B decays see, for example, V. Khoze and M. Uraltsev, Yad. Fiz. 47 (1988) 1687; I. Bigi et al., SLAC-PUB-4476 (1987); P. Krawczyk et al., DESY Report 87-171 (1987).

[59] H. Albrecht et al., ARGUS Collaboration, DESY Report 88-056 (1988).

[60] A. Ali et al., to be published.

[61] J. Ellis, J. S. Hagelin and S. Rudaz, Phys. Lett. 192B (1987) 201; J Maalampi and M. Roos, Phys. Lett. 195B (1987) 489; V. Barger et al., Phys. Lett. 194B (1987) 312; L.L. Chau and W.Y. Keung, Univ. California Davis Report, UCD-87-02(1987); H. Harari and Y. Nir, Phys. Lett. 195B (1987) 586; V.A. Khoze and N. G. Uraltsev, Yad. Fiz. 47 (1988) 1687; I. Bigi and A. Sanda, SLAC-PUB-4299(1987); L. Angelini et al., Phys. Lett. 195B (1987) 468; G. Altarelli and P. Franzini, CERN Report, CERN-TH 4745 (1987); S. Bertolini, F. Borzumati and A. Masiero, Phys. Lett. 194B (1987) 545; F. Donoghue et al., Phys. Lett. 195B (1987) 285; A. Ali in [22].

[62] J. S. Hagelin, Nucl. Phys. B193 (1981) 123; A. J. Buras, W. Slominski and H. Steger, Nucl. Phys. B245 (1984) 369; M. A. Shifman and M. V. Voloshin, ITEP Reports 86-54, 86-83 (1986).

[63] T. Schaad et al. MARK II Collaboration, Phys. Lett. 160B (1985) 188.

[64] L. B. Okun, V. I. Zakharov and B. M. Pontecorvo, Lett. Nuov. Cim. 13 (1975) 218; A. Pais and S.B. Treiman, Phys. Rev. D12 (1975) 2744.

[65] F. Barreiro, Invited talk at the 6th INFN ELOISATRON Project Workshop on heavy flavour physics, Erice-Trapani, Italy, 1988.

[66] D. Denegri, Invited talk at the 6th INFN ELOISATRON Project Workshop on heavy flavour physics, Erice-Trapani, Italy, 1988.

[67] V. Barger, A.D. Martin and R.J.N. Phillips, Phys. Lett. 125B (1983) 339, 343; Phys. Rev. D28 (1983) 145.

[68] R. K. Ellis and P. Nason, Fermilab-PUB-88/54/T (1988)

[69] Z. Kunszt, Phys. Lett. 207B (1988) 103

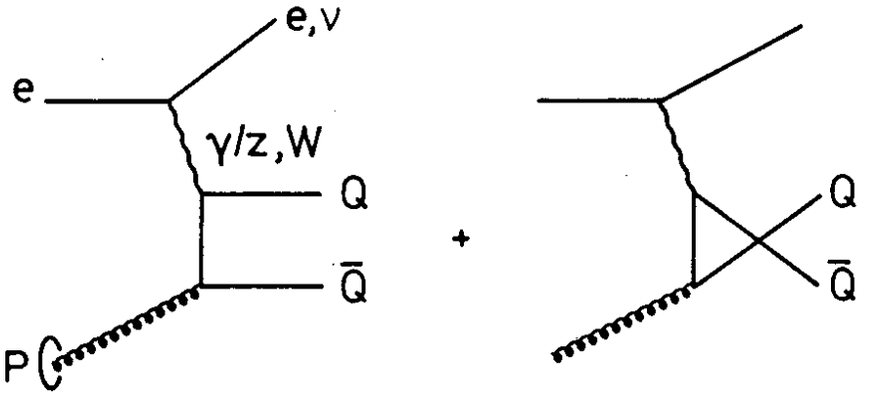

Figure 1.1 Lowest order QCD diagrams for boson-gluon fusion into a heavy quark-antiquark pair.

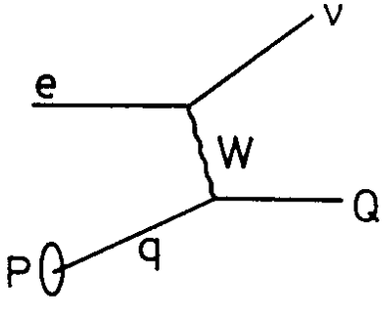

Figure 2.1 Quark Parton Model diagram contributing to the charged current interaction giving a single heavy quark.

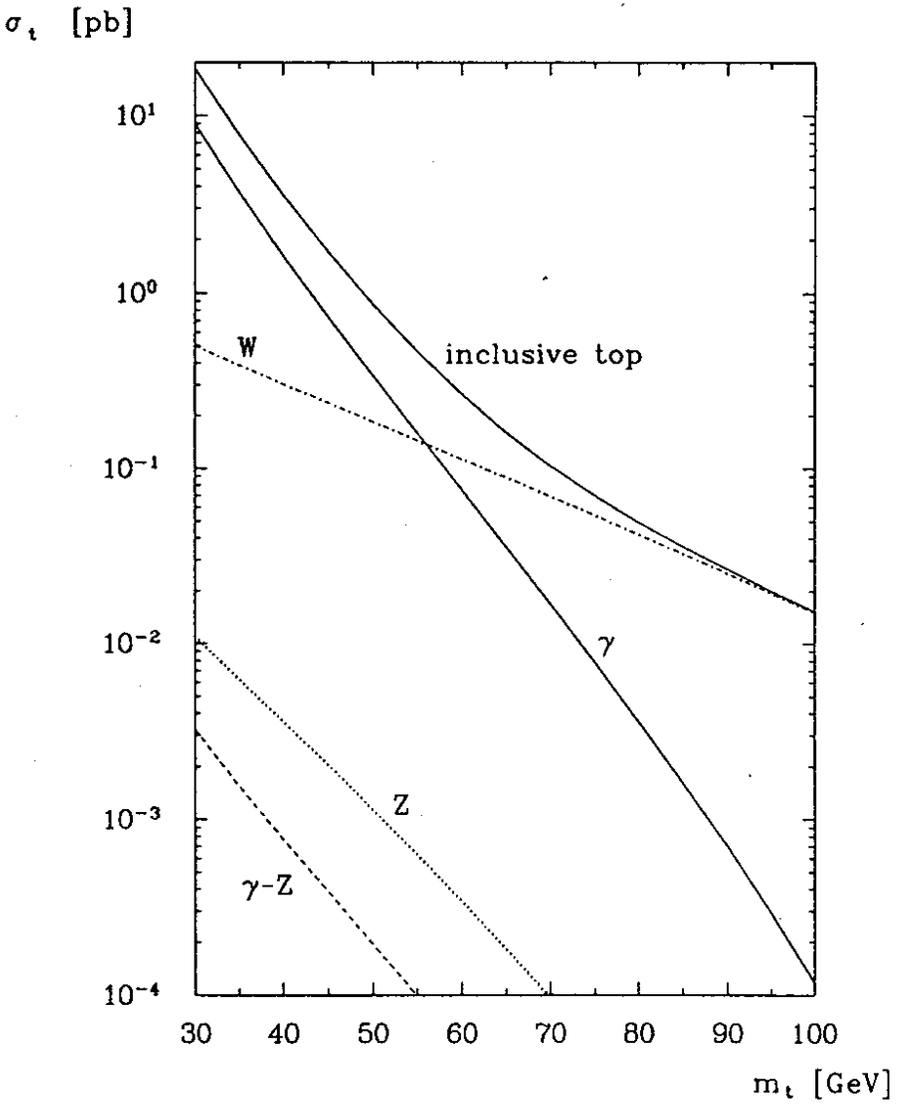

Figure 2.2 Inclusive cross-section for top quark production via boson-gluon fusion as a function of the top quark mass. Curves are for charged current interactions (W), and in the neutral current case separately for pure γ, pure Z and their interference $\gamma - Z$. The inclusive cross-section is defined in Eq. (2.35) (From ref. [18]).

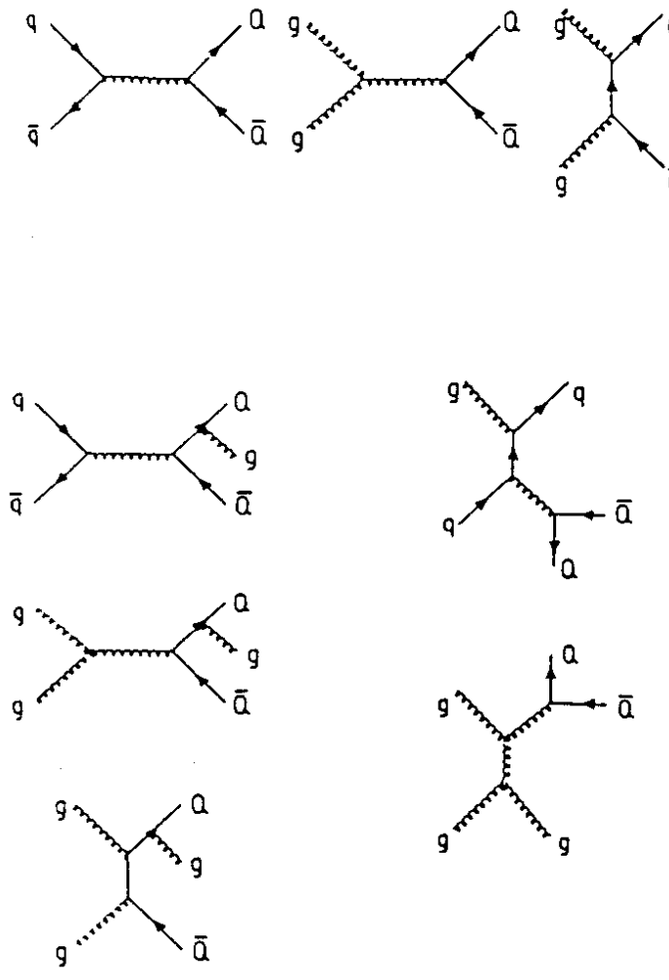

Figure 2.3 Leading $O(\alpha_s^2)$ and $O(\alpha_s^3)$ diagrams contributing to heavy quark production in hadron-hadron collisions.

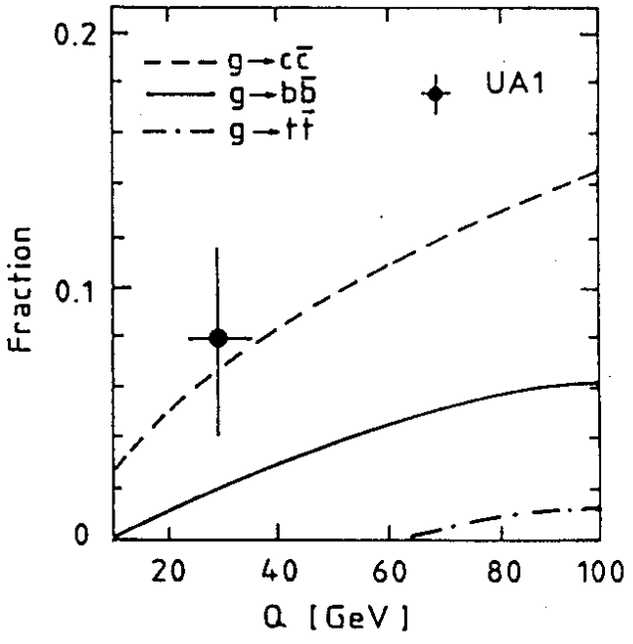

Figure 2.4 Perturbative estimates of heavy quark fraction in a gluon jet in $pp/p\bar{p}$ as a function of the parton-parton c.m.s. energy Q compared with the UA1 data [2]. Theoretical curves are from Müller and Nason in ref. [37].

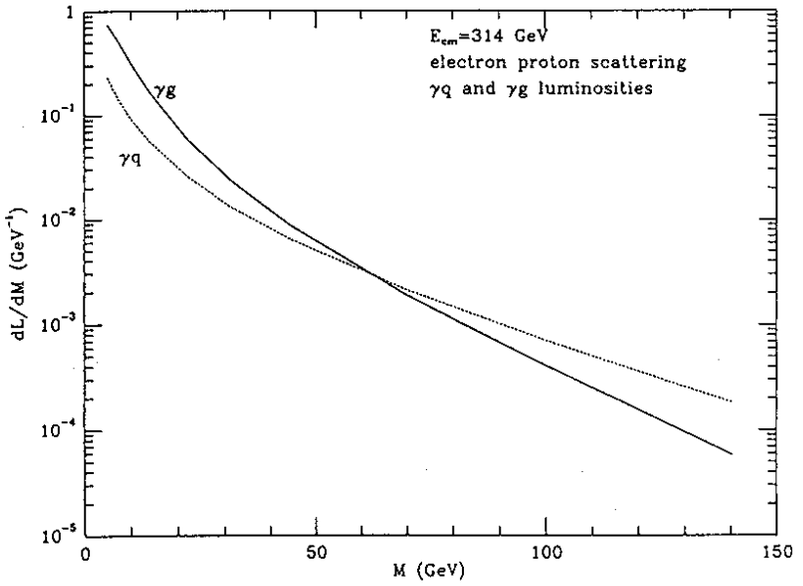

Figure 2.5 Luminosity functions for initial parton combinations γg and γq in ep collisions at $\sqrt{s}$ = 314 GeV. M denotes the subenergy of the parton collisions. (From ref. [29]).

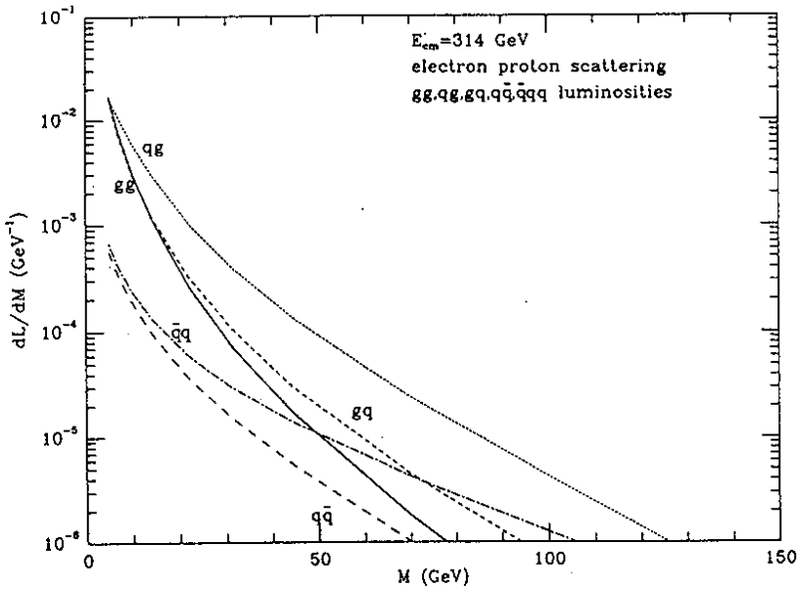

Figure 2.6 Luminosity functions for gg, gq, qg, $\bar{q}q$ and $q\bar{q}$ parton collisions in electron proton scattering at HERA energy, $\sqrt{s}$ = 314GeV (From ref. [29]).

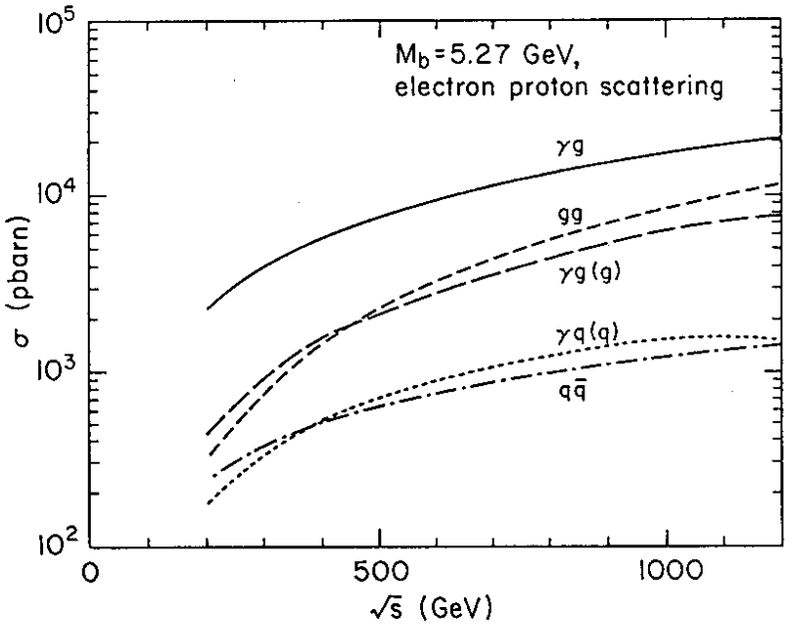

Figure 2.7 Total cross sections for bottom quark production in ep collisions. The contributions of the five production mechanisms (2.46) are separately indicated. (From ref. [29]).

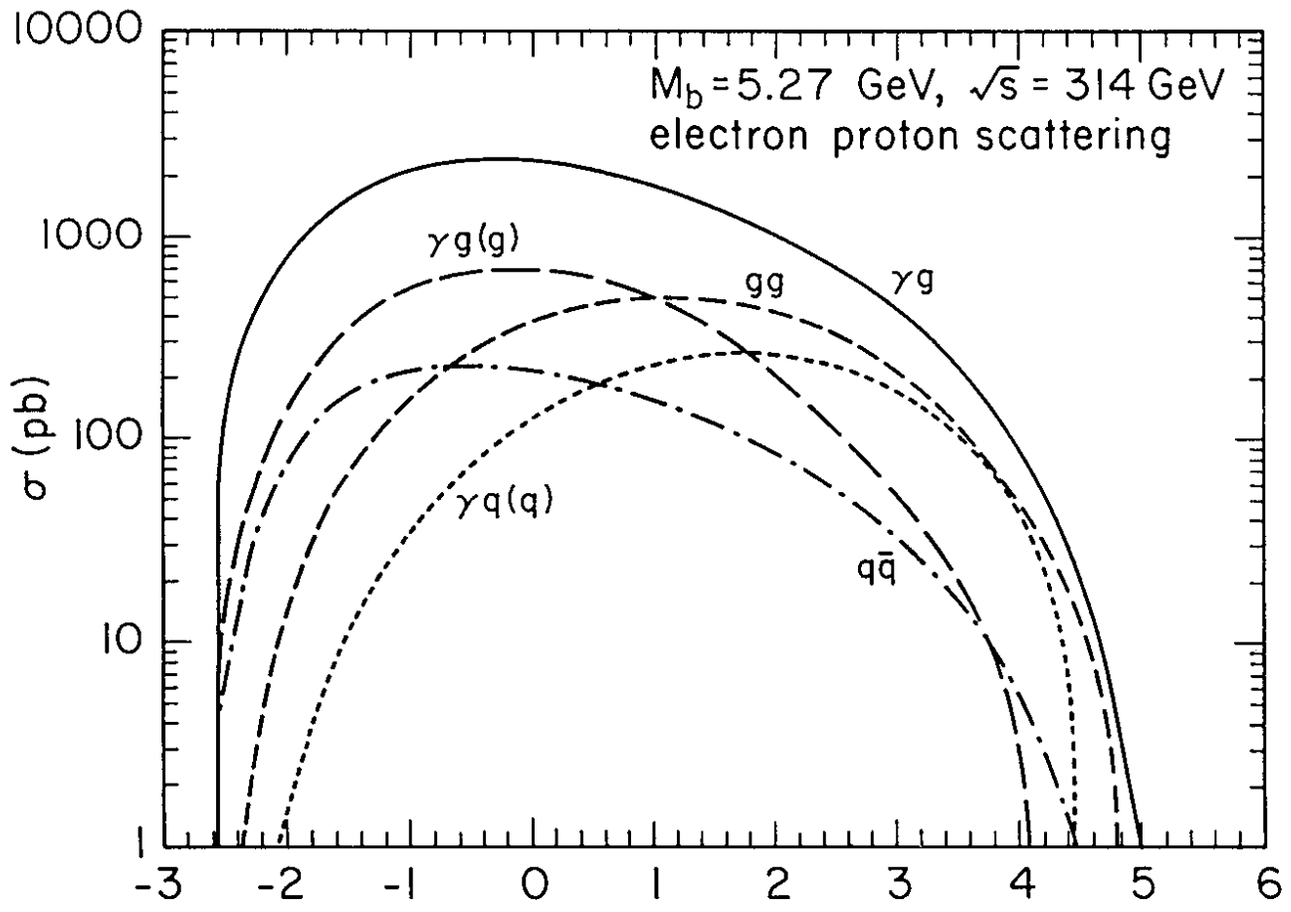

Figure 2.8 Rapidity distributions for bottom pair production in ep collisions at HERA energy. The contributions of the five production mechanisms in (2.46) are separately indicated. (From ref. [29]).

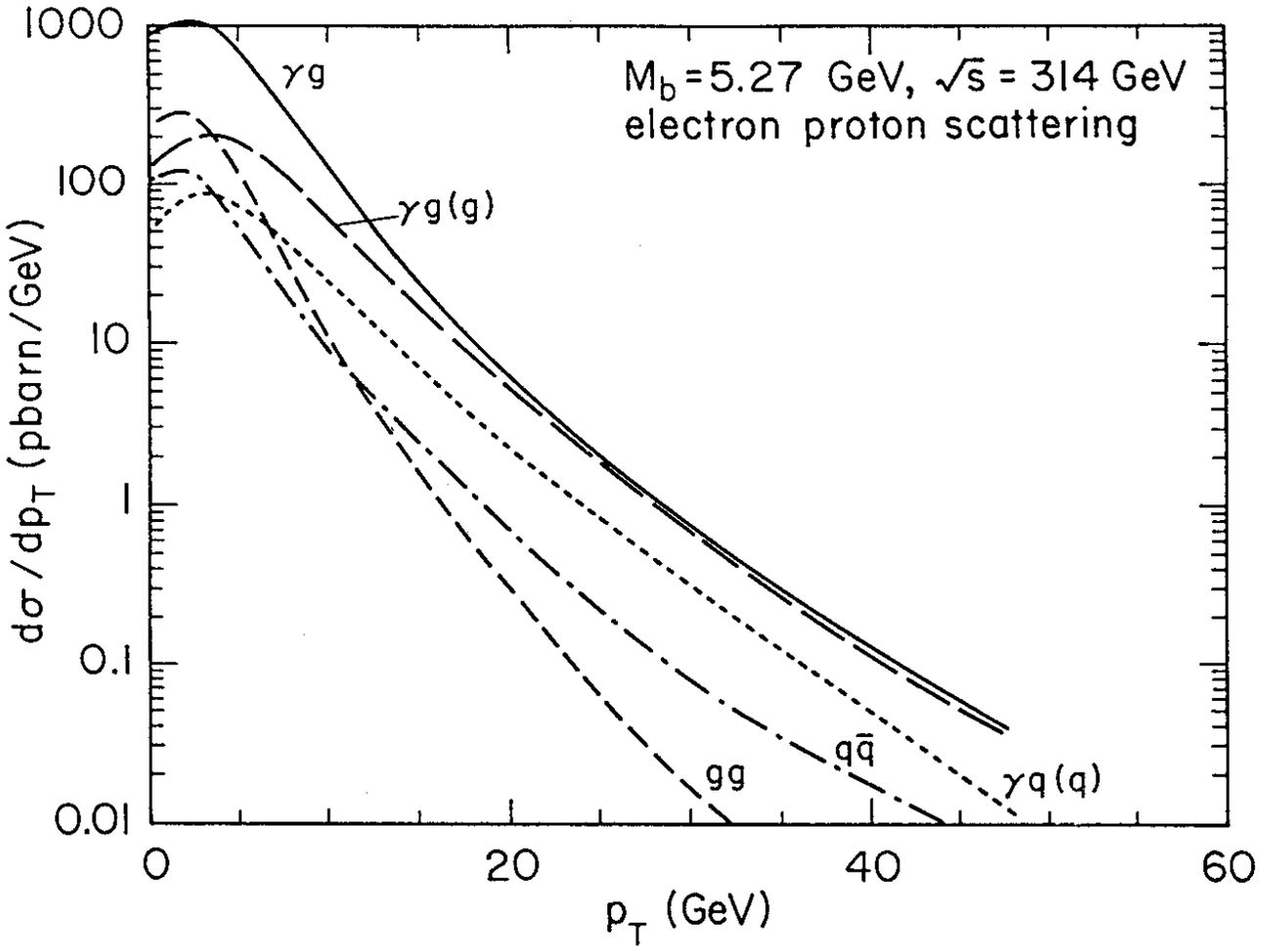

Figure 2.9 Transverse momentum distribution of the bottom quark produced in ep collisions at HERA energy. The contributions of the five production mechanisms (2.46) are separately indicated. (From ref. [29]).

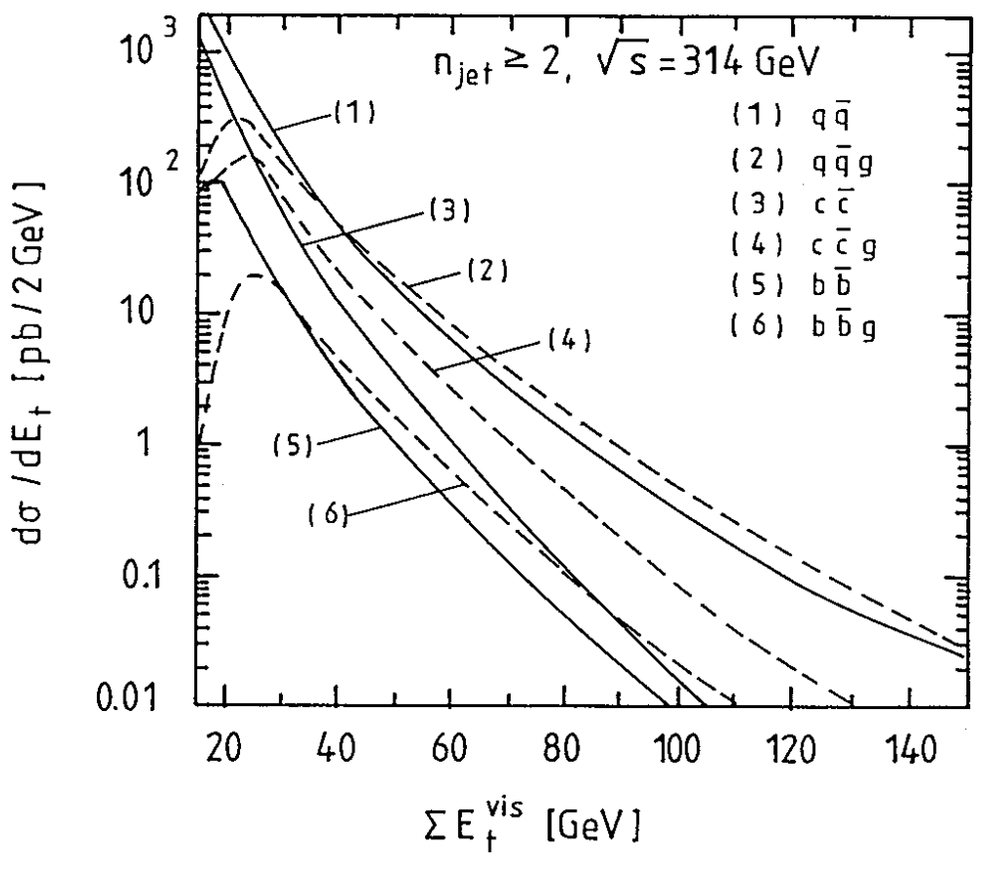

Figure 2.10 Total visible transverse energy distributions in ep collisions at $\sqrt{s} = 314$ GeV obtained by requiring that at least two jets are observed in the detector of angular acceptance of $|\sin\theta| \geq 0.1$. The curves with labels $q\bar{q}$, $q\bar{q}g$ correspond to the subprocess contributions (2.46) and the labels $c\bar{c}$, $c\bar{c}g$, $b\bar{b}$ and $b\bar{b}g$ correspond to $\gamma g \to Q\bar{Q}, Q\bar{Q}g$ and $\gamma q \to Q\bar{Q}q$ for charm and bottom. (From ref. [16]).

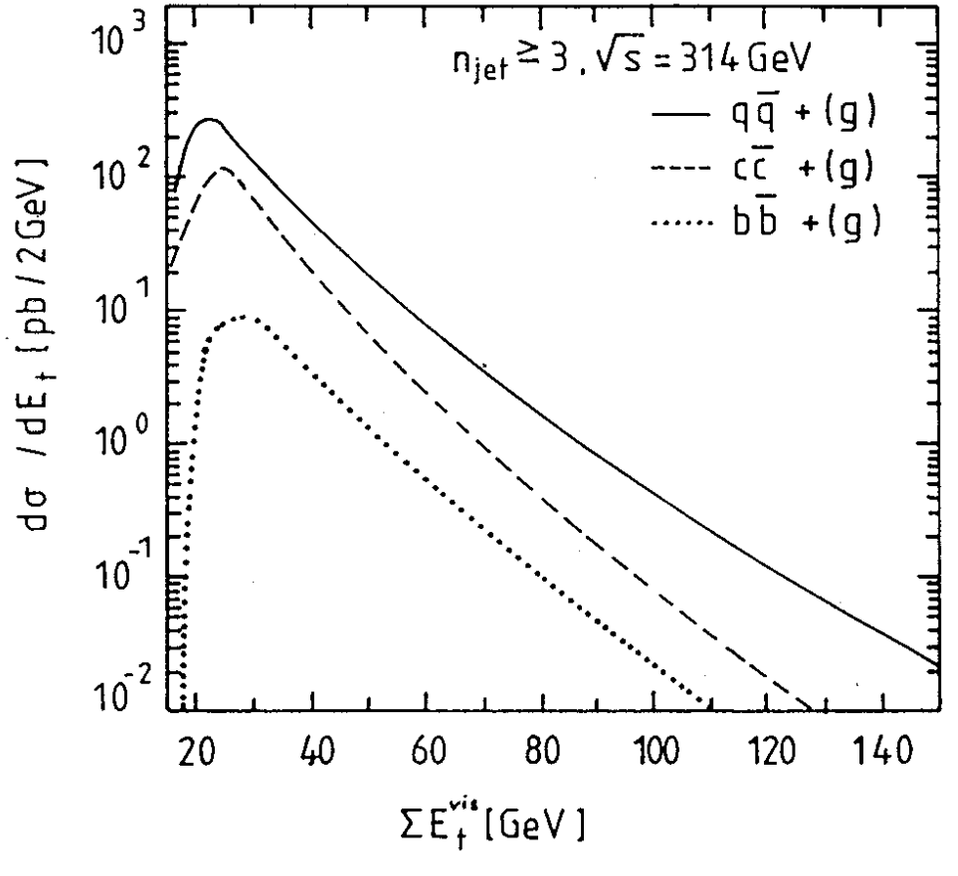

Figure 2.11 Total visible transverse energy distributions in ep collisions at HERA energy $\sqrt{s} = 314$ GeV. It is required that at least three jets are found in the detector of angular acceptance of $|\sin\theta| \geq 0.1$. The curves with labels $q\bar{q}(g)$, $c\bar{c}(g)$, $b\bar{b}(g)$ correspond to the sum of the contributions of the subprocess (2.46) and to the sum of the heavy quark processes $\gamma g \to Q\bar{Q}, Q\bar{Q}g$ and $\gamma q \to Q\bar{Q}q$ for charm and bottom. (From ref. [16]).

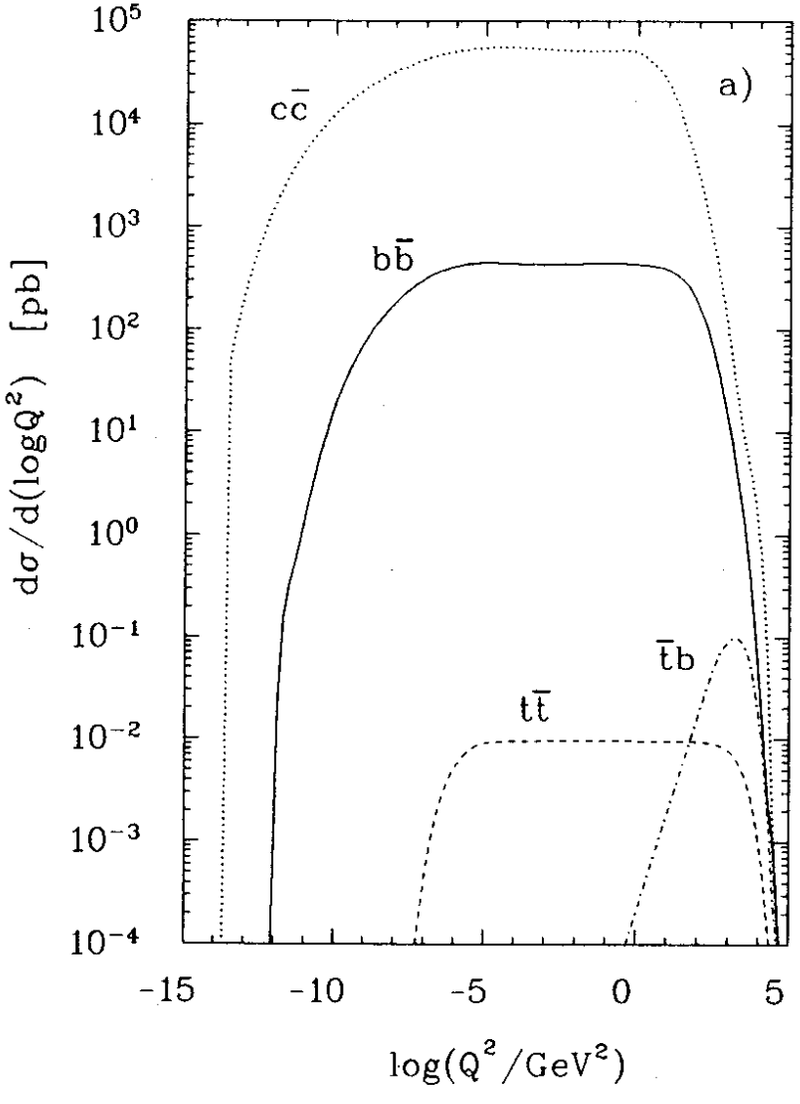

Figure 2.12

Q^2 dependence of the cross-sections for neutral current production of $c\bar{c}$, $b\bar{b}$ and $t\bar{t}$, and charged current production of $\bar{t}b$. (From ref. [18]).

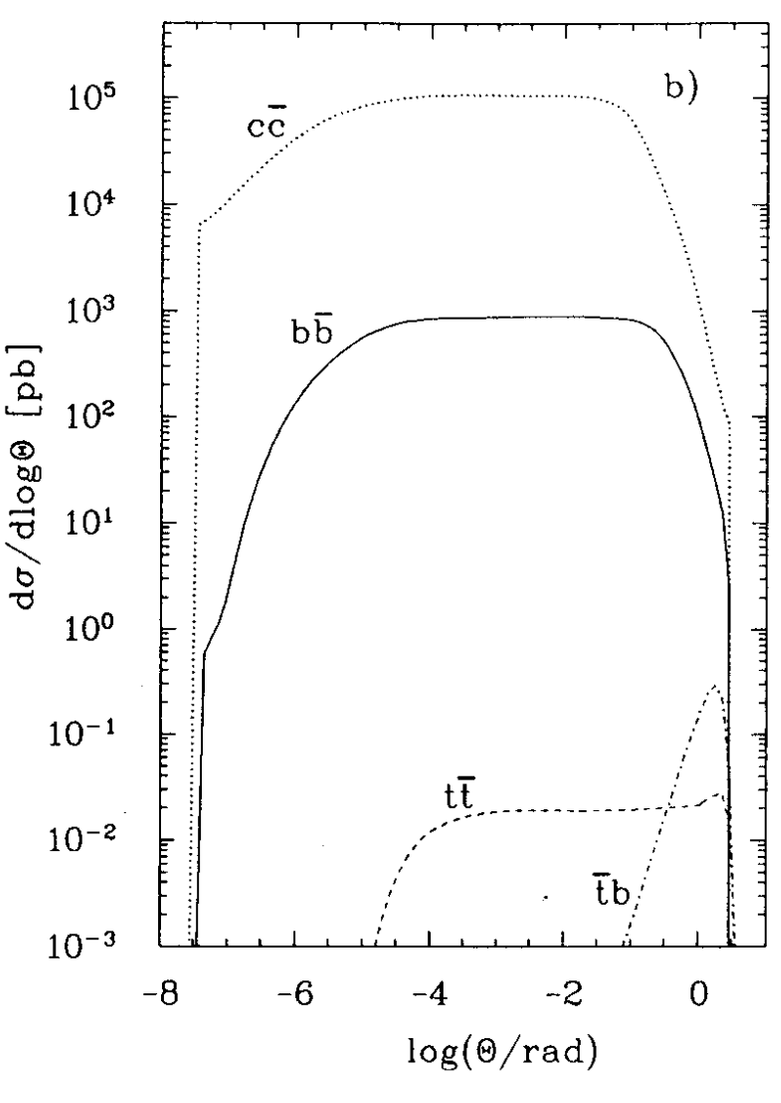

Figure 2.13

Laboratory angle of the scattered lepton. Curves as in Fig. 2.12. (From ref. [18]).

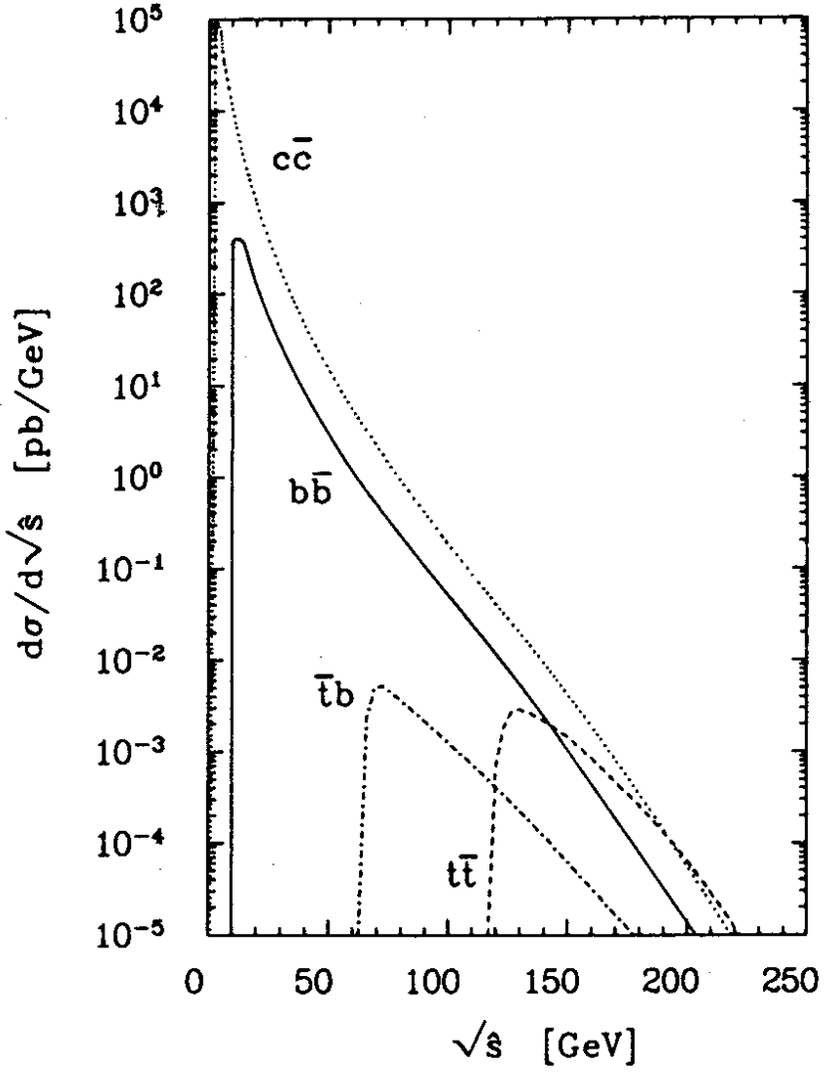

Figure 2.14 Dependence of the heavy quark cross-section on the invariant mass, $\sqrt{\hat{s}}$, of the heavy quark-antiquark system. (From ref. [18]).

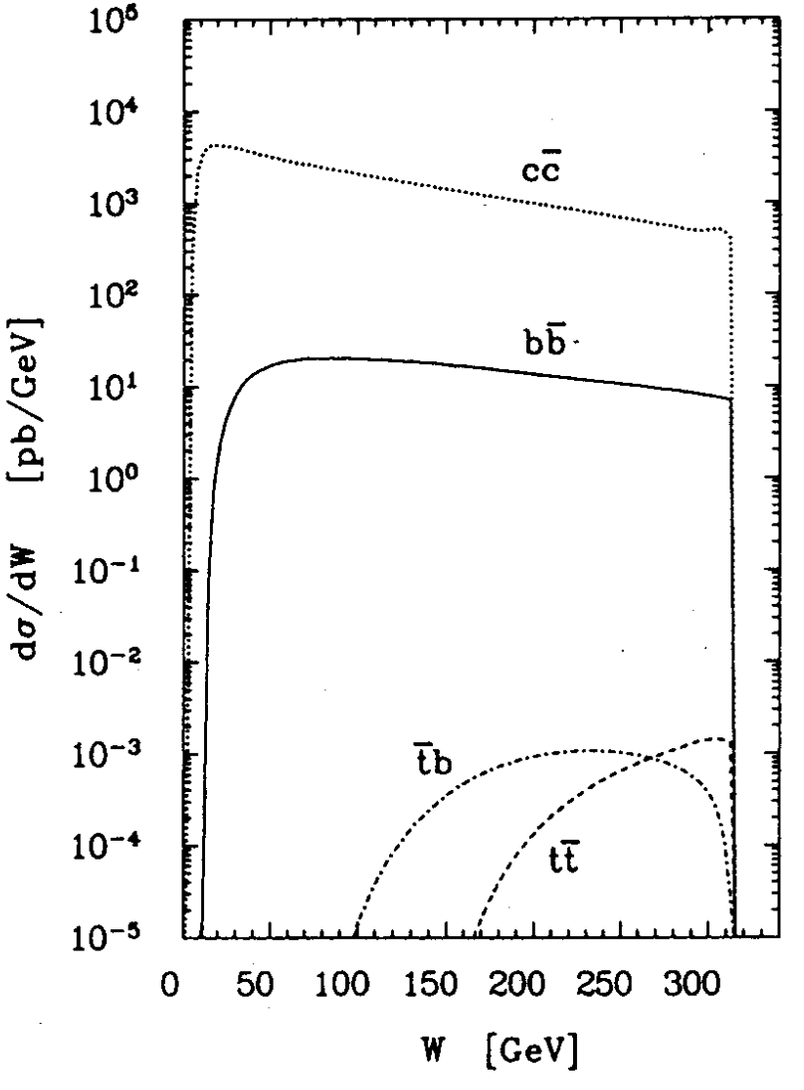

Figure 2.15 Dependence of the heavy quark cross-section on the invariant mass, W, of the total hadronic system including the target remnant. (From ref. [18]).

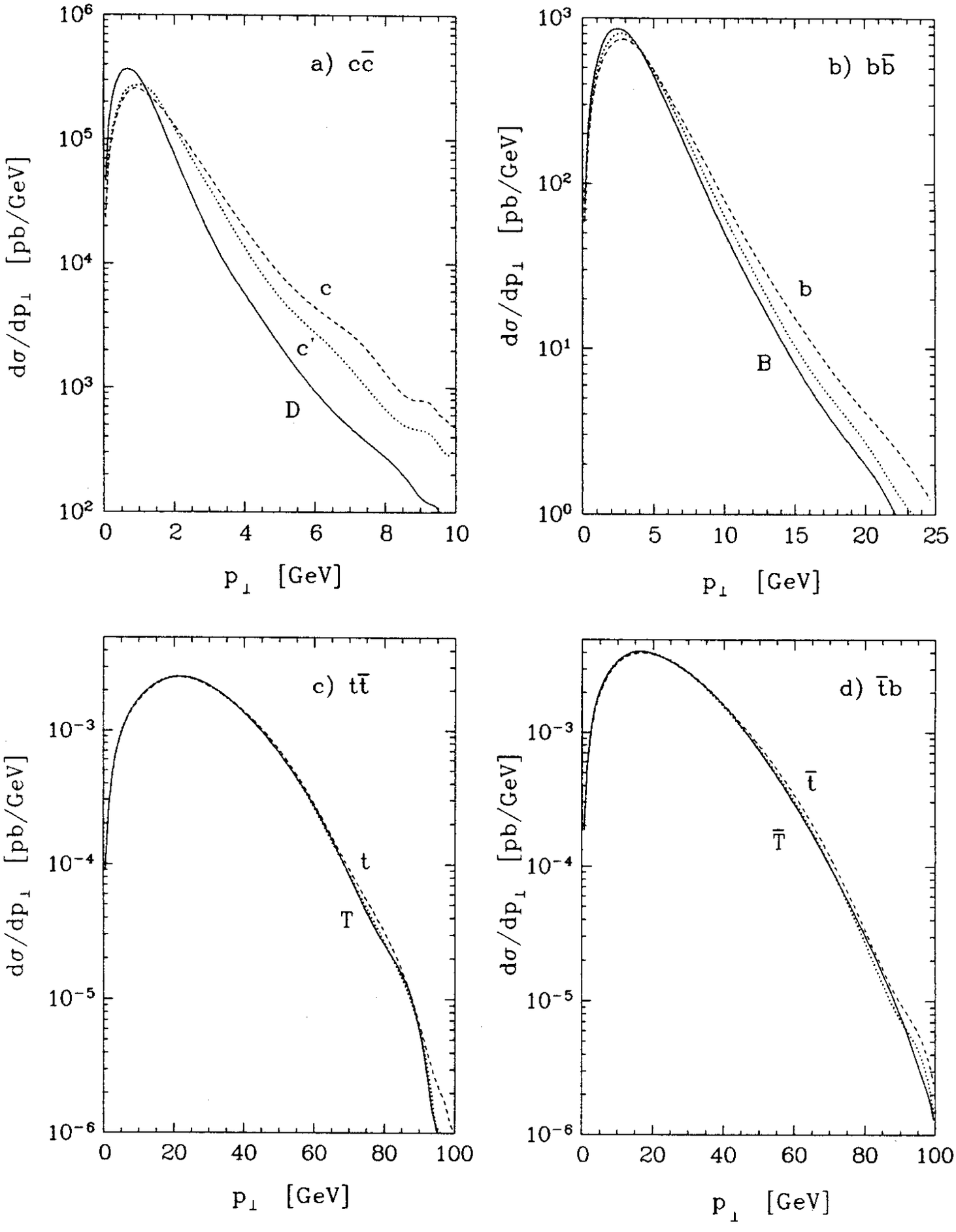

Figure 2.16 Transverse momentum distributions in the HERA laboratory frame for the heavy quark before (dashed) and after parton shower gluon emission (dotted), and for the corresponding hadrons after the LUND string fragmentation (full). (From ref. [18]).

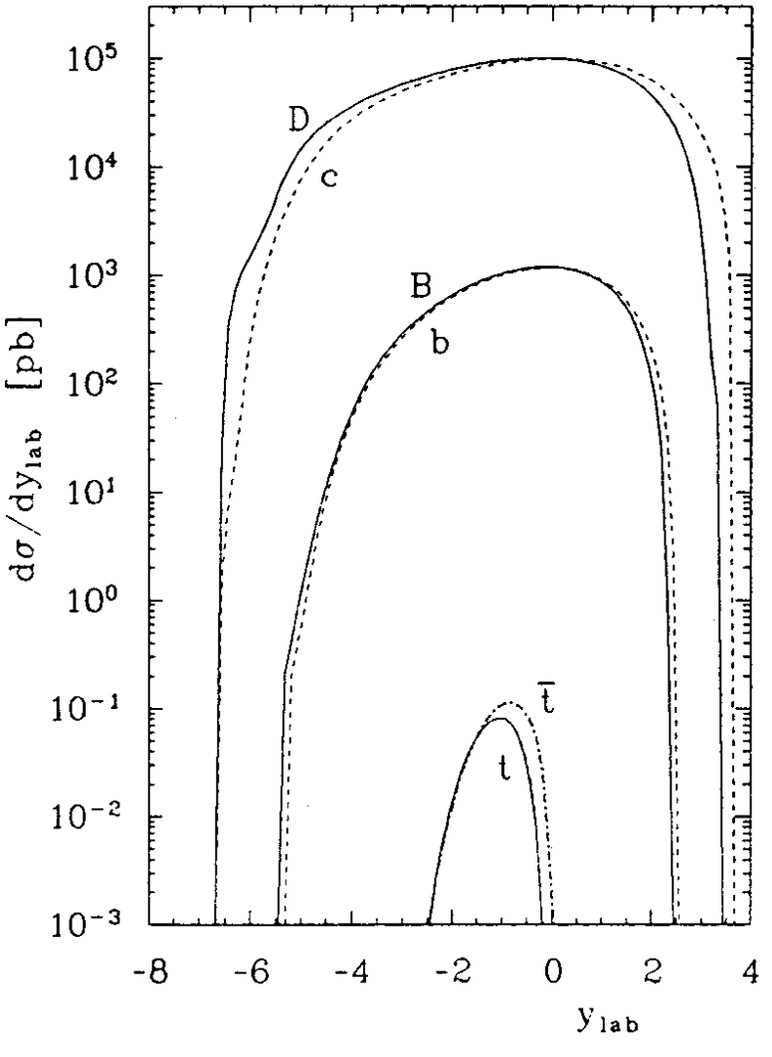

Figure 2.17 Rapidity distributions of heavy quarks, dotted curves, and hadrons, solid curves, (sum of mesons and baryons of the corresponding flavour) in the HERA laboratory frame. The separate curves are for $c\bar{c}$, $b\bar{b}$, $t\bar{t}$ and $\bar{t}b$ production, respectively. (Top quark and hadron curves overlap.) (From ref. [18]).

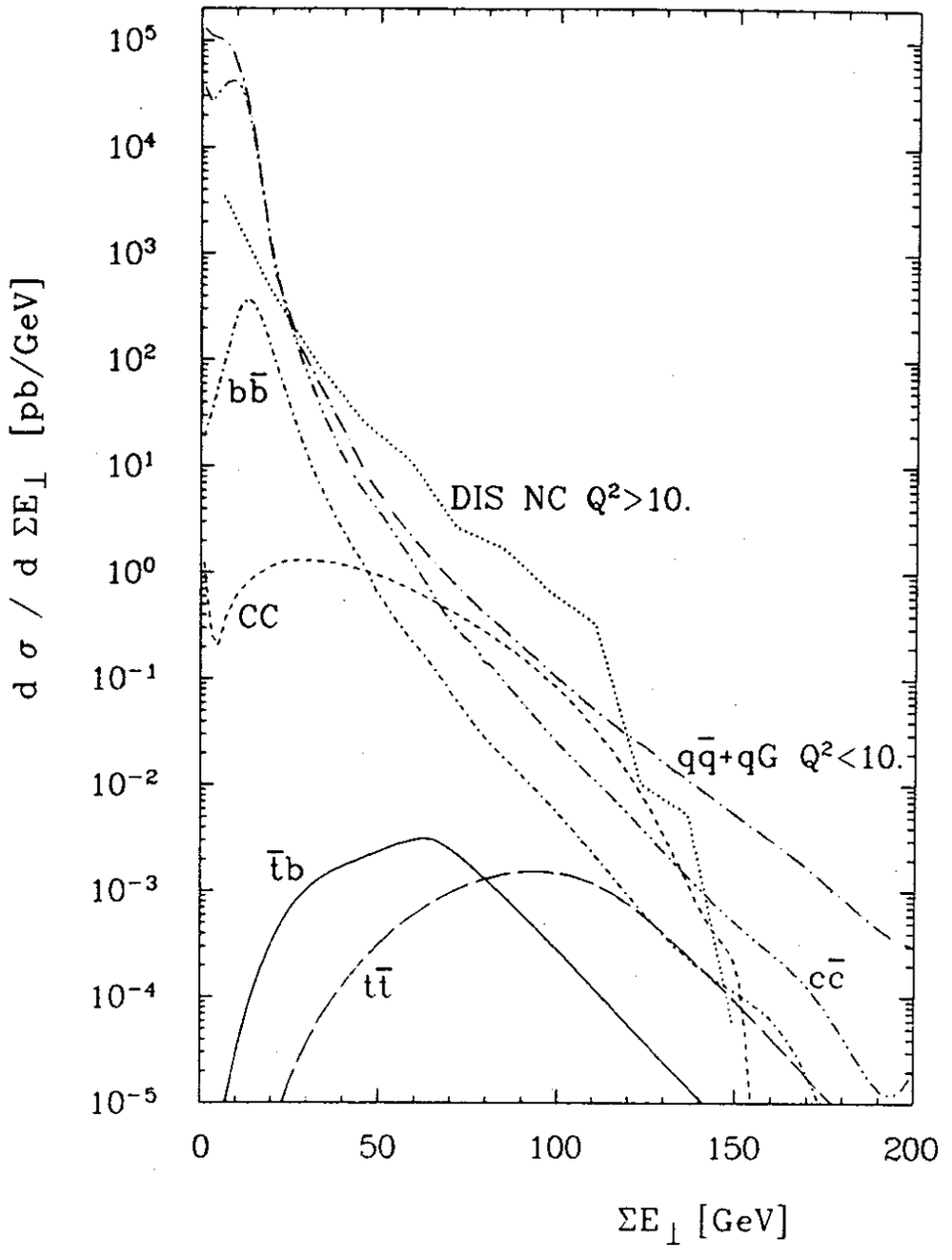

Figure 2.18 Distribution of the total transverse energy, $\sum E_\perp$, of all stable particles outside a beam pipe cut of 100 mrad, with curves corresponding to tt, tb events and the various background processes. (From ref. [49]).

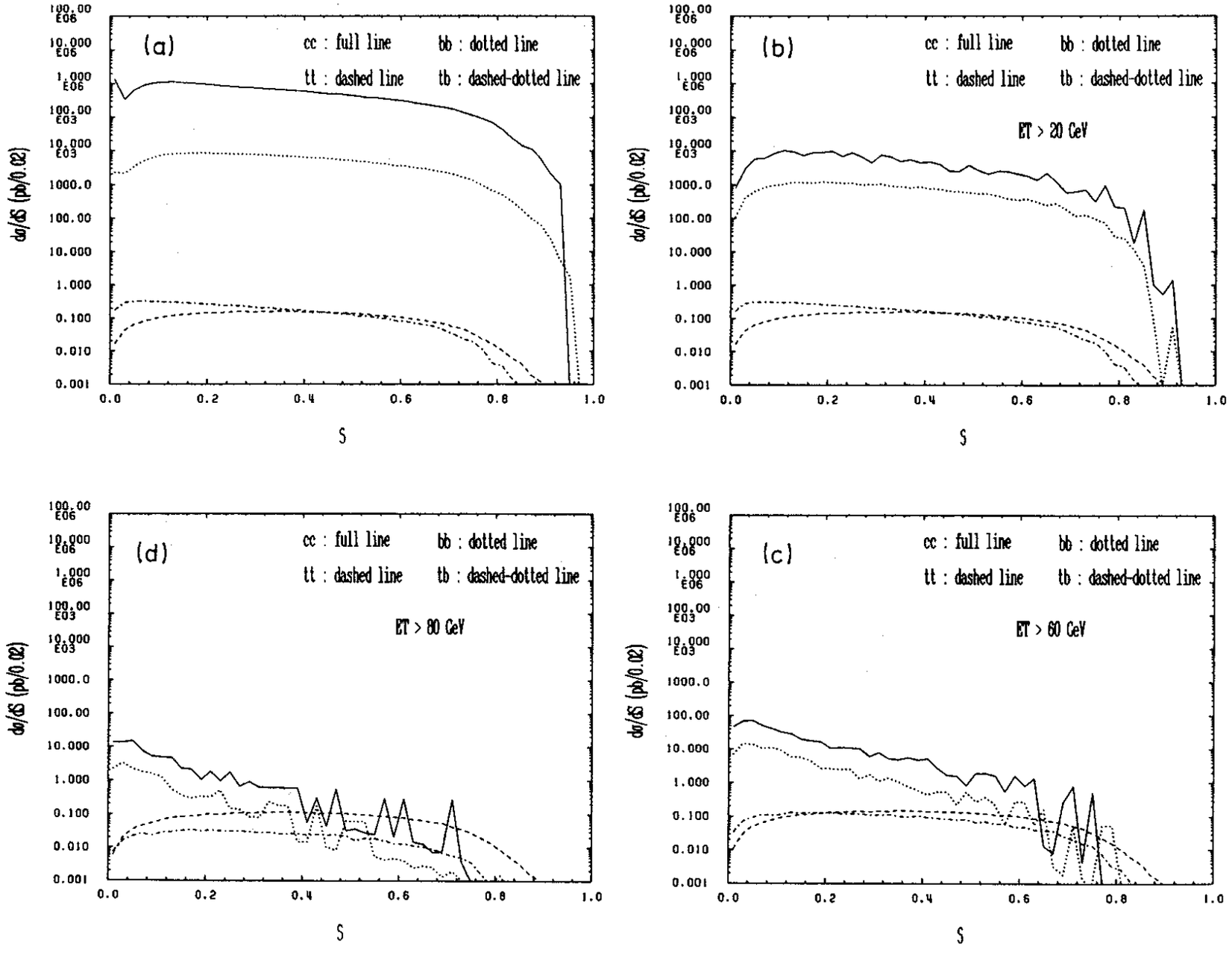

Figure 2.19 The sphericity distribution for $c\bar{c}$, $b\bar{b}$, $t\bar{t}$, and $\bar{t}b$ final states at HERA, $\sqrt{s} = 314GeV$, for various trigger cuts on $\sum E_T$: a) All $\sum E_T$, b) $\sum E_T \leq 20GeV$, c) $\sum E_T \leq 60GeV$, d) $\sum E_T \leq 80GeV$. (From ref. [60].

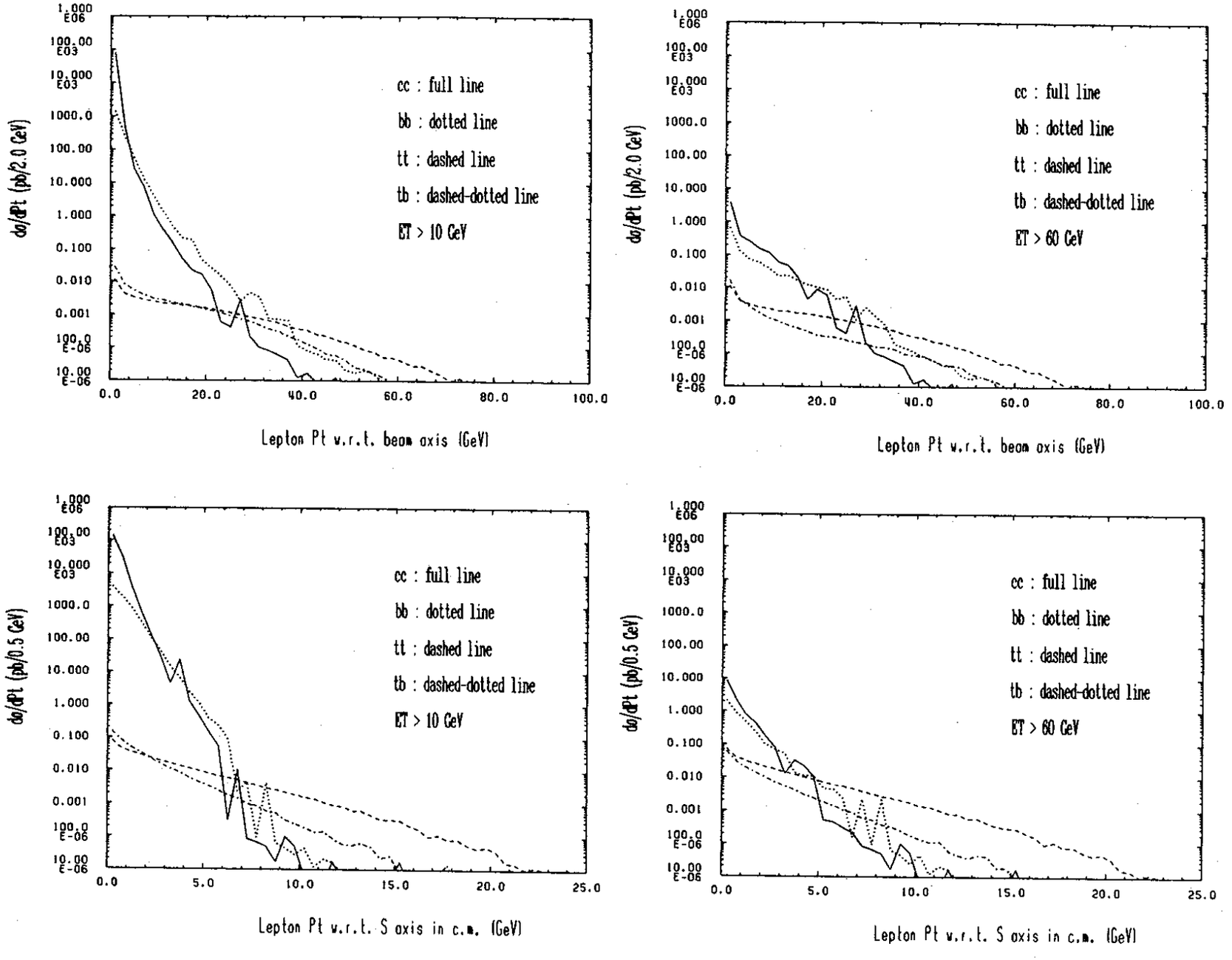

Figure 2.20 Lepton p_T distribution in the process $cp \rightarrow l^{\pm} X$ from the heavy quark (b,c,t) production and decays measured w.r.t. to the sphericity and beam axis for two values of $\sum E_{\perp}$. (From ref. [60]).

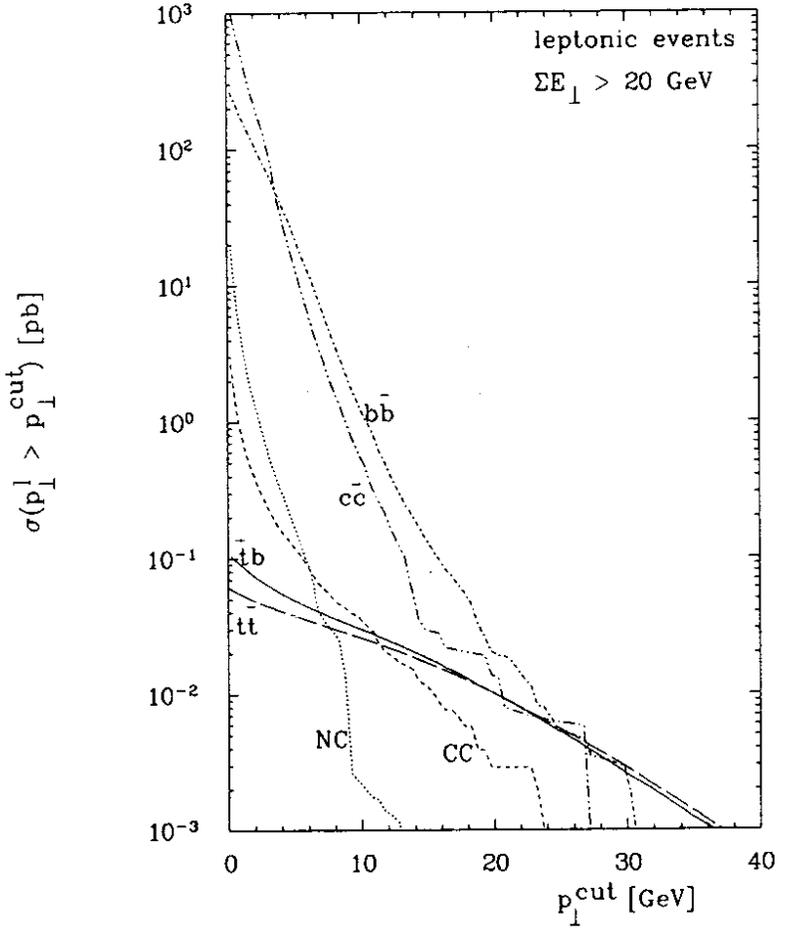

Figure 3.1 Cross section [pb] for single lepton events versus the lower cutoff in the (hardest) lepton transverse momentum $p_\perp^{cut}(l)$ measured w.r.t. the beam axis. The total transverse energy $\sum E_\perp$ is required to be larger than 20 GeV, the beam pipe cut is 100 mrad, and $Q^2 \leq 10\,\mathrm{GeV}^2$ for NC events. (From ref. [49]).

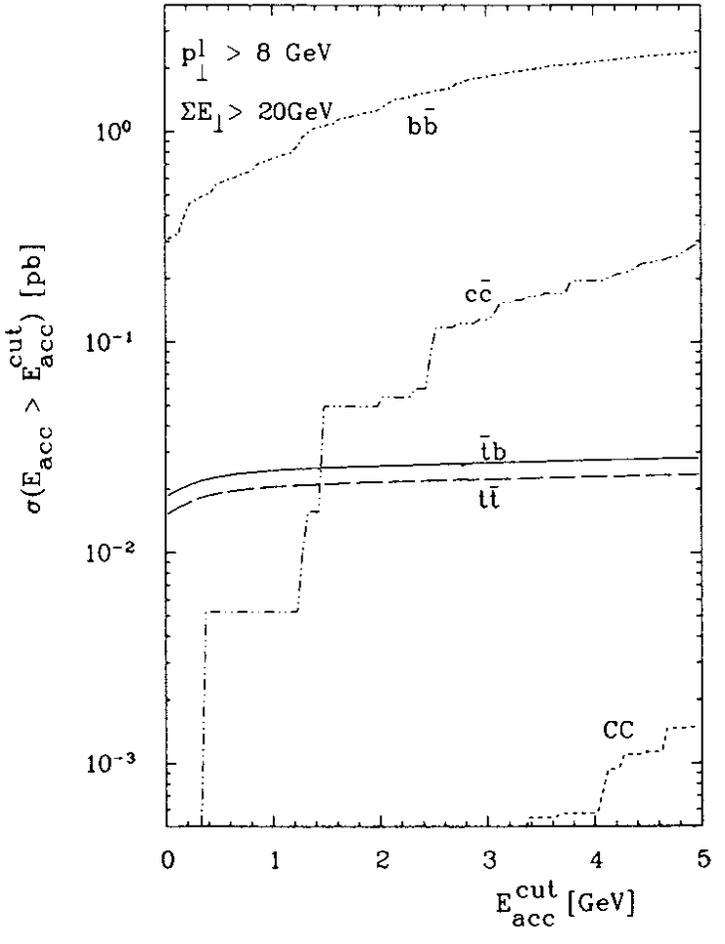

Figure 3.2 Cross section [pb] for single lepton events versus E_{acc}^{cut}, the upper cutoff in the total transverse energy within a cone of $\Delta R = 0.4$ accompanying the hardest lepton of transverse momentum $p_\perp(l) \geq 8\,\mathrm{GeV}$. The total transverse energy $\sum E_\perp$ is required to be larger than 20 GeV, the beam pipe cut is 100 mrad, and $Q^2 \leq 10\,\mathrm{GeV}^2$ for NC events. (From ref. [49]).

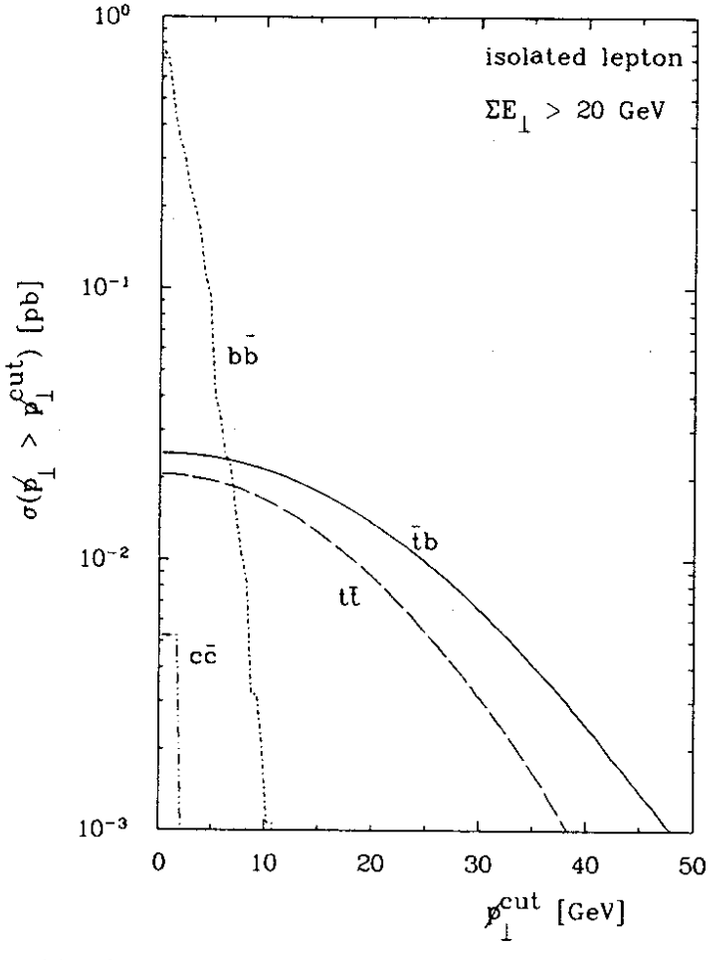

Figure 3.3 Cross section [pb] for isolated lepton events versus the lower cutoff $\not{p}_\perp^{cut}$ in the missing transverse momentum. The total transverse energy $\sum E_\perp$ is required to be larger than 20 GeV, the beam pipe cut is 100 mrad, and $Q^2 \leq 10\,\mathrm{GeV}^2$ for NC events. (From ref. [49]).

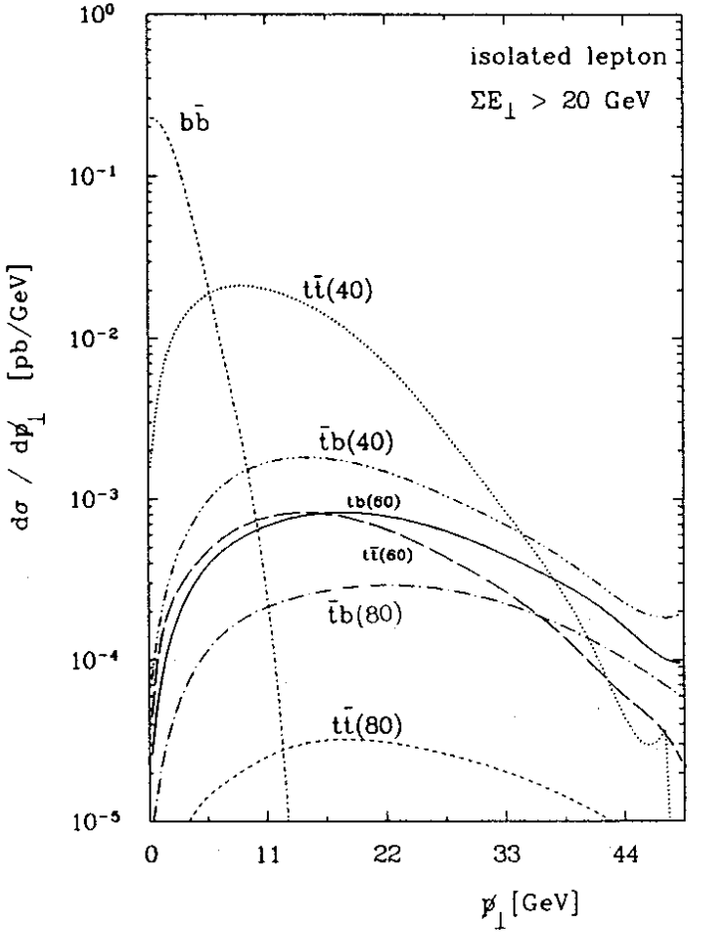

Figure 3.4 Differential cross section $d\sigma/d\not{p}_\perp$ [pb/GeV] in missing transverse momentum for the total background and the top signal for three different top masses. The applied cuts are: events contain an isolated lepton, the total transverse energy $\sum E_\perp \geq 20$ GeV, the beam pipe cut is 100 mrad, and $Q^2 \leq 10\,\mathrm{GeV}^2$ for NC events. (From ref. [49]).

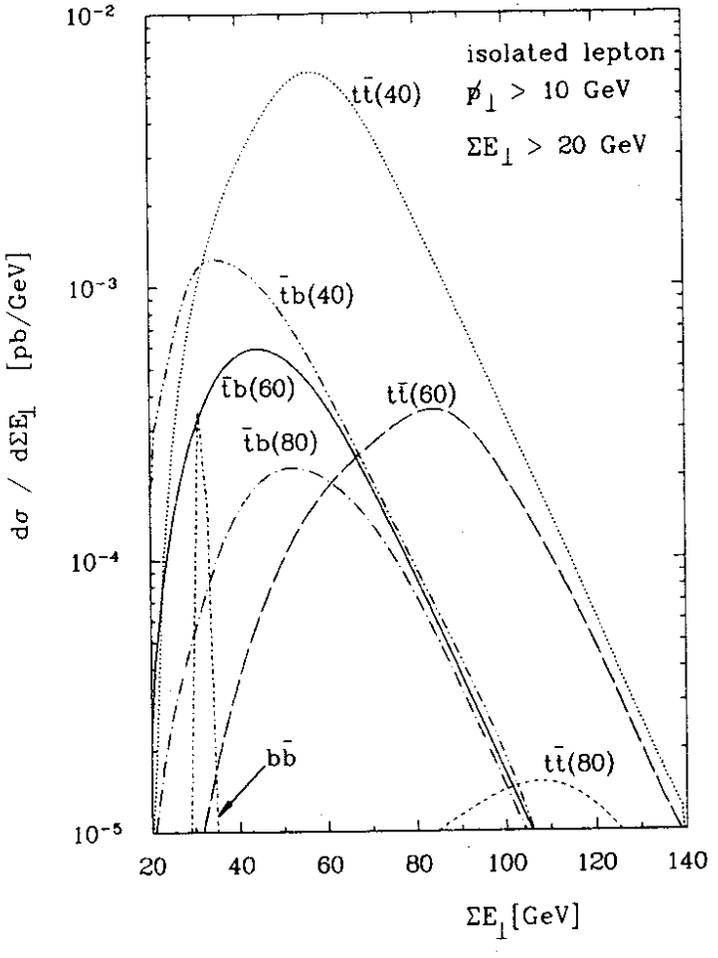

Figure 3.5 Differential cross section $d\sigma/d\sum E_\perp$ [pb/GeV] in the total transverse energy for the total background and the top signal for three different top masses. The applied cuts are: events contain an isolated lepton, the total transverse energy $\sum E_\perp \geq 20$ GeV, the missing transverse momentum $\not{p}_\perp \geq 10$ GeV, the beam pipe cut is 100 mrad, and $Q^2 \leq 10\,\mathrm{GeV}^2$ for NC events. (From ref. [49]).

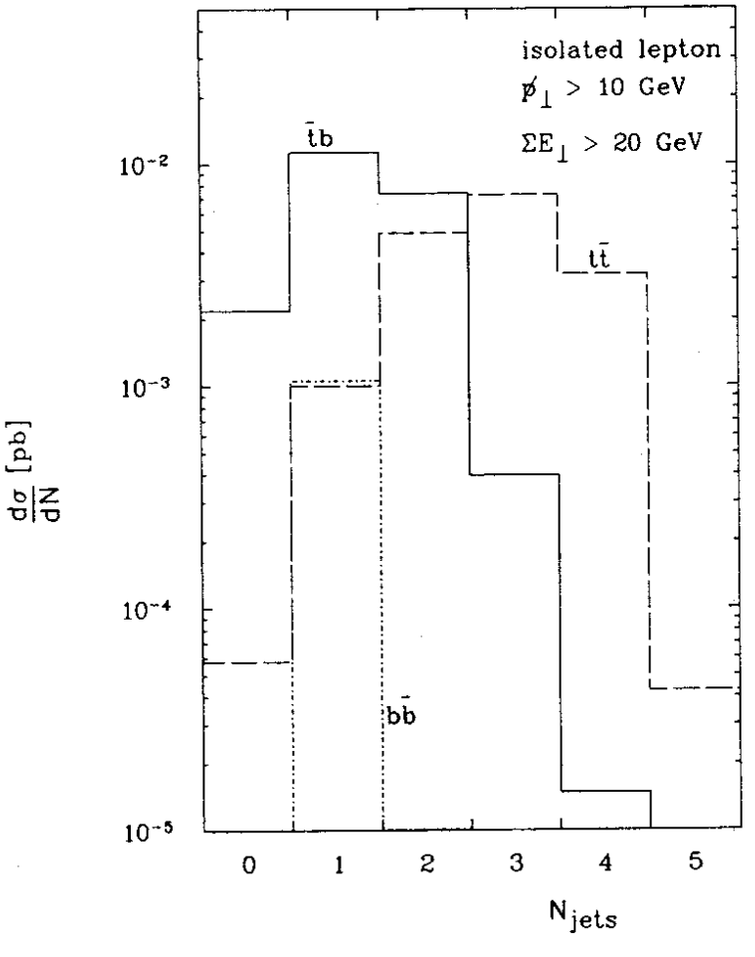

Figure 3.6 Differential cross section $d\sigma/d\,N\,jets$ [pb] in number of jets for the background and the top signal (m_t = 60 GeV). The applied cuts are: events contain an isolated lepton, the total transverse energy $\sum E_\perp \geq 20$ GeV, the missing transverse momentum $\not{p}_\perp \geq 10$ GeV, the beam pipe cut is 100 mrad, and $Q^2 \leq 10\,\mathrm{GeV}^2$ for NC events. (From ref. [49]).

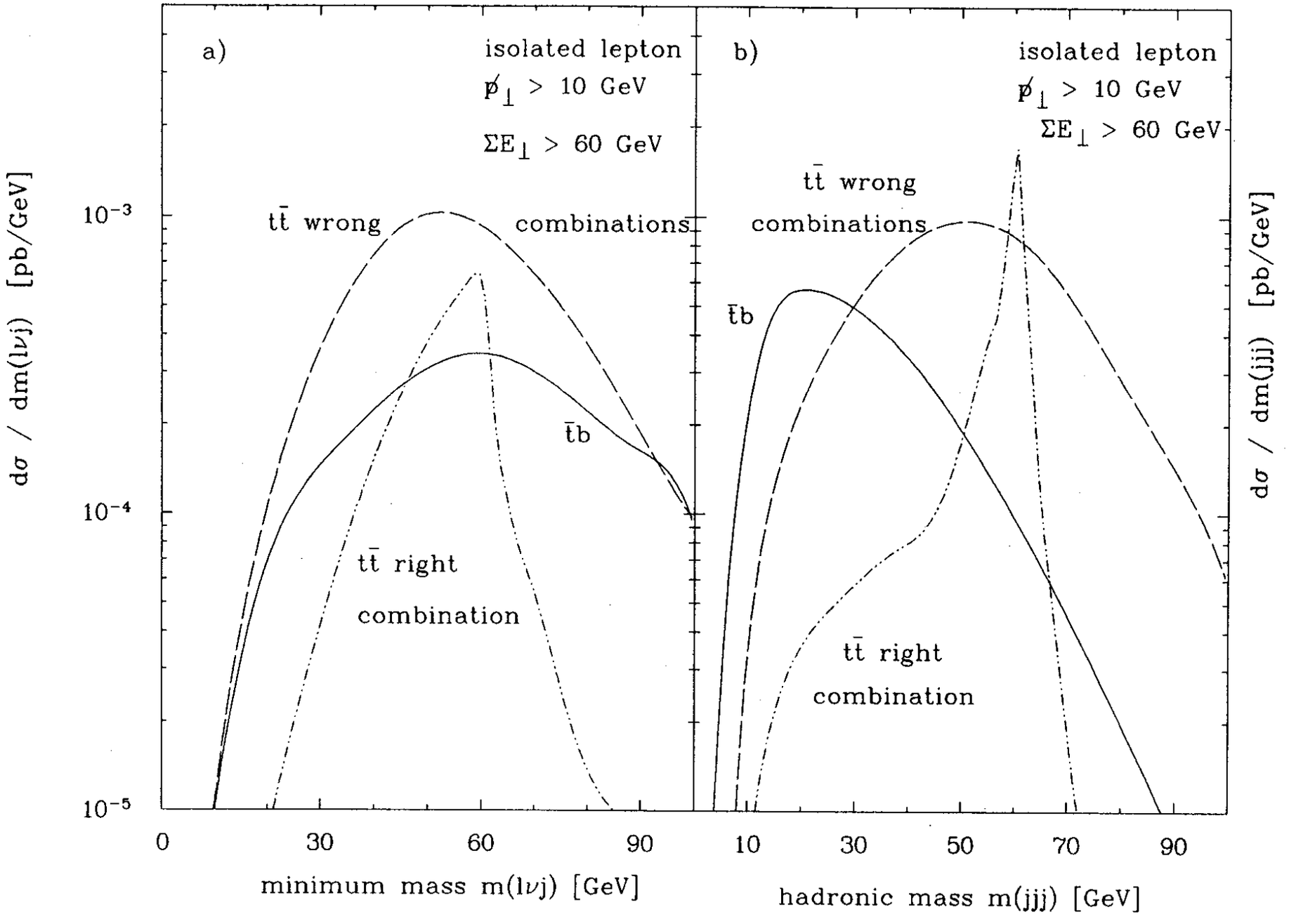

Figure 3.7 Differential cross section $d\sigma/dm$ [pb/GeV] in the reconstructed minimum (leptonic) mass $m_l \equiv m(l\nu j)$ (a) and hadronic mass $m_h \equiv m(jjj)$ (b). The applied cuts are: events contain an isolated lepton, the total transverse energy $\sum E_\perp \geq 60$ GeV, the missing transverse momentum $\not{p}_\perp \geq 10$ GeV, the beam pipe cut is 100 mrad, and $Q^2 \leq 10$ GeV^2 for NC events. (From ref. [49]).

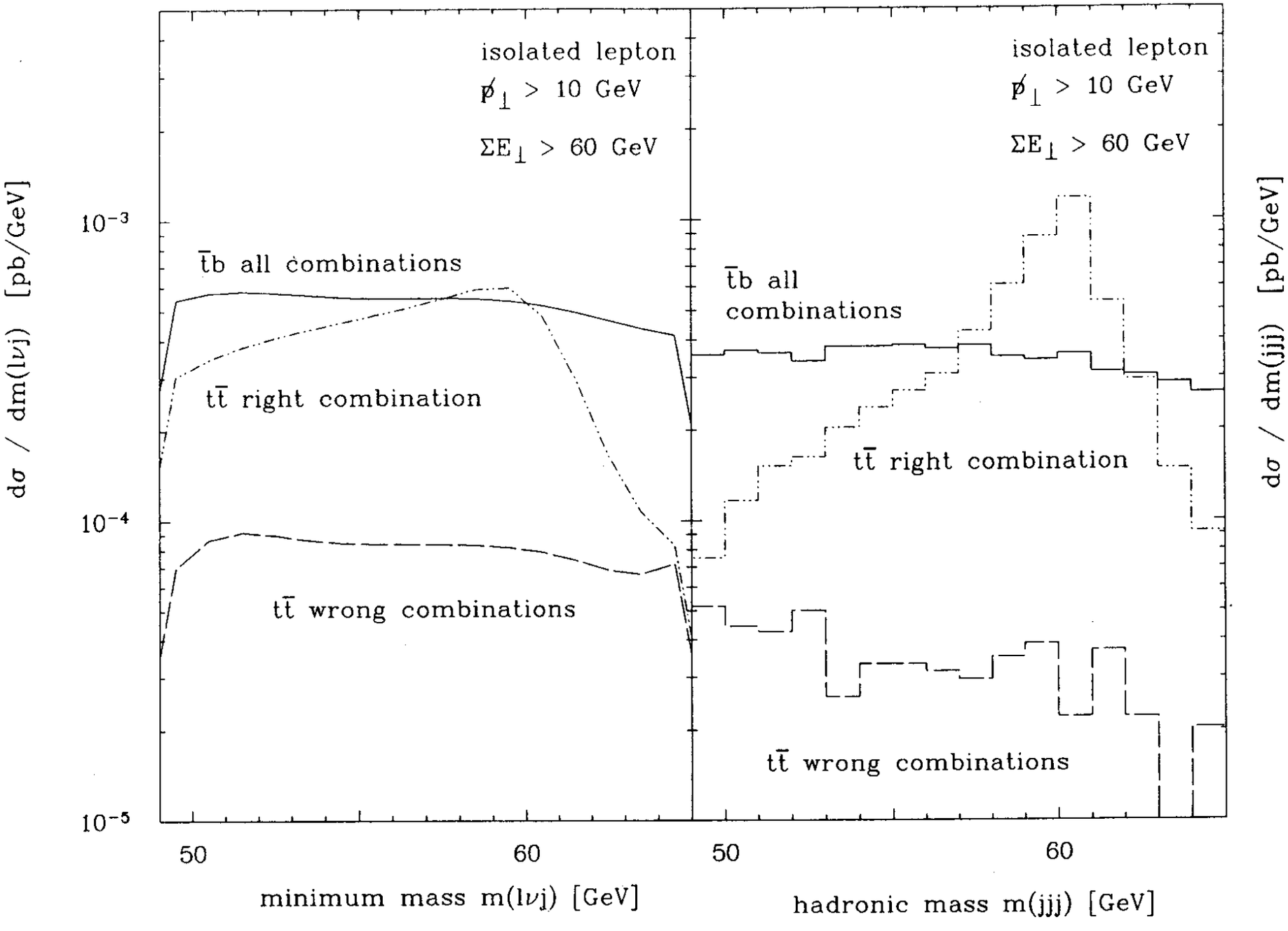

Figure 3.8 The same as Figure 3.7 but after a selection of a window in the hadronic (leptonic) mass for the leptonic (a) (hadronic (b)) mass distribution: $m_h \in [40\,\text{GeV}, 65\,\text{GeV}]$, $m_l \in [50\,\text{GeV}, 65\,\text{GeV}]$. (From ref. [49]).

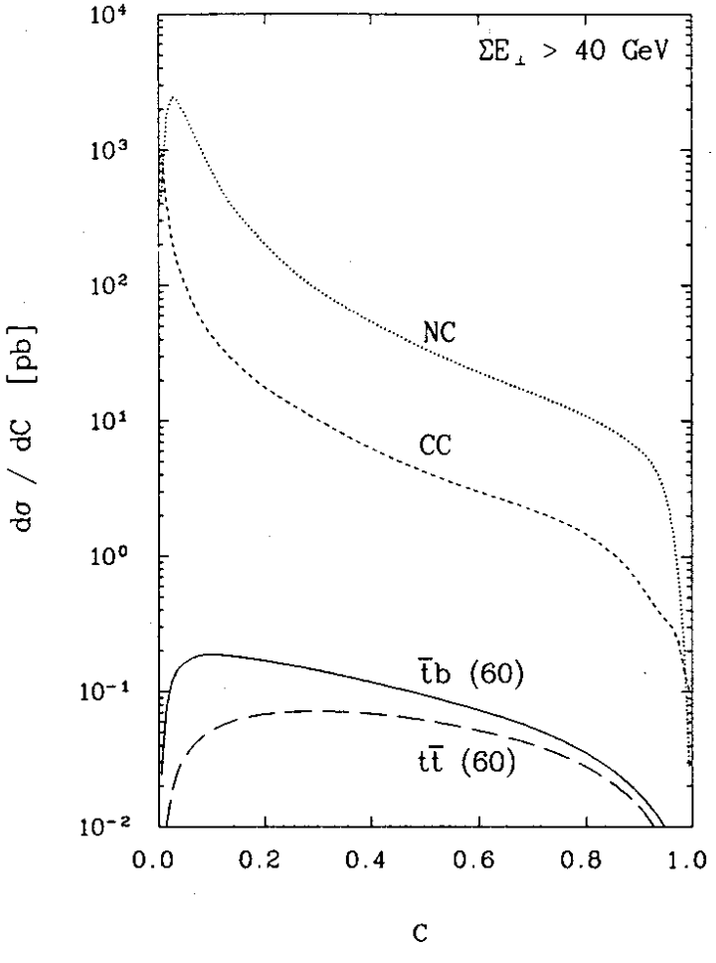

Figure 3.9 Differential cross section $d\sigma/dC$ [pb] in circularity for total NC background, total CC background and the top signal, seperatly for $\bar{t}b$ and $t\bar{t}$ events. The applied cuts are: events do not contain an isolated lepton, the total transverse energy $\sum E_\perp \geq 40\,\mathrm{GeV}$, $Q^2 \leq 10\,\mathrm{GeV}^2$ for NC events, and the beam pipe cut is 100 mrad. (From ref. [49]).

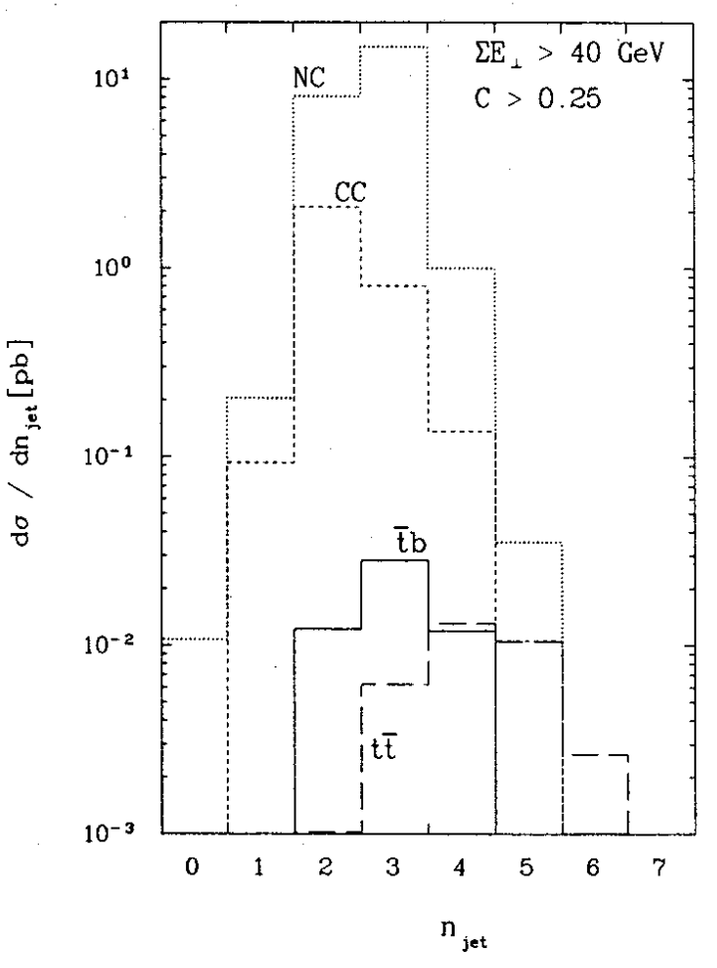

Figure 3.10 Differential cross section $d\sigma/d\,Njets$ [pb] in the number of jets for the total NC and CC background and the top signal ($m_t = 60\,\mathrm{GeV}$). The applied cuts are: events do not contain an isolated lepton, the total transverse energy $\sum E_\perp \geq 40\,\mathrm{GeV}$, $Q^2 \leq 10\,\mathrm{GeV}^2$ for NC events, the circularity $C \geq 0.25$, and the beam pipe cut is 100 mrad. (From ref. [49]).

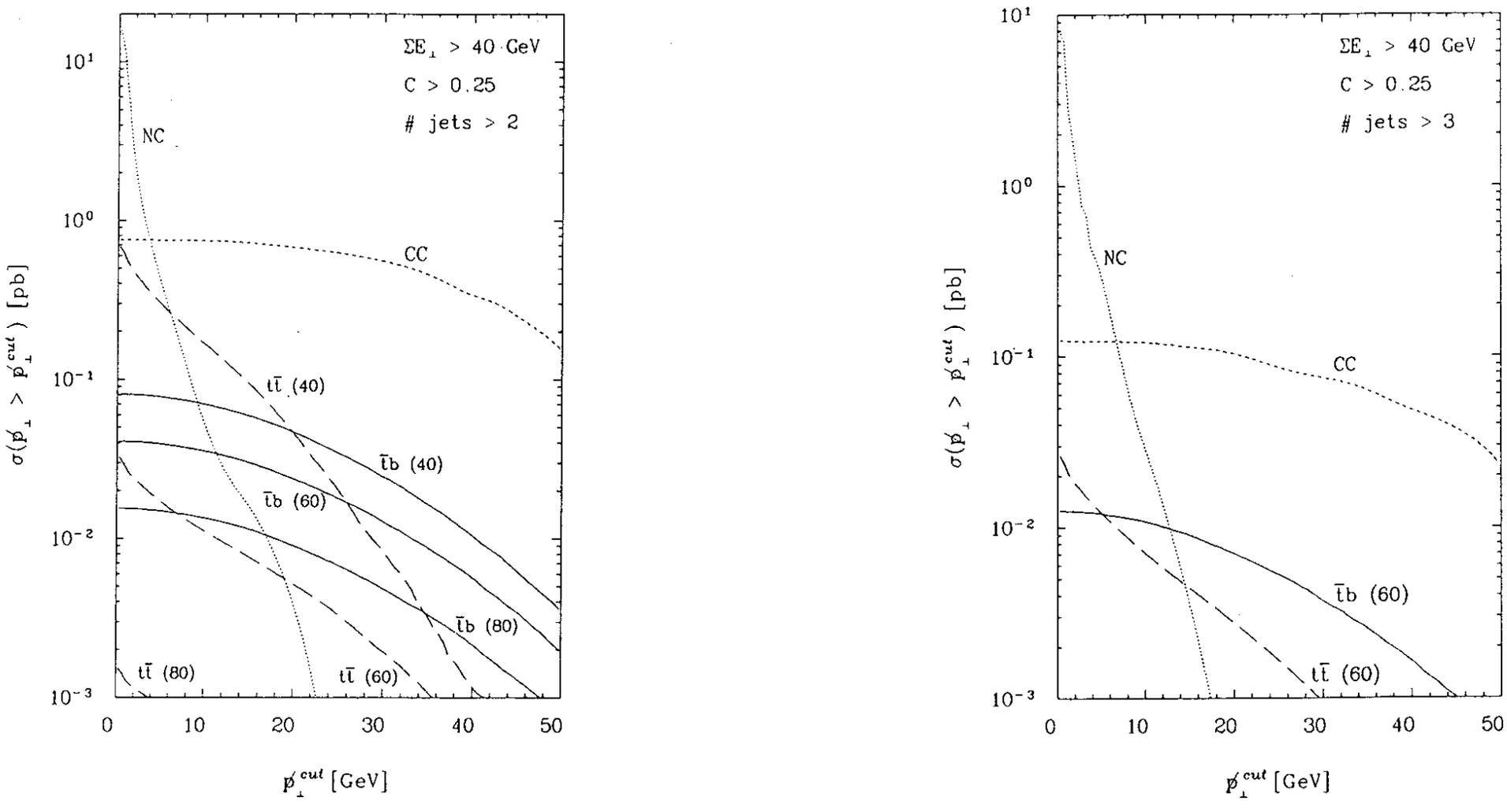

Figure 3.11 Integrated cross section $\sigma(\not{p}_\perp \geq \not{p}_\perp^{cut})$ for the total NC and CC background and the top signal. a) The distributions for events containing at least three jets, with the top mass 40, 60 and 80 GeV . b) The distributions for events containing at least four jets with $m_t = 60$ GeV. The additional cuts for both a) and b) are: events do not contain an isolated lepton, the total transverse energy $\sum E_\perp \geq 40\,\mathrm{GeV}$, $Q^2 \leq 10\,\mathrm{GeV}^2$ for NC events, the circularity $C \geq 0.25$, and the beam pipe cut is 100 mrad. (From ref. [49]).

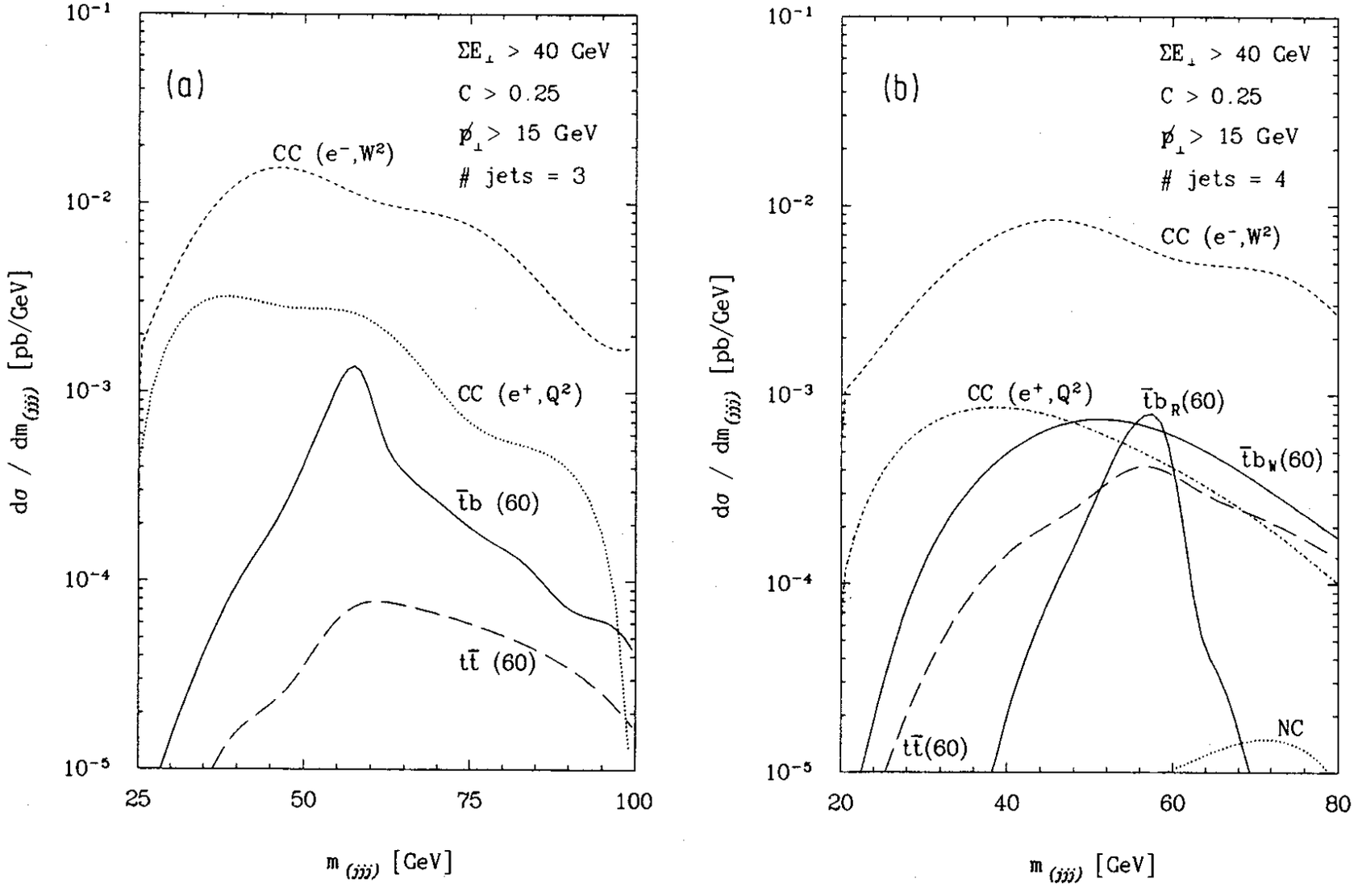

Figure 3.12 Differential cross section $d\sigma/dm$[pb/GeV] for the reconstructed mass $m(jjj)$ (m_t = 60 GeV) where $m(jjj)$ is the invariant mass of three jets. Figure 3.12 a) is for three jet events, (b) for four jet events. In (b) the sum of all four combinations of $\bar{t}t$ and background events, and the sum of the three wrong combinations and the right combination of $\bar{t}b$ events are shown. The curve marked by $CC(e^-, W^2)$ ($CC(e^+, Q^2)$) gives the CC background in electron (positron) scattering using W^2 (Q^2) as mass scale in the parton cascades. All other cuts are as in Figure 3.11. (From ref. [49]).

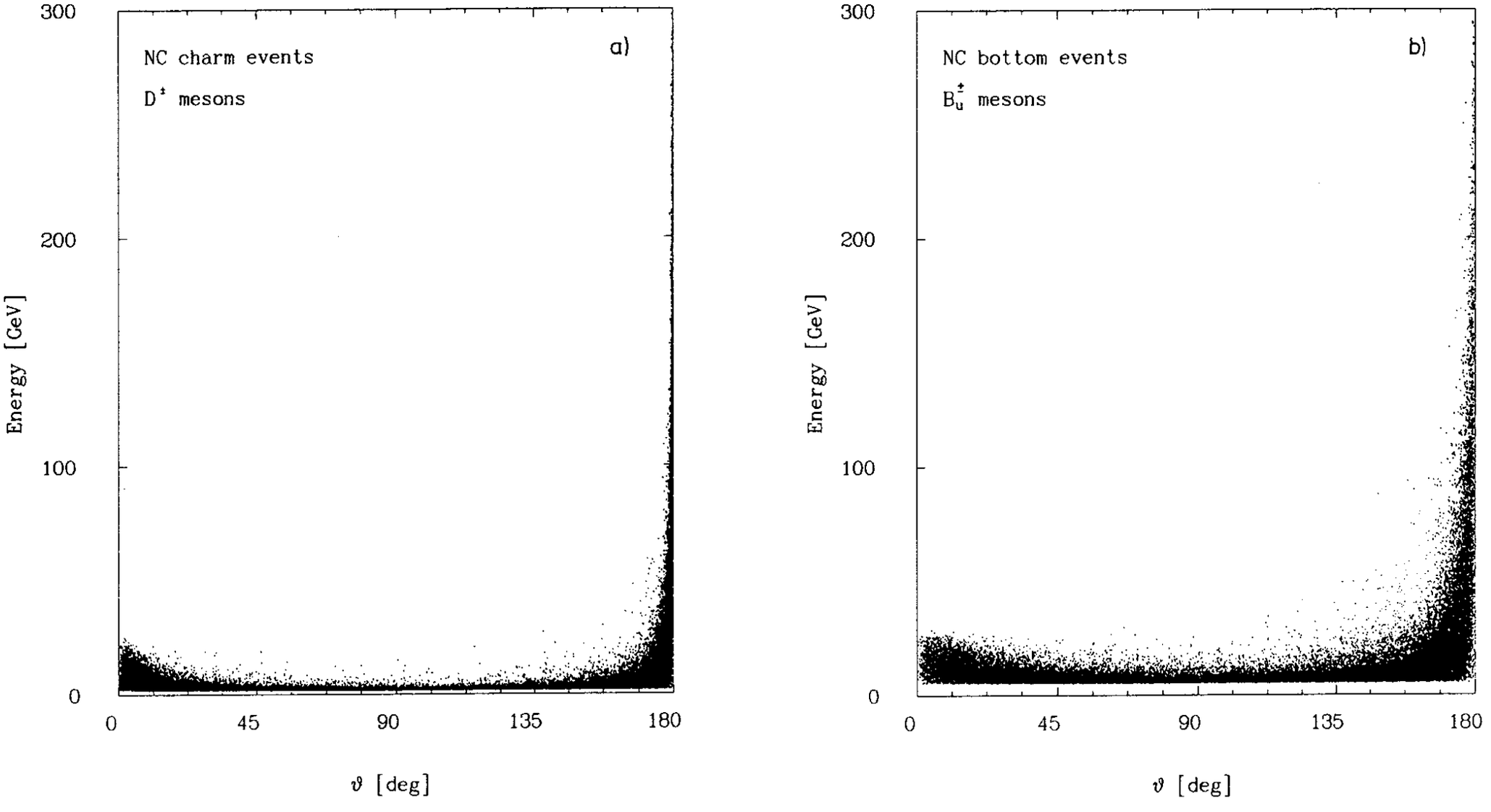

Figure 4.1 Scatter plot showing the correlation between the energy and polar angle of the heavy mesons produced in the NC process $ep \rightarrow eQ\bar{Q}X$, a) Q=c, b) Q=b. (From ref. [60])

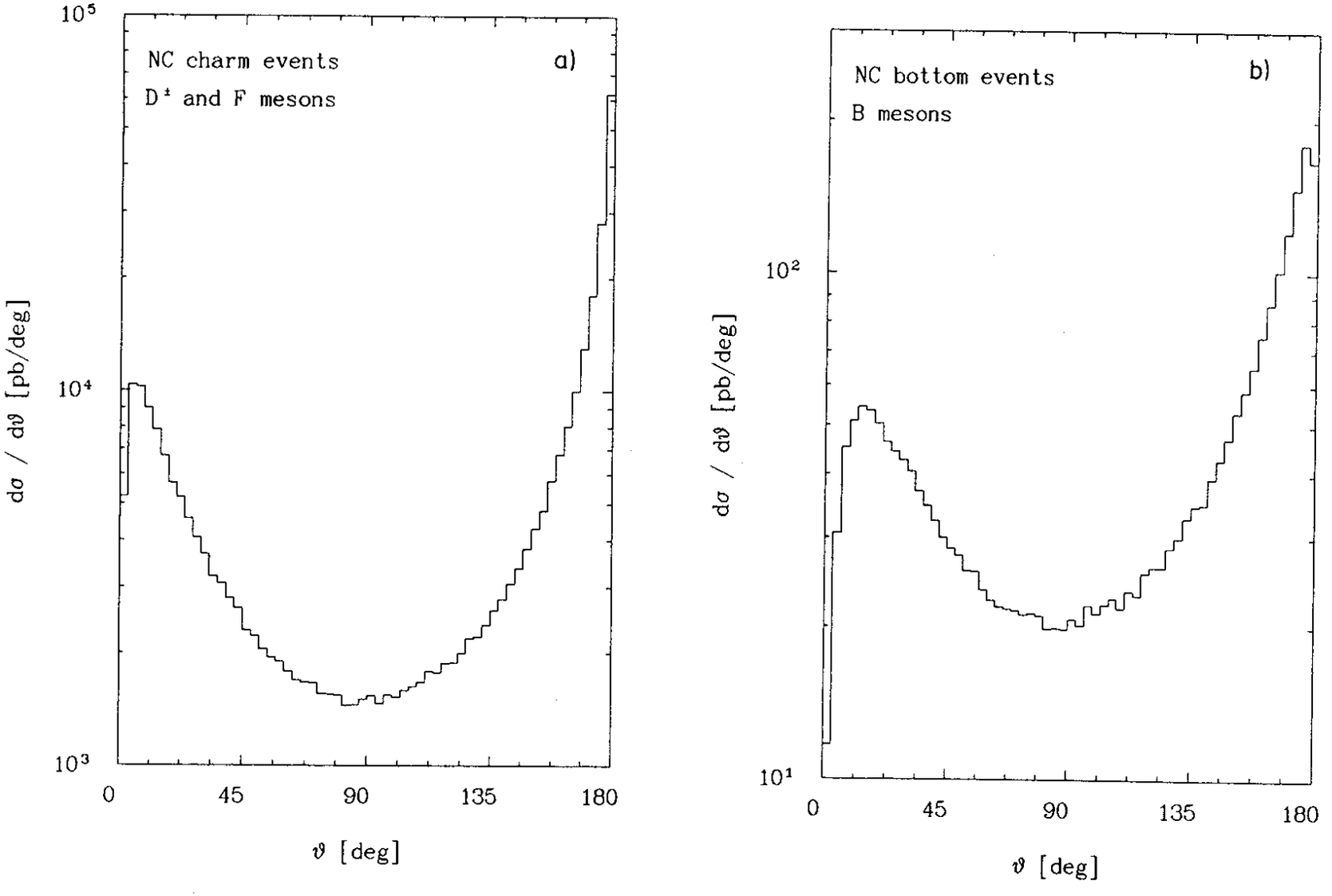

Figure 4.2 Polar angle distribution of the heavy mesons produced in the NC process $ep \to eQ\bar{Q}X$ calculated at HERA energy $\sqrt{s} = 314\ GeV$, a) Q=c, b)Q=b. (From ref. [60])

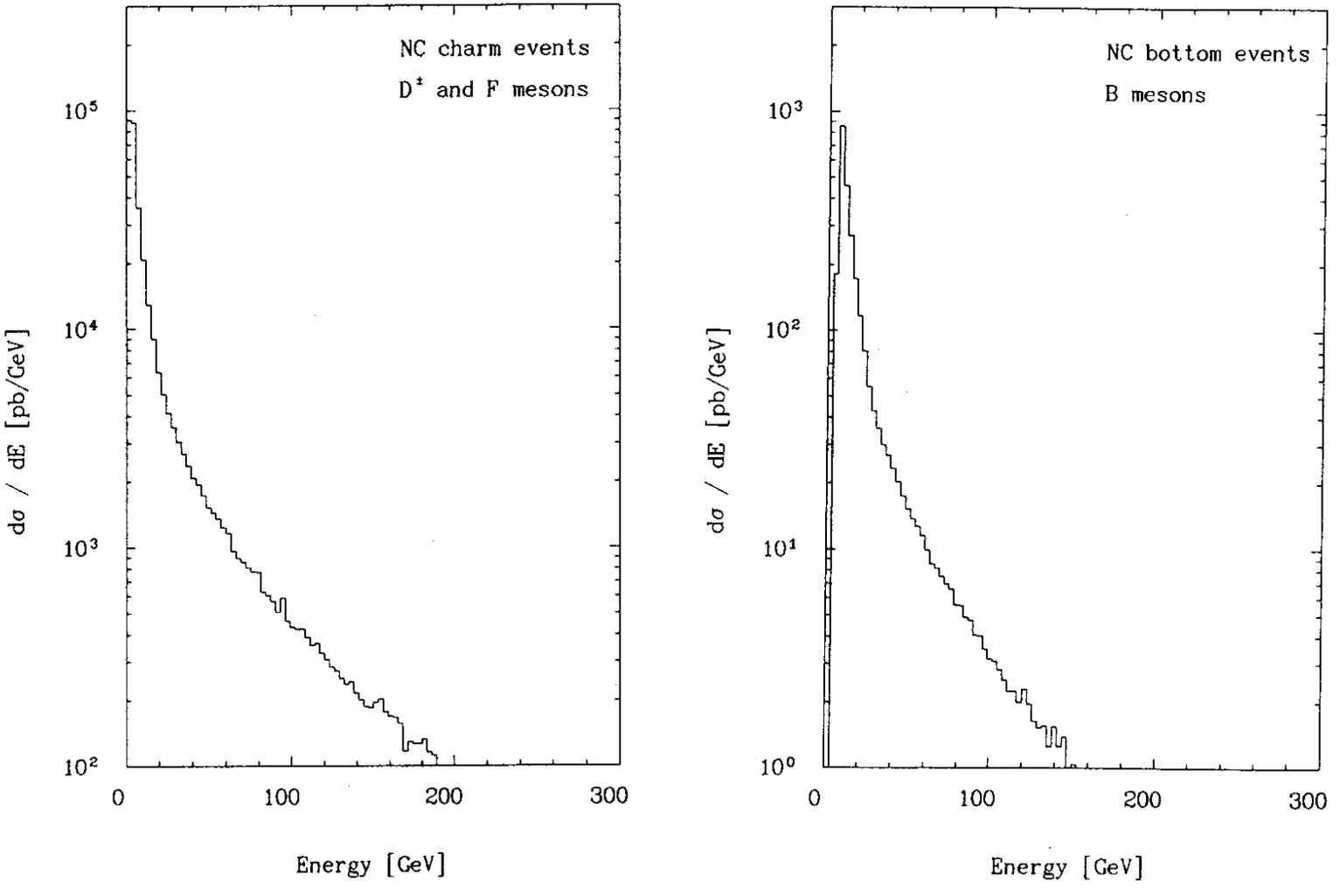

Figure 4.3 Energy distribution for bottom mesons produced in the NC process $ep \to eb\bar{b}X$ calculated at HERA energy $\sqrt{s} = 314\ GeV$. (From ref. [60])

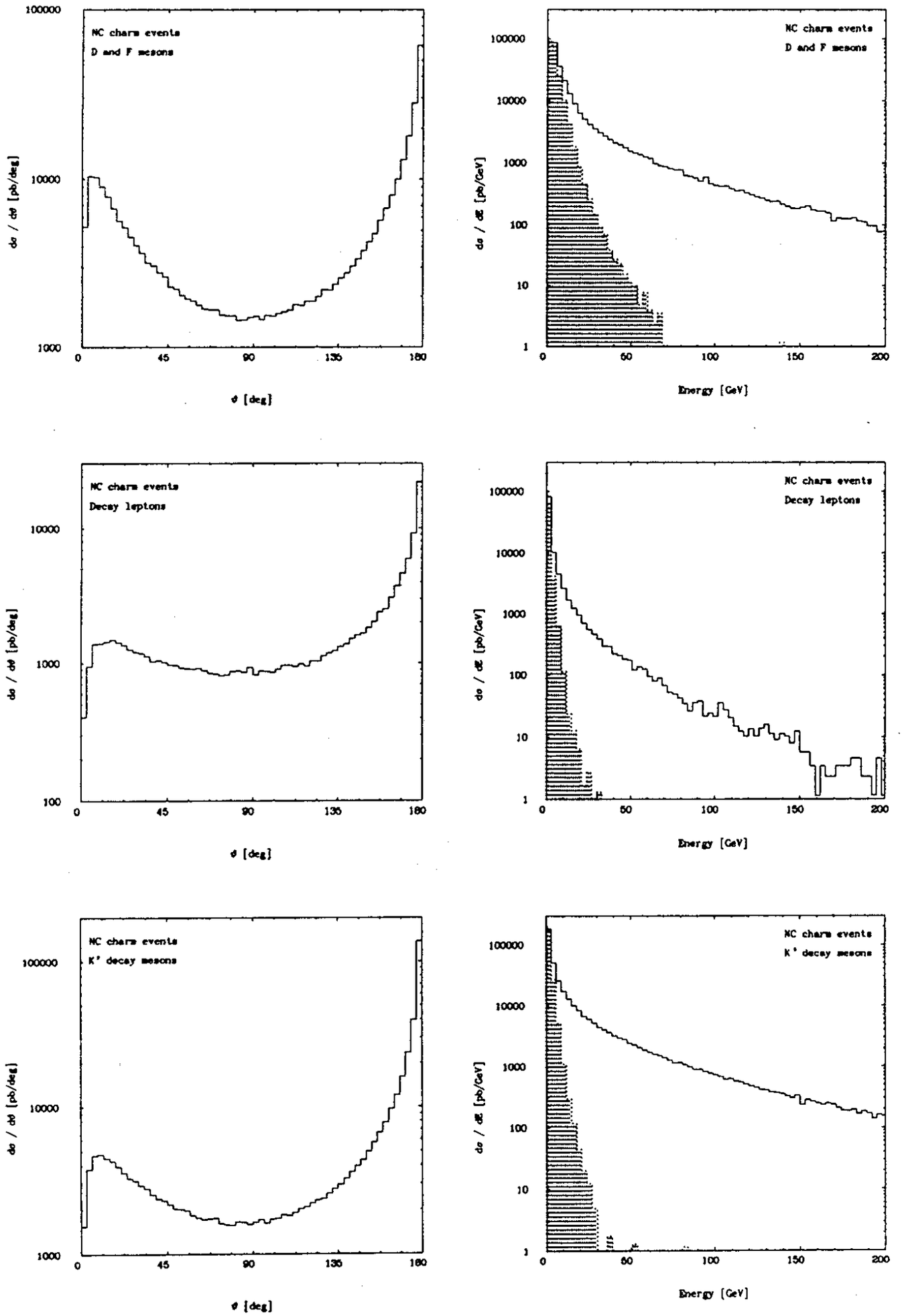

Figure 4.4 Energy and polar angle distributions for D and F mesons, decay kaons and leptons, produced in the NC process $ep \rightarrow e c\bar{c} X$ and subsequent charm decays calculated at HERA energy $\sqrt{s} = 314\ GeV$. The energy distributions resulting after imposing a beam pipe cut of 100 mrad are represented by the shaded areas. (From ref. [60])

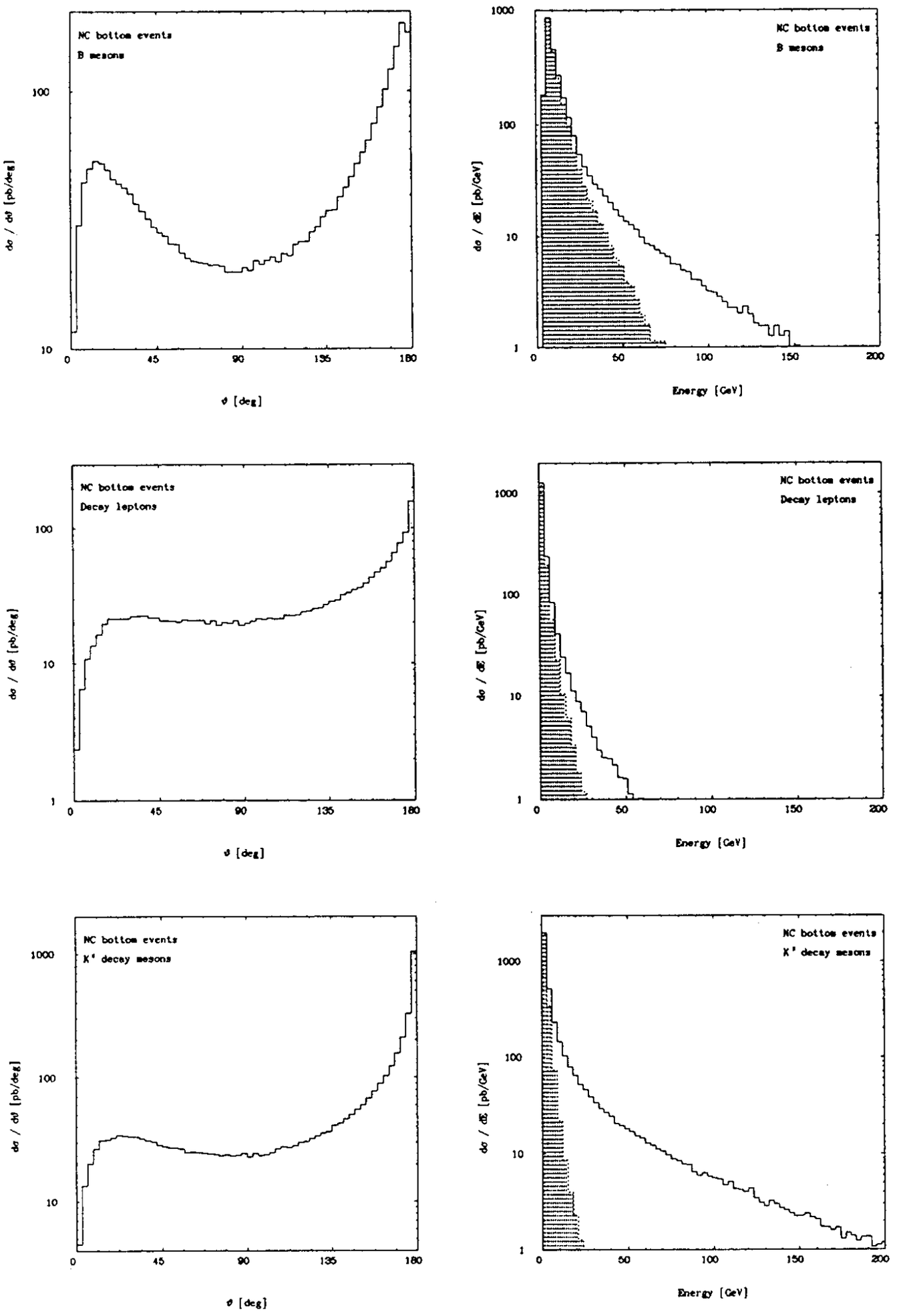

Figure 4.5 Energy and polar angle distributions for B mesons, decay kaons and leptons, produced in the NC process $ep \rightarrow eb\bar{b}X$ and subsequent bottom decays calculated at HERA energy $\sqrt{s} = 314\ GeV$. The energy distributions resulting after imposing a beam pipe cut of 100 mrad are represented by the shaded areas. (From ref. [60])

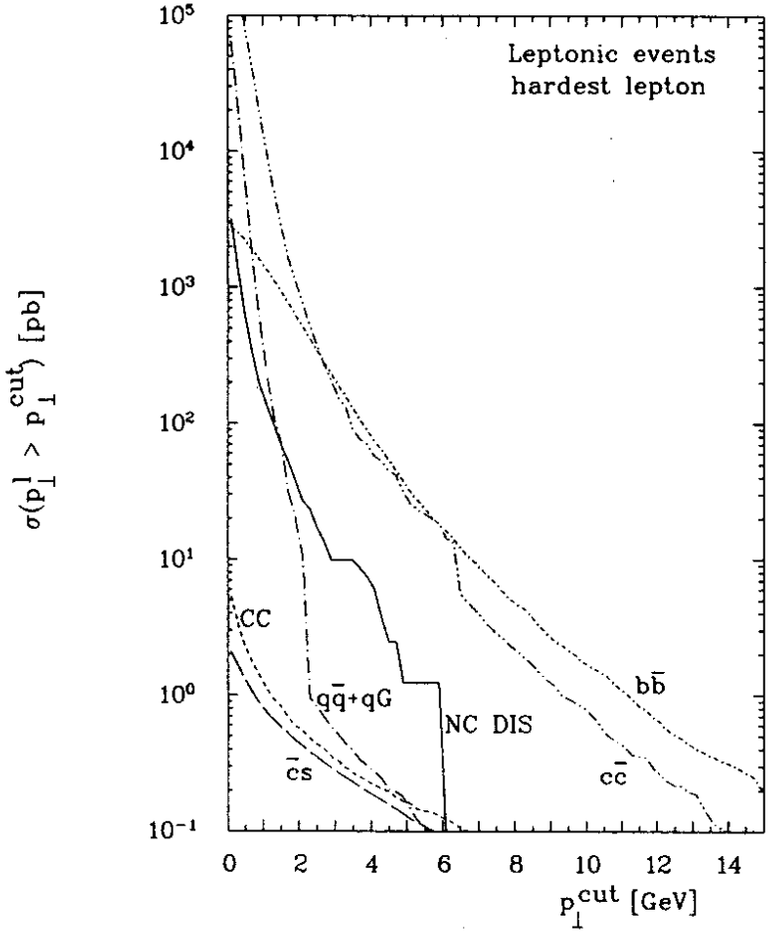

Figure 4.6 Integrated cross section for the process $ep \to (e, \nu_e)l^{\pm}X$ as a function of a cut on the $p_\perp$ of the hardest lepton at HERA energy $\sqrt{s} = 314\ GeV$. The beam pipe cut is 100 mrad. (From ref. [60])

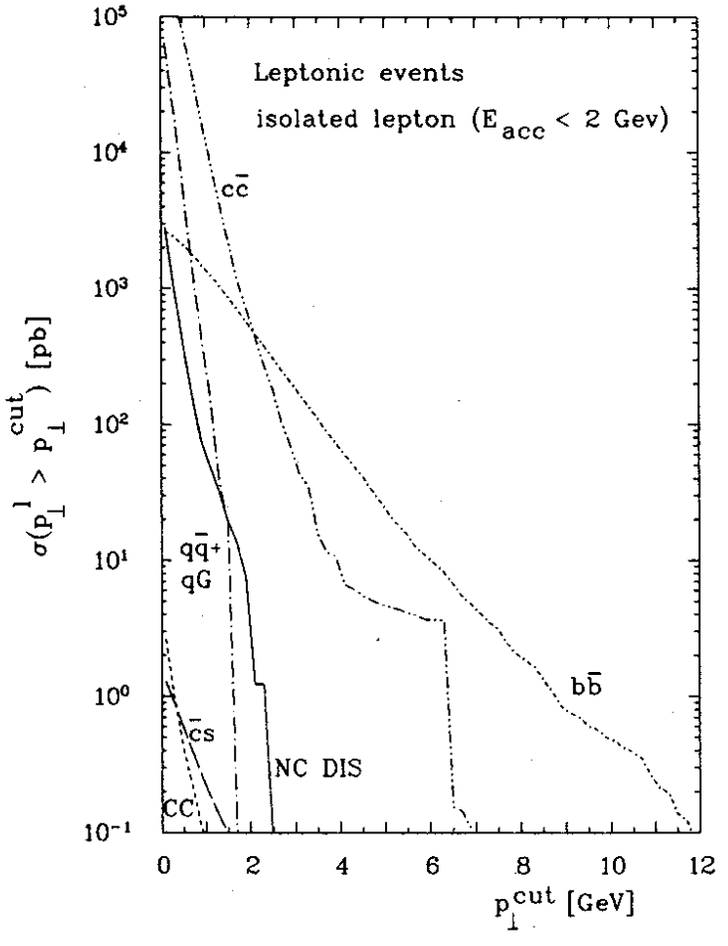

Figure 4.7 Same as Fig. 4.6 but for an isolated lepton defined by $E_{acc} \leq 2$ GeV. (From ref. [60])

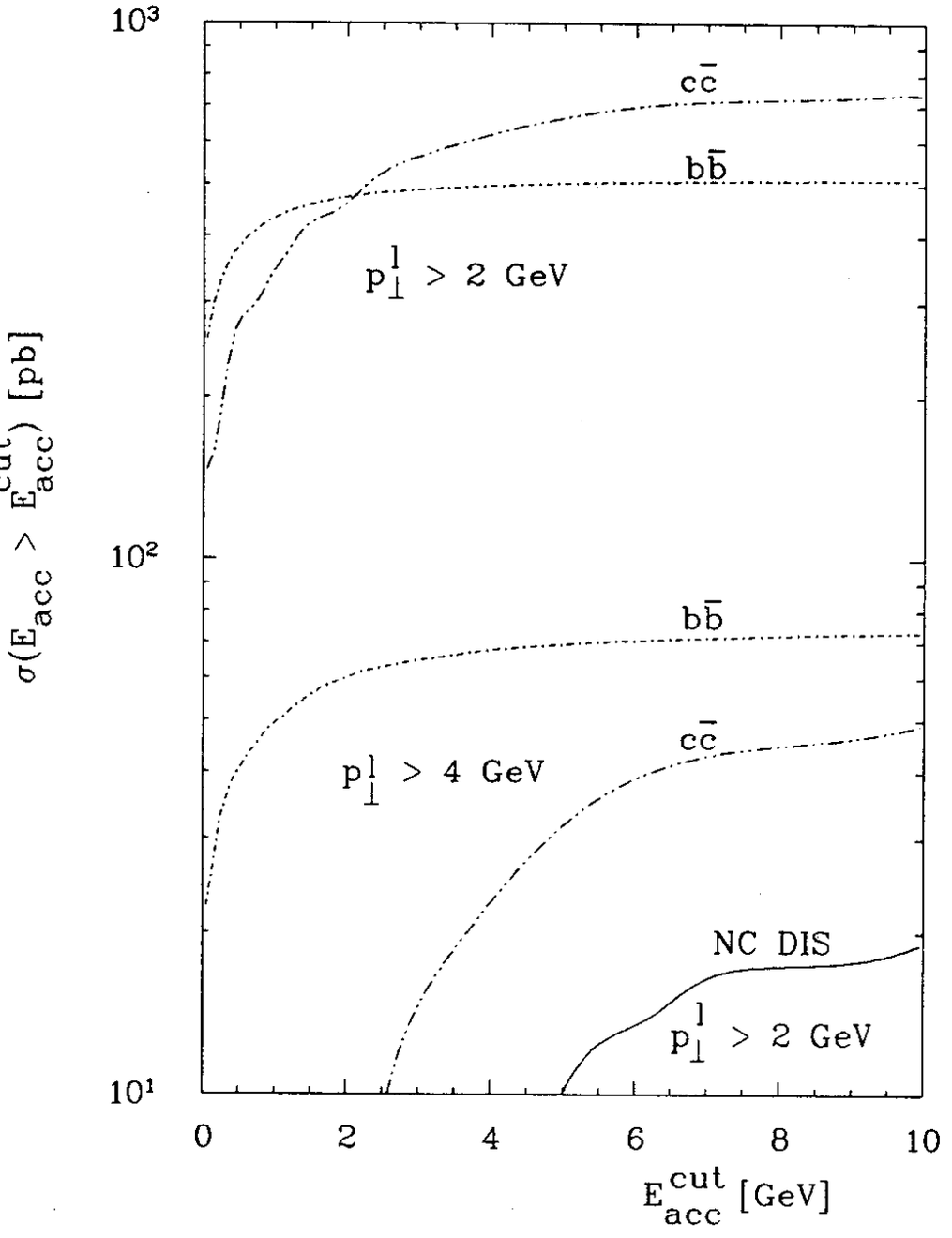

Figure 4.8 Integrated cross section $\sigma(E_{acc} \geq E_{acc}^{cut})$ for the process $ep \rightarrow (e, \nu_e)l^{\pm}X$ as a function of a cut on the energy accompanying the hardest lepton in a cone defined by $\Delta R \leq 0.7$. Shown are the two cases where the hardest lepton is required to have a minimum $p_\perp$ of at least 2 and 4 GeV. The beam pipe cut is 100 mrad.

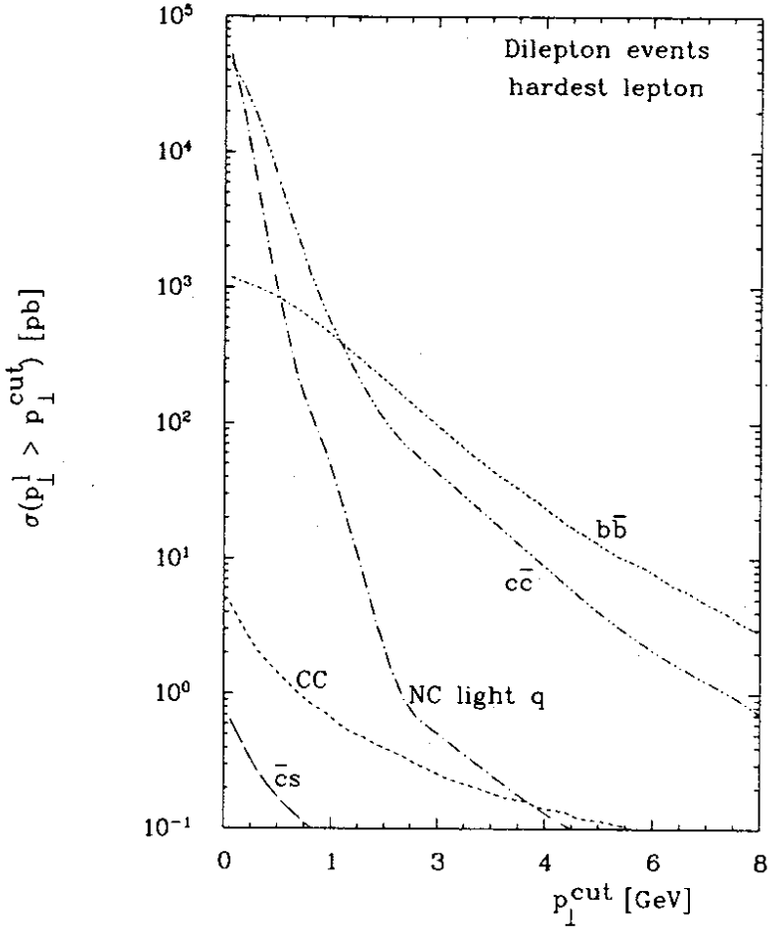

Figure 4.9 Integrated cross section for the process $ep \to (e, \nu_e) l^- l^+ X$ as a function of the cut on the p_T of the hardest lepton in dilepton events for charm, bottom, light quark and gluon, and CC production processes at HERA energy $\sqrt{s} = 314\ GeV$. The beam pipe cut is $100 mrad$. (From ref. [60])

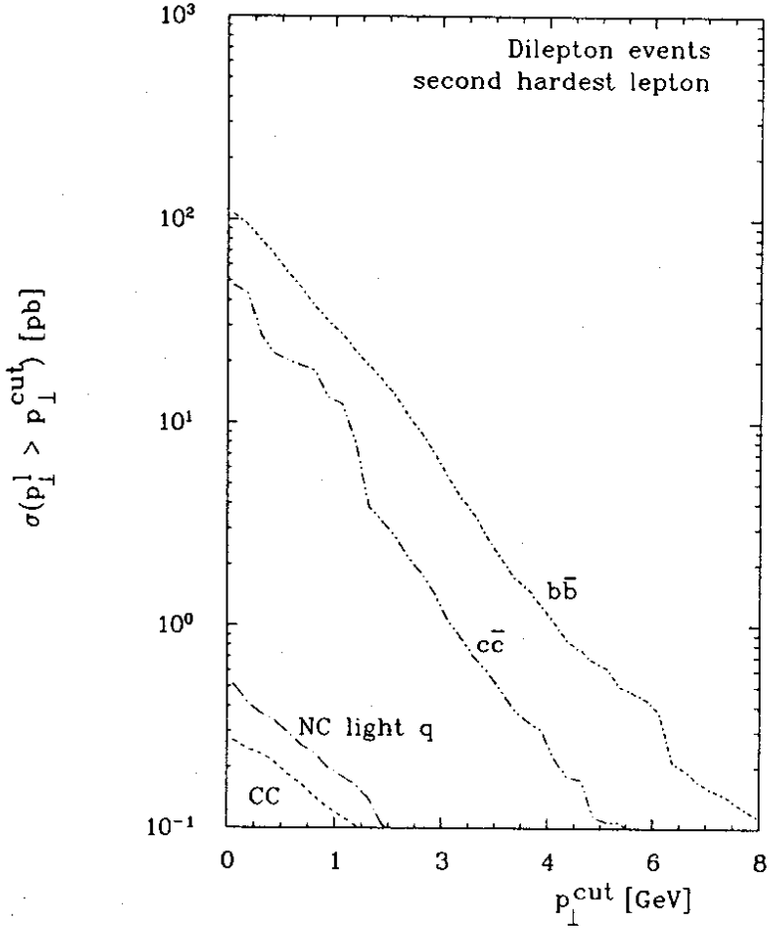

Figure 4.10 Integrated cross section for the process $ep \to (e, \nu_e)\ l\ l\ X$ as a function of a cut on the $p_\perp$ of the second hardest lepton in dilepton events for charm, bottom, light quark + gluon and CC production processes at HERA energy $\sqrt{s}$ = 314 GeV. The hardest lepton is required to have $p_\perp \geq 2$ GeV. The beam pipe cut is 100 mrad. (From ref. [60])

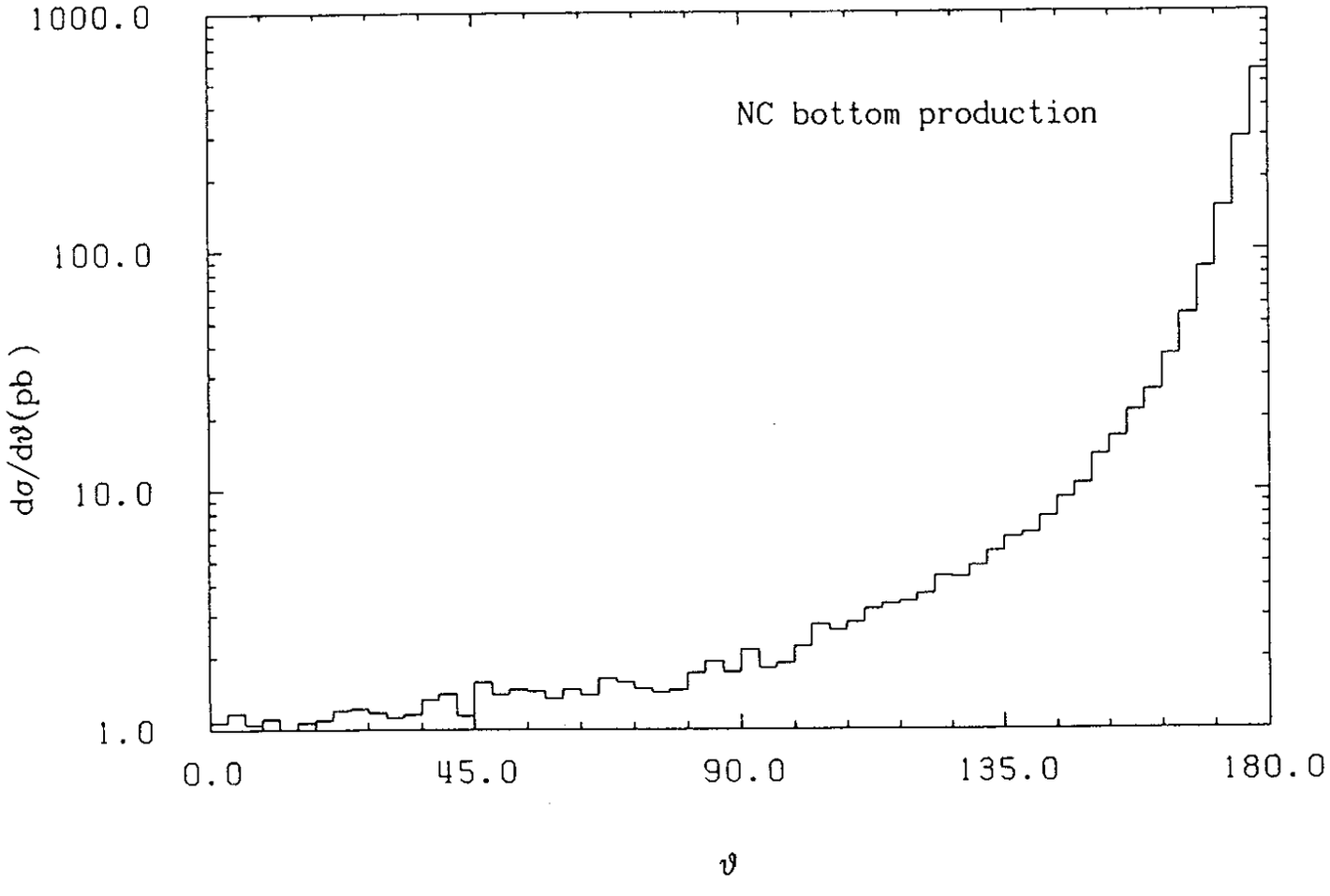

Figure 4.11 Azimuthal angle distribution in the process $ep \to e b\bar{b} X$ evaluated for HERA energy $\sqrt{s} = 314$ GeV. (From ref. [60])

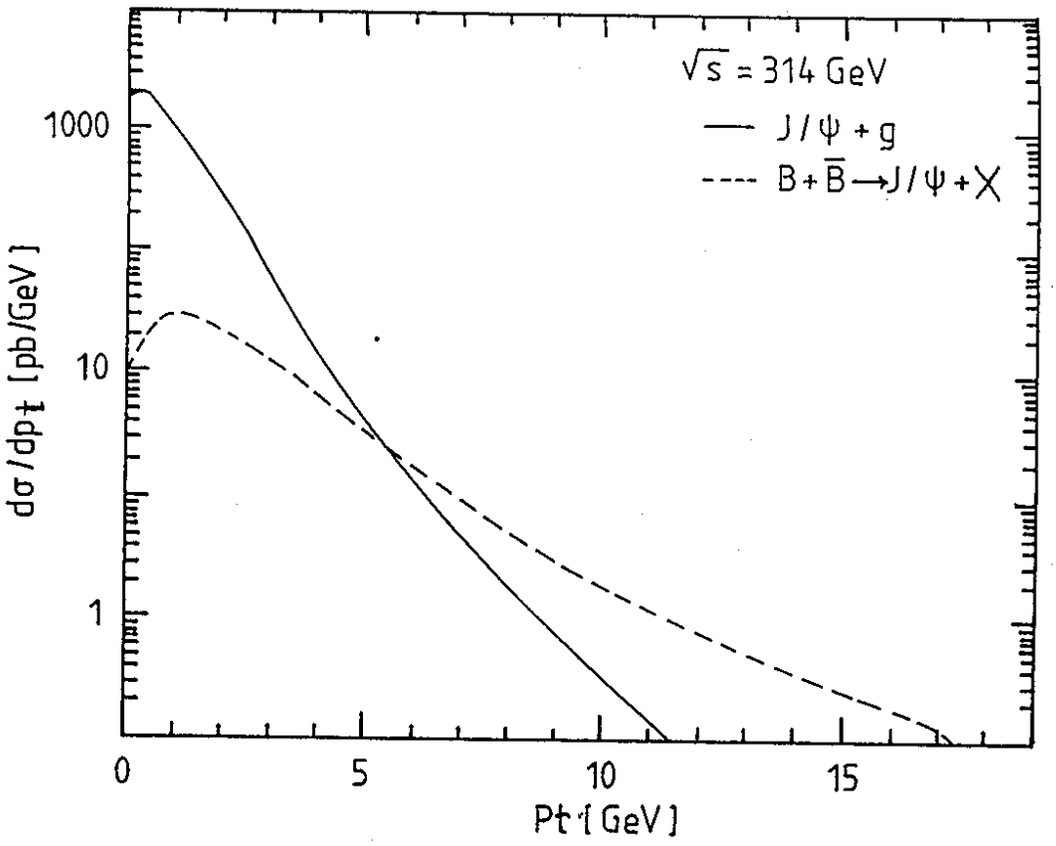

Figure 4.12 Transverse momentum distributions of J/Ψ produced via the subprocess (4.2) (solid line) and via bottom production and decay into J/Ψ (4.3) (dashed line) in ep collisions at HERA energy $\sqrt{s} = 314$ GeV. (From ref. [16])

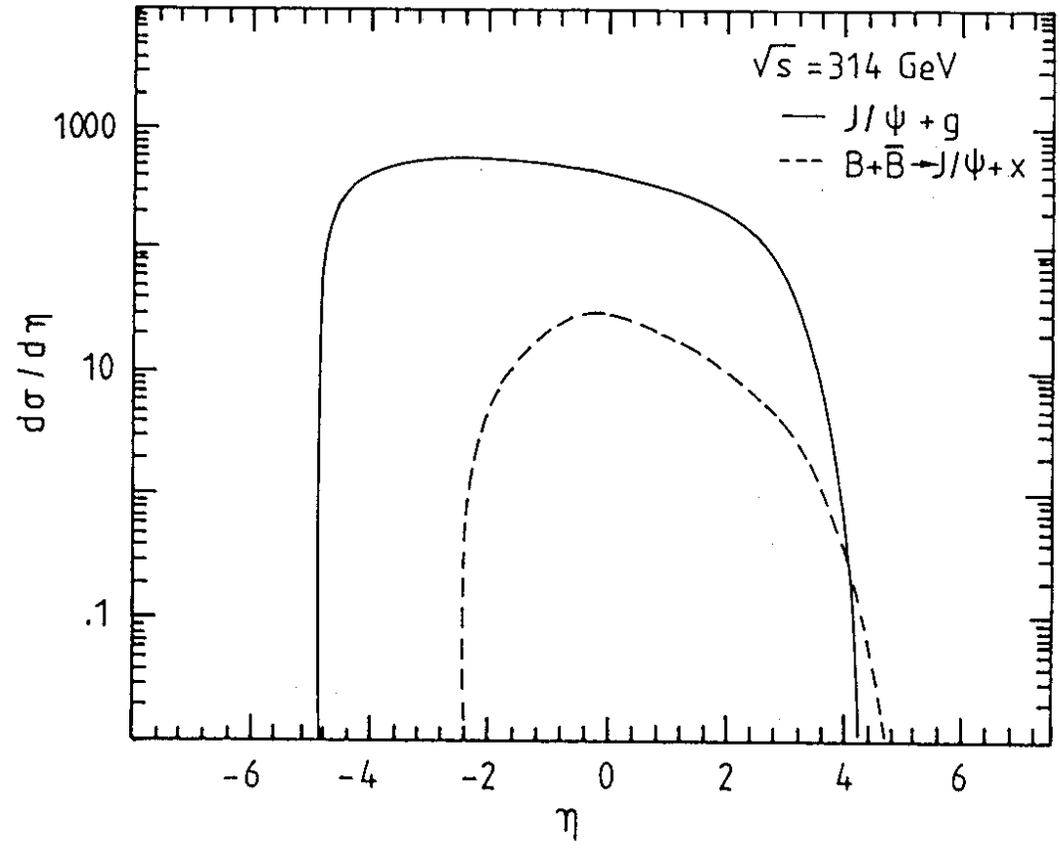

Figure 4.13 Rapidity distributions of J/Ψ produced via the subprocess (4.2) (solid line) and via bottom production and decay into J/Ψ (dashed line) in ep collisions at HERA energy $\sqrt{s} = 314GeV$. (From ref. [16])

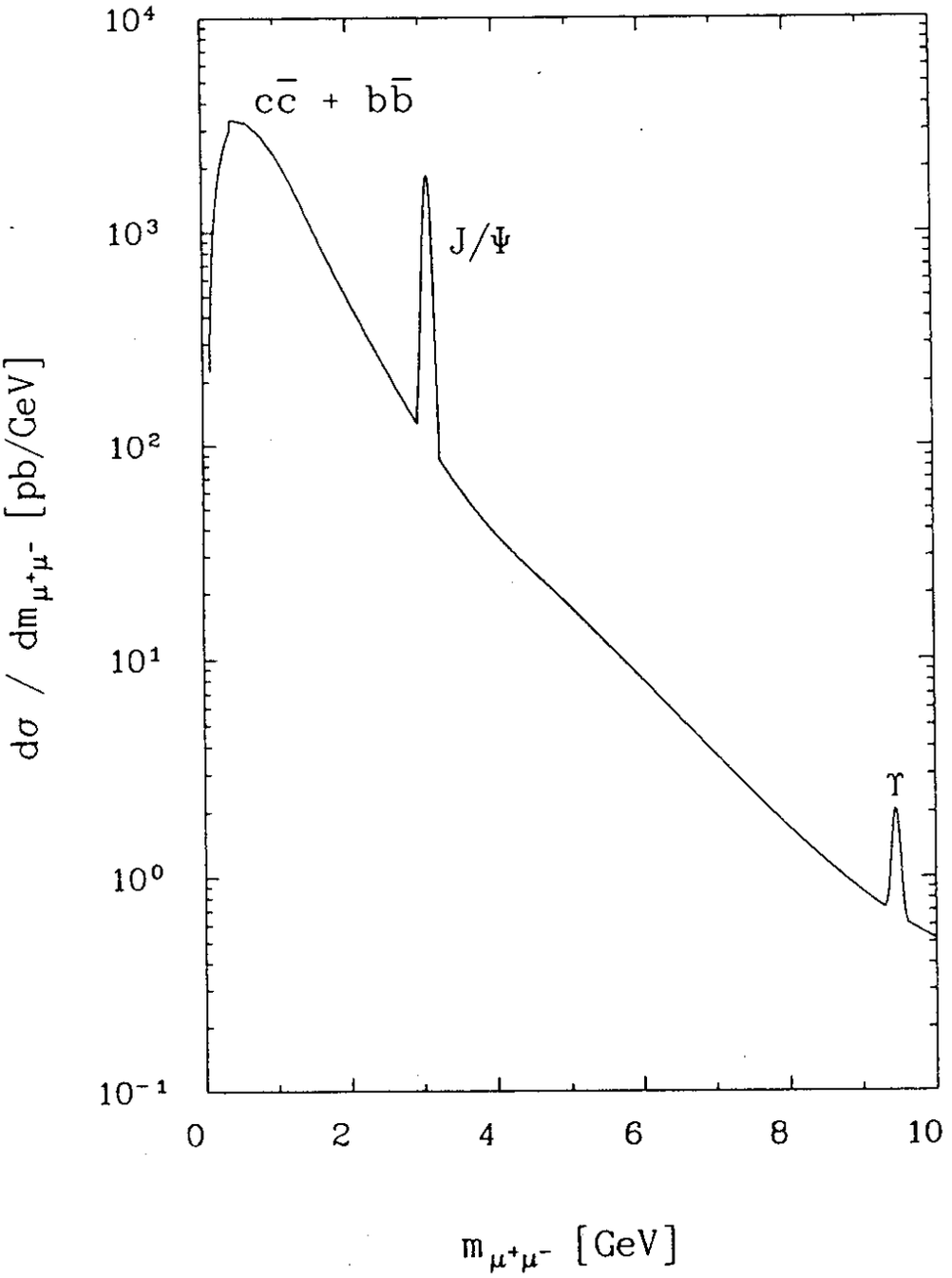

Figure 4.14 The dimuon invariant mass distribution $\frac{d\sigma}{dm_{\mu\mu}}$ from heavy quark production processes $ep \to eQ\bar{Q}X \to \mu^+\mu^- X$. Also shown are the QCD distributions from $ep \to J/\Psi X$ with $J/\Psi \to \mu^+\mu^-$ and $ep \to \Upsilon X$ with $\Upsilon \to \mu^+\mu^-$, folded with a Gaussian resolution $\Delta m_{\mu\mu} = 50\,\text{MeV}$. (From ref. [60]).

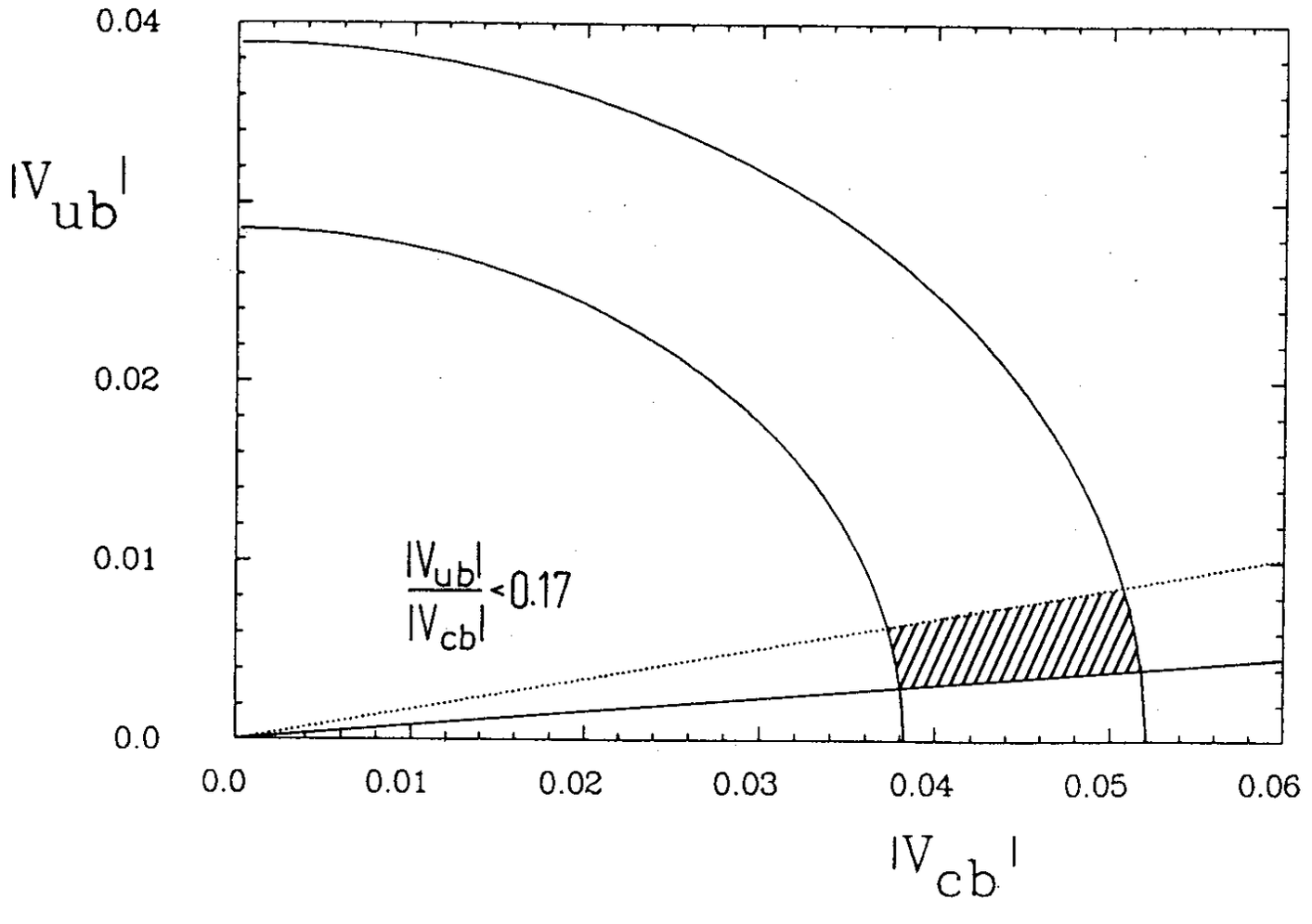

Figure 4.15 Constraints on the CKM matrix elements $|V_{ub}|$ and $|V_{cb}|$ from present data on B decays from Eqs. (4.12), (4.14) and (4.16). (From ref. [27]).

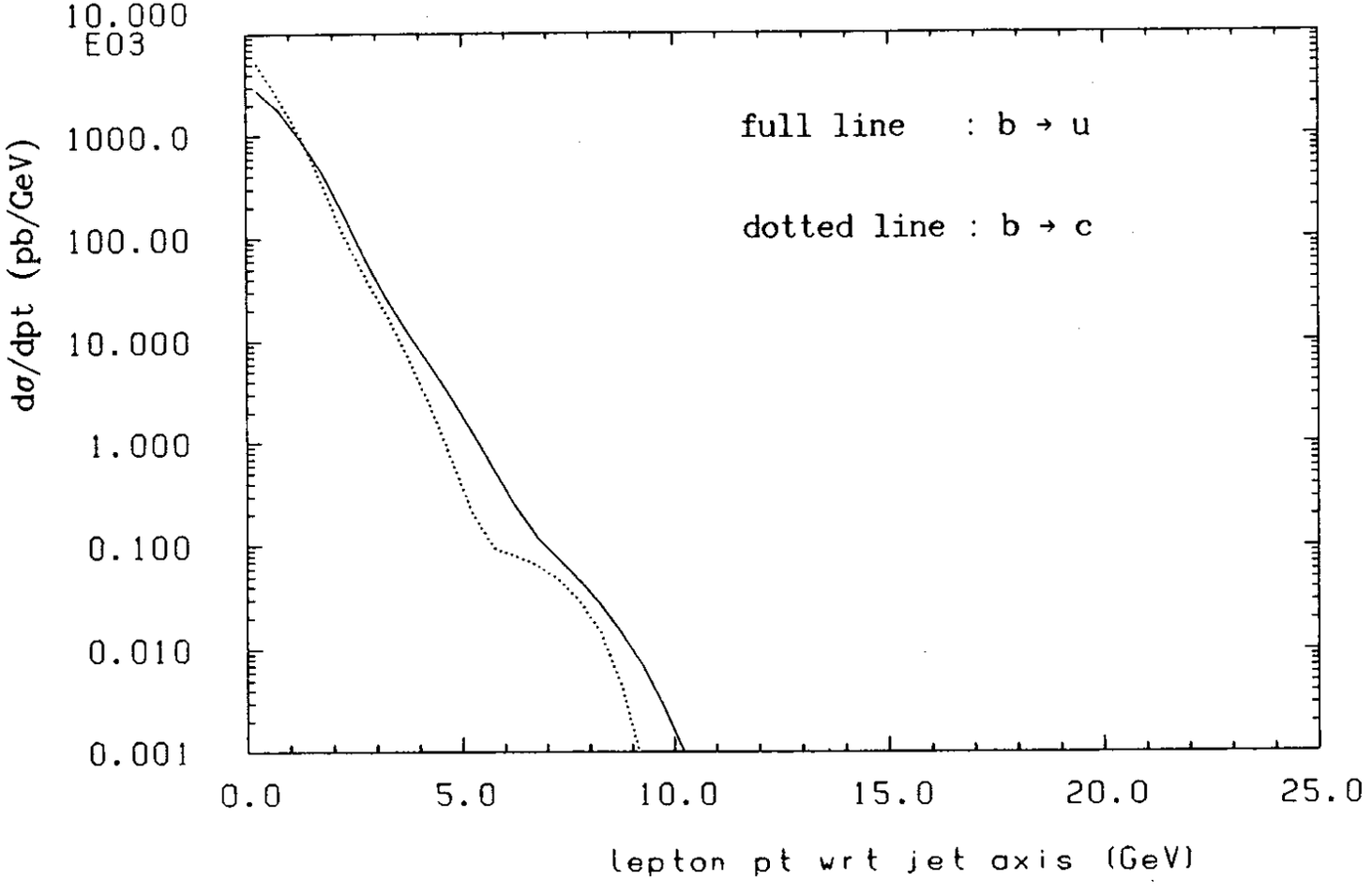

Figure 4.16 Normalized distribution $\frac{1}{\sigma}\frac{d\sigma}{dp_T^l}$ (p_T^l measured w.r.t. jet axis) for the process $ep \to eb\bar{b}X$ with $b \to cl\nu_l$ and $ep \to eb\bar{b}X$ with $b \to ul\nu_l$. (From ref. [60])

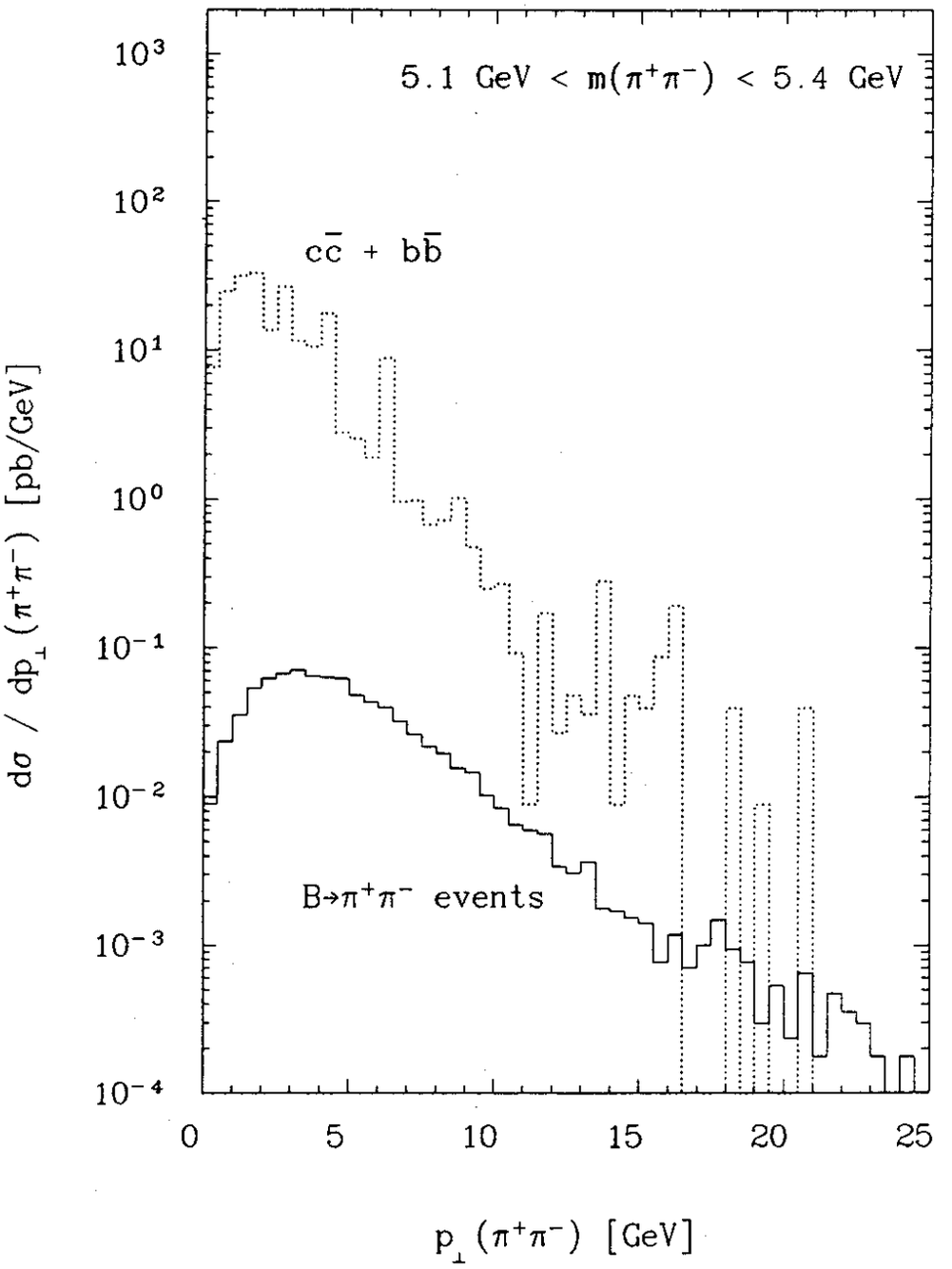

Figure 4.17 The transverse momentum distributions for dipion pairs produced in the process $ep \rightarrow Q\bar{Q}X$, Q=c,b and for $B \rightarrow \pi^+\pi^-$. (From ref. [60]).

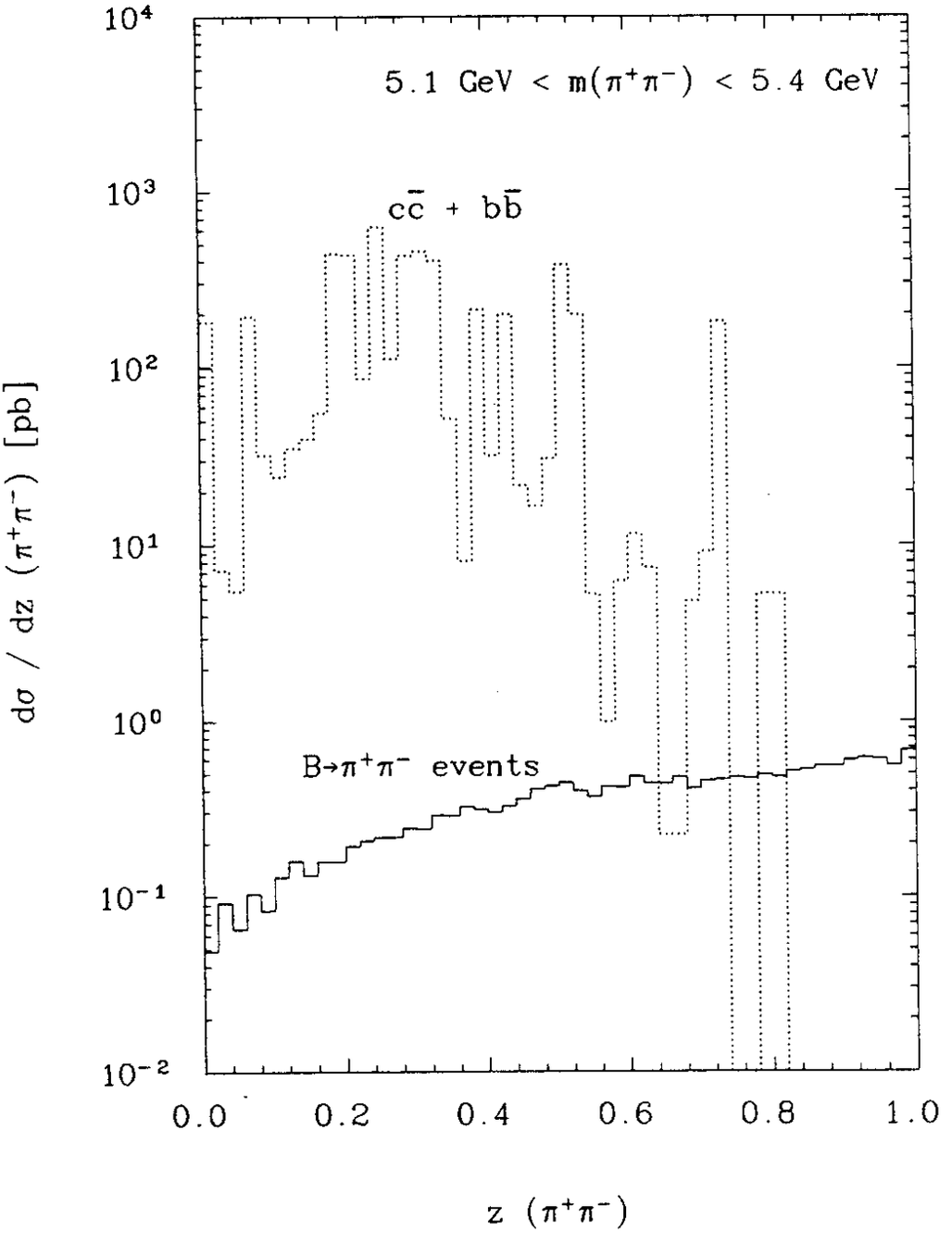

Figure 4.18 The scaled energy distribution in $z(\pi^+\pi^-) = \frac{E(\pi^+\pi^-)}{E_{jet}}$ for dipion pairs produced in the process $ep \rightarrow Q\bar{Q}X$, Q=c,b and for $B \rightarrow \pi^+\pi^-$. (From ref. [60]).

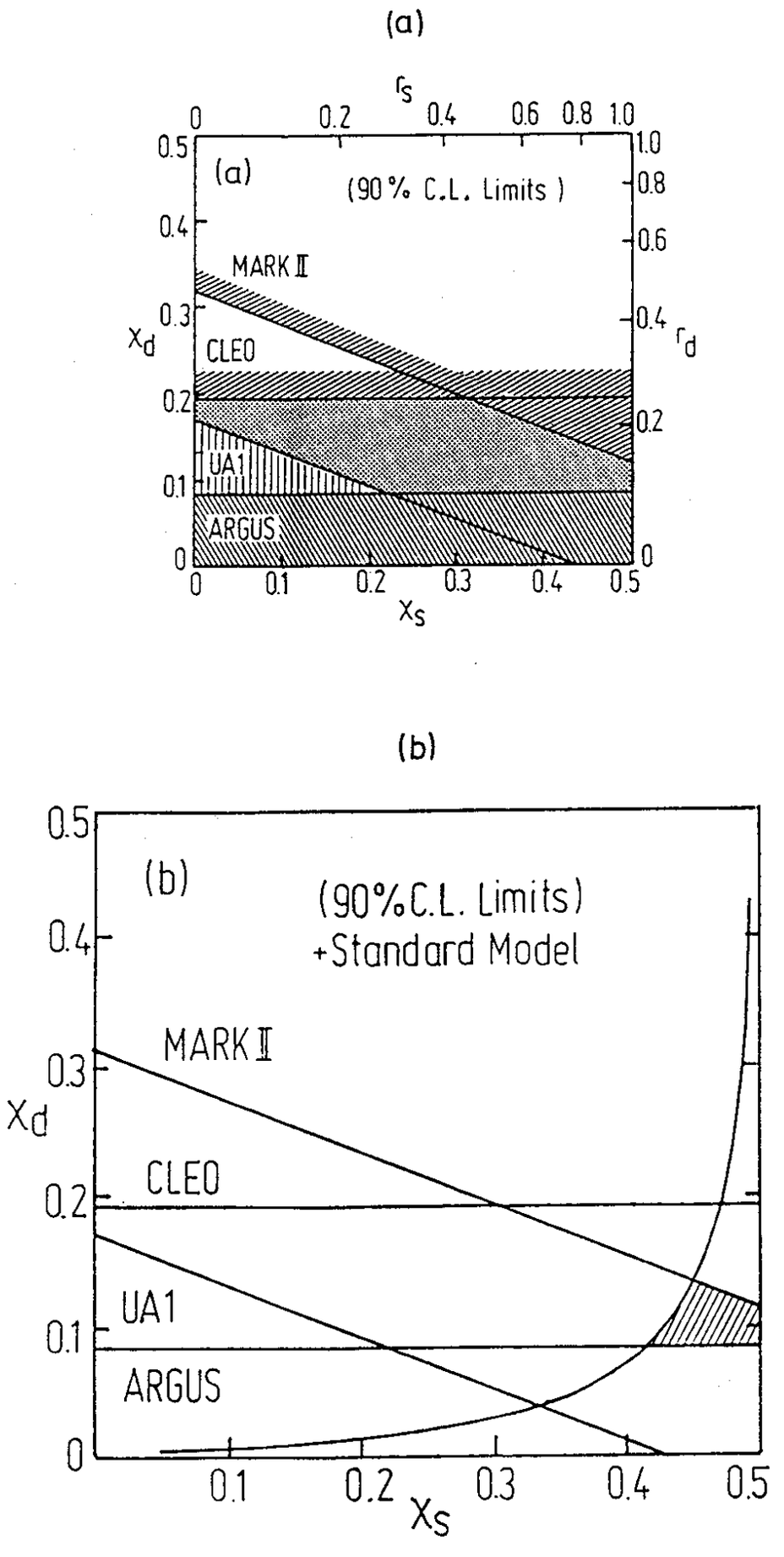

Figure 4.19 a) Allowed region in the χ_s, χ_d plane (dots) obtained from the 90%*C.L.* limits given in Eqs. (4.35), (4.40) and (4.41). The limits on χ from MARK II and UA1 have been converted into χ_d and χ_s by assuming $P_d = 0.375$ and $P_s = 0.15$ b) The experimentally allowed region (shaded area) in the χ_d, χ_s plane from Fig. 4.19 a) and the CKM model constraint 4.25 and 4.44. (From ref. [22])

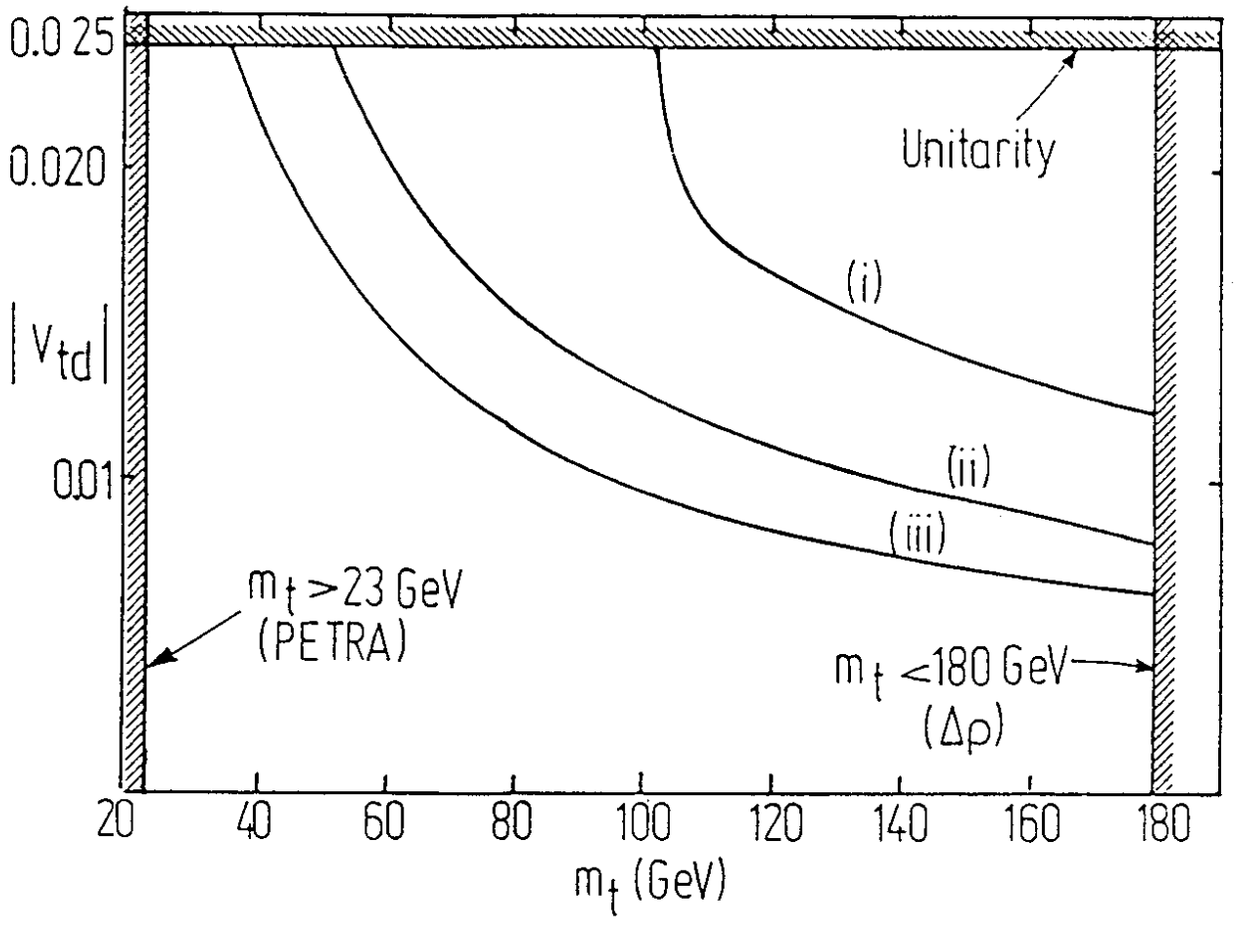

Figure 4.20 Upper bound on the matrix element $|V_{td}|$ from unitarity and $\bar{R} \leq 0.08$, and the lower bounds from $x_d \geq 0.44$ and $m_t \leq 180GeV$ for the three values of the coupling constants i) $B_d f_{B_d}^2 = (0.1GeV)^2$, ii) $B_d f_{B_d}^2 = (0.15GeV)^2$ and iii) $B_d f_{B_d}^2 = (0.20GeV)^2$. (From ref. [22])

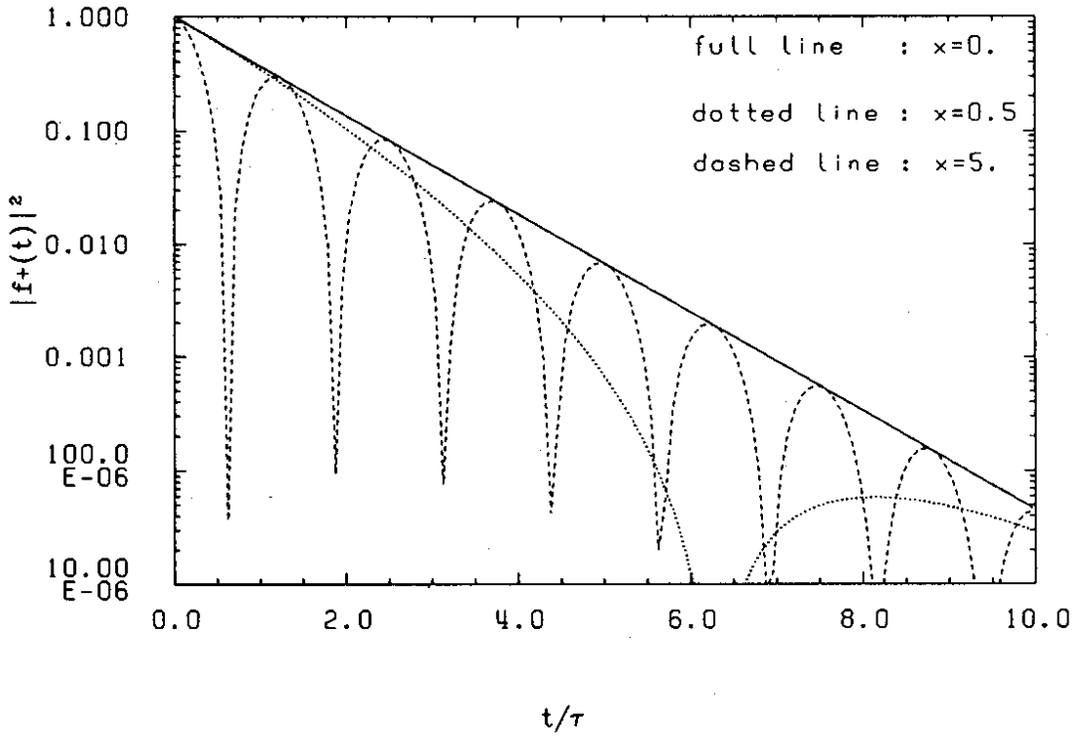

Figure 4.21 The function $| f_+(t) |^2$ as defined in (4.57), for $x = 0.5, 5,\ 0$.

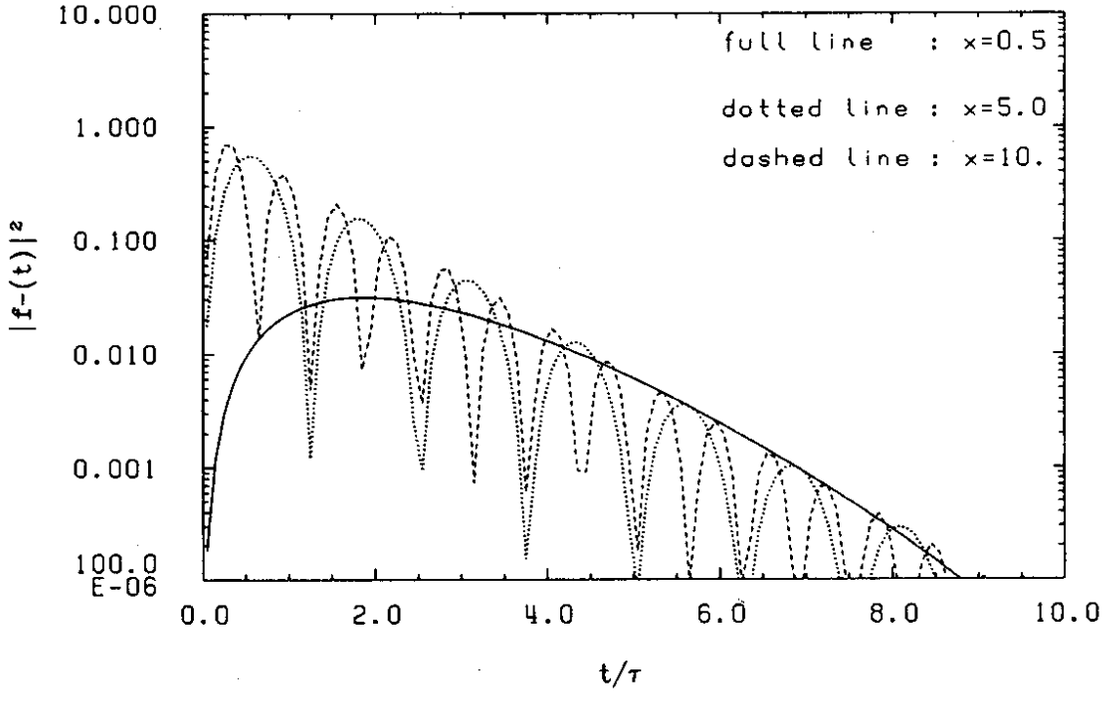

Figure 4.22 The function $| f_-(t) |^2$ as defined in (4.58), for $x = 0.5, 5, 10$.

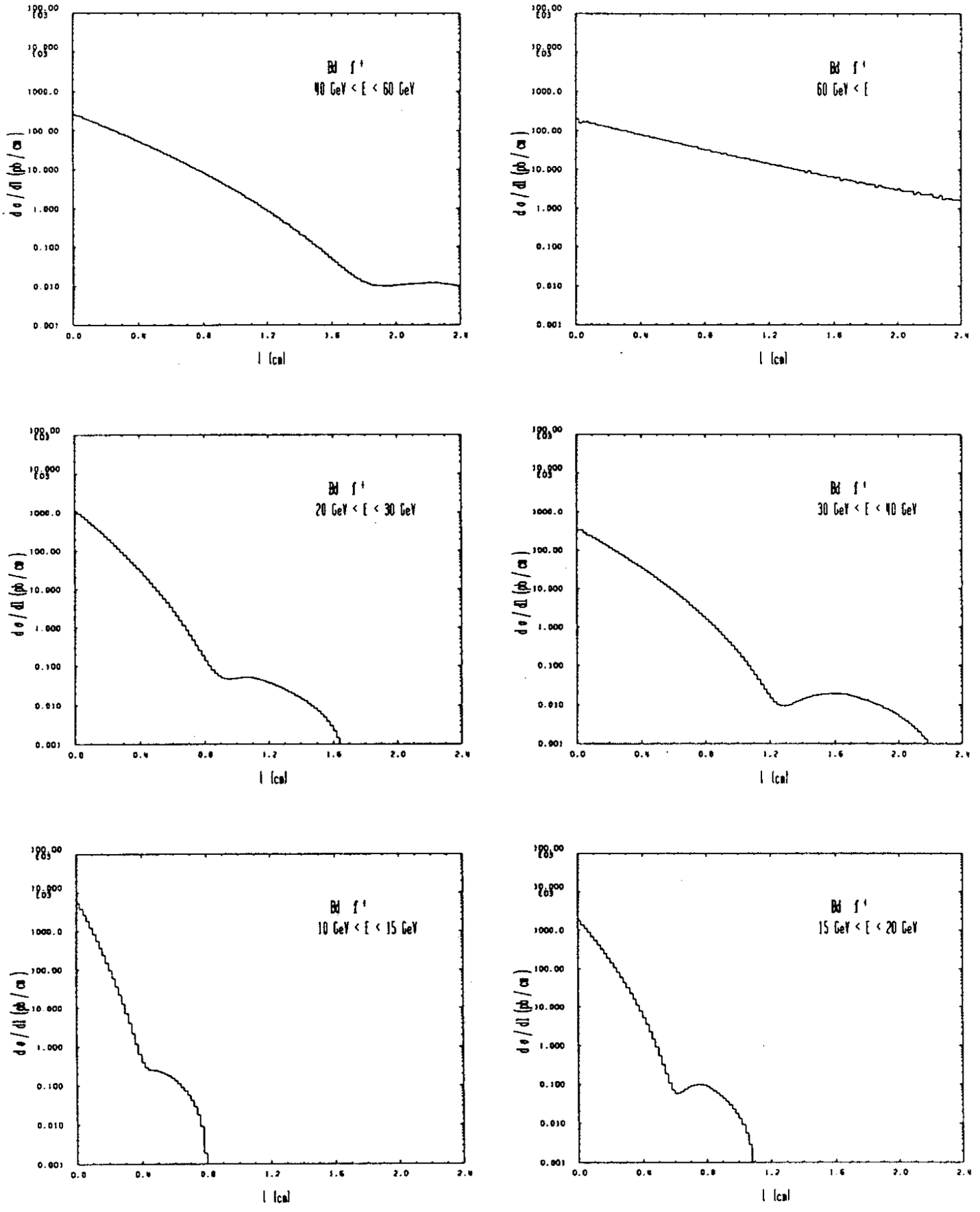

Figure 4.23 Distribution in decay length, $d\sigma/dl$, for the "right sign meson" $B_d^0 \to B_d^0$ with $x_d = 0.5$ in the process $ep \to eb\bar{b}X \to B_d X$ at HERA energy $\sqrt{s} = 314GeV$. The distribution is obtained by fixing the flavour of the other b quark. Decay lengths in the indicated E_B bins are plotted separately. (From ref. [60])

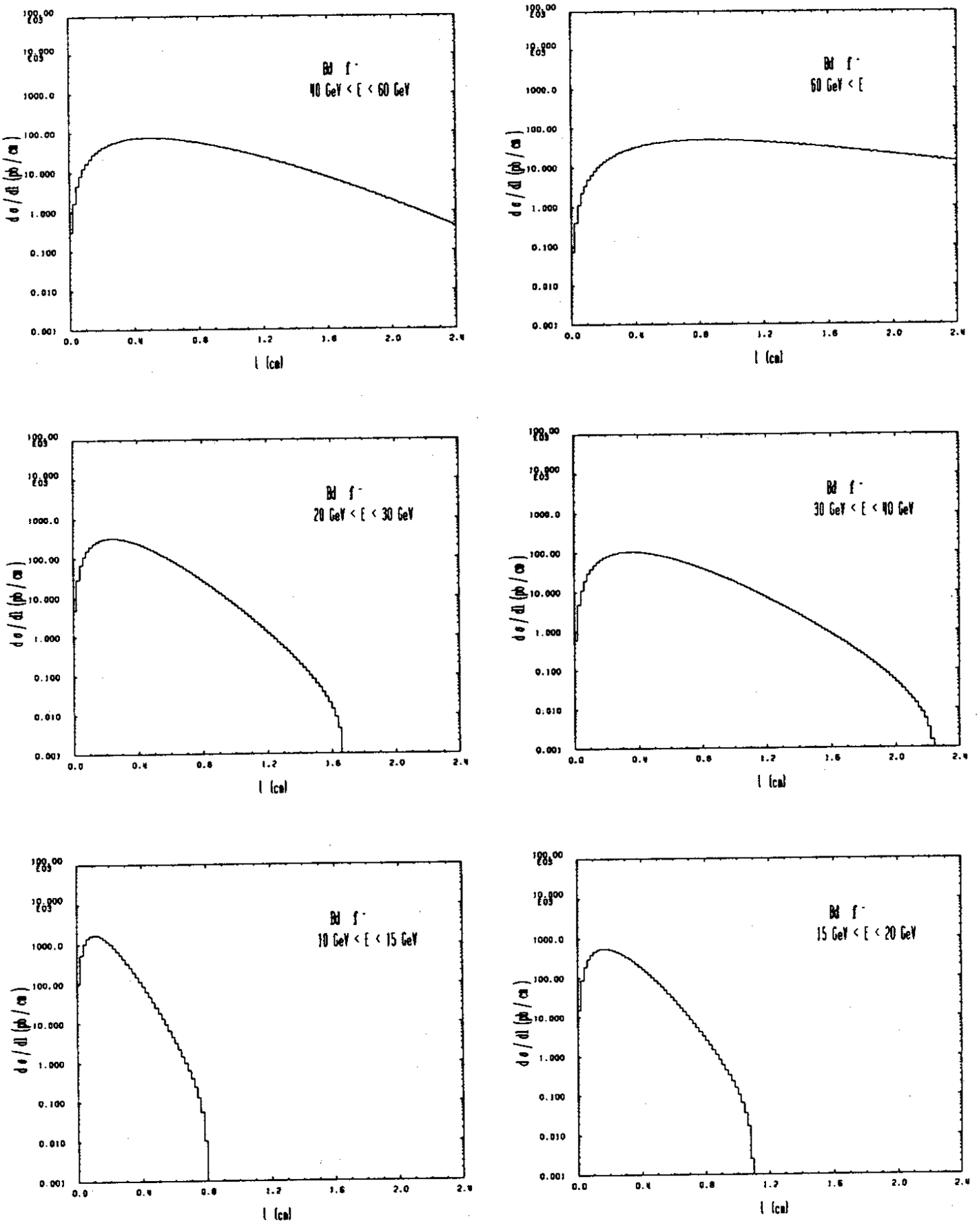

Figure 4.24 Same as Fig. 4.23 but for the "wrong sign meson" $B_d^0 - \bar{B}_d^0$ with $x_d = 0.5$.

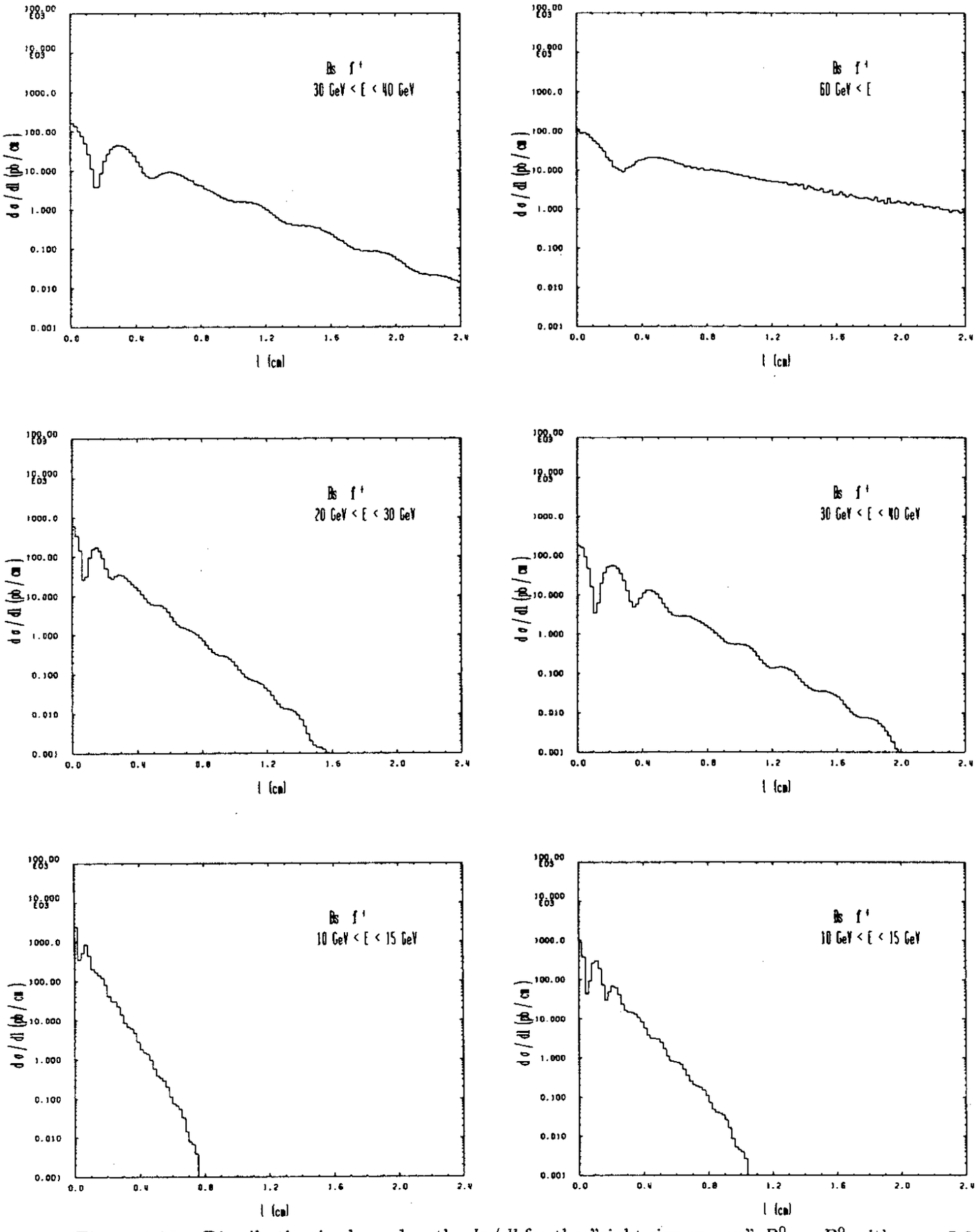

Figure 4.25 Distribution in decay length, $d\sigma/dl$,for the "right sign meson" $B_s^0 \rightarrow B_s^0$ with $x_s = 5.0$ in the process $ep \rightarrow eb\bar{b}X \rightarrow B_sX$.

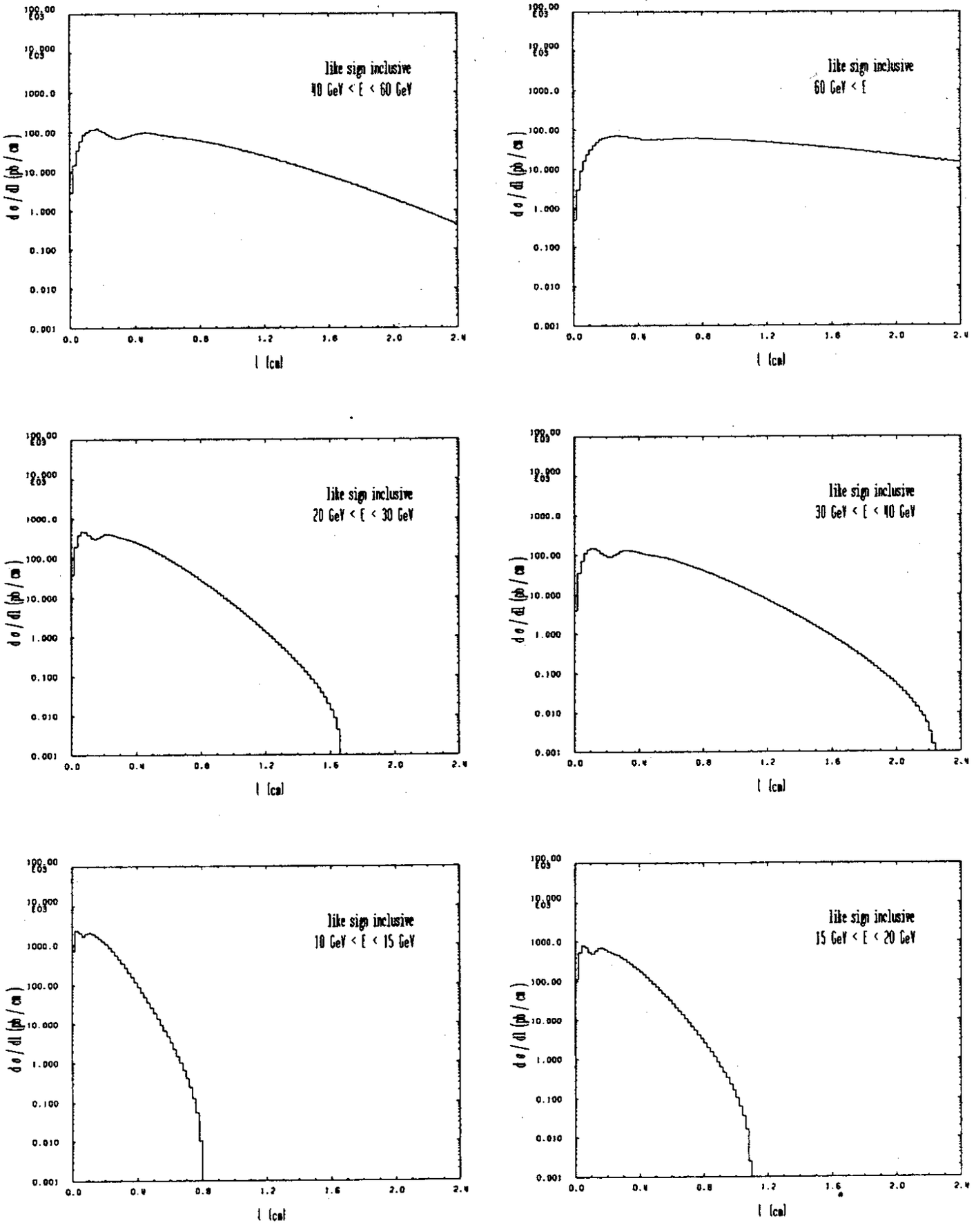

Figure 4.26 Same as Fig. 4.25 but for the "wrong sign meson" $B_s^0 \to \bar{B}_s^0$ with $x_s = 5.0$.

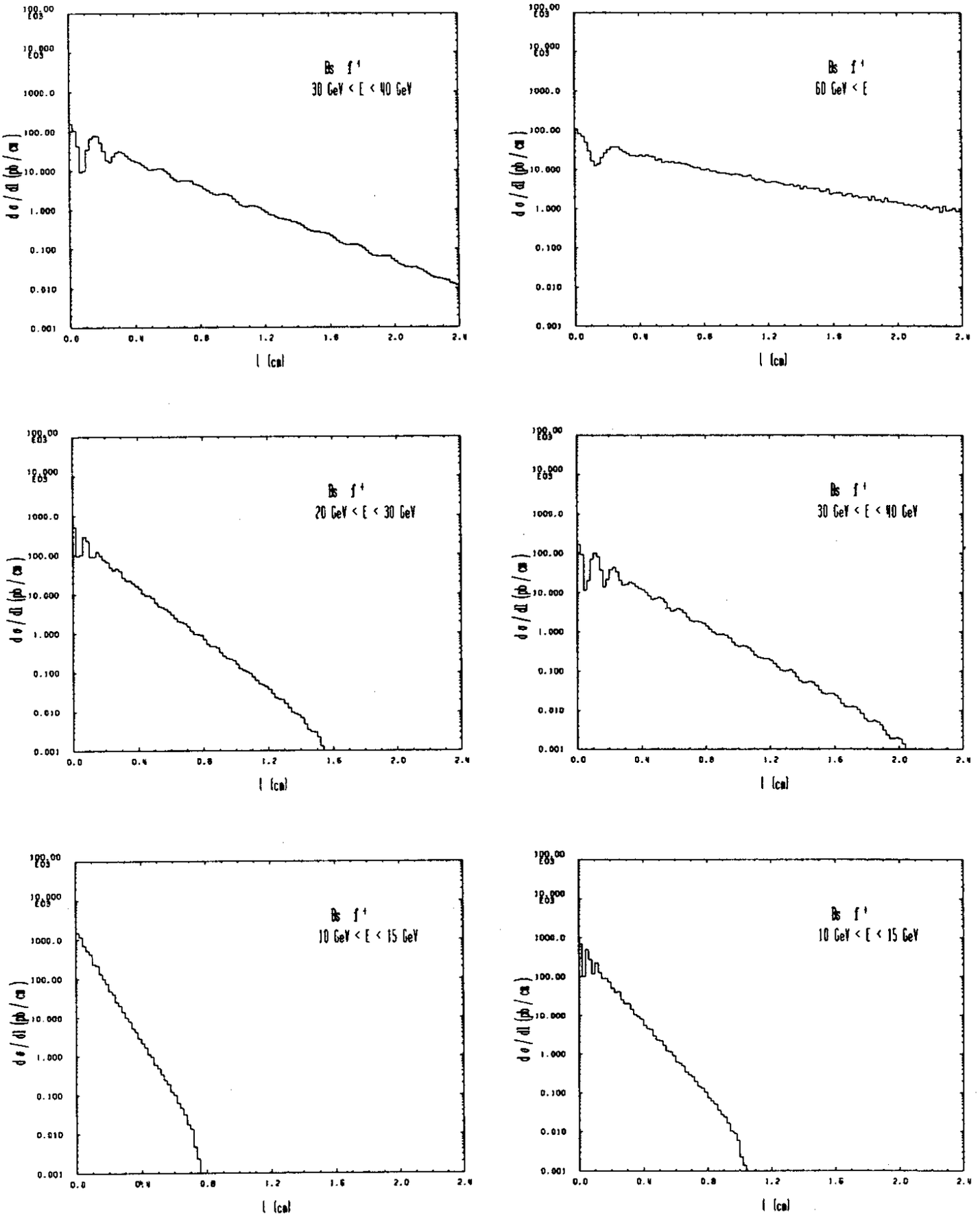

Figure 4.27 Same as Fig. 4.25 for $B_s^0 \to B_s^0$ but with $x_s = 10.0$.

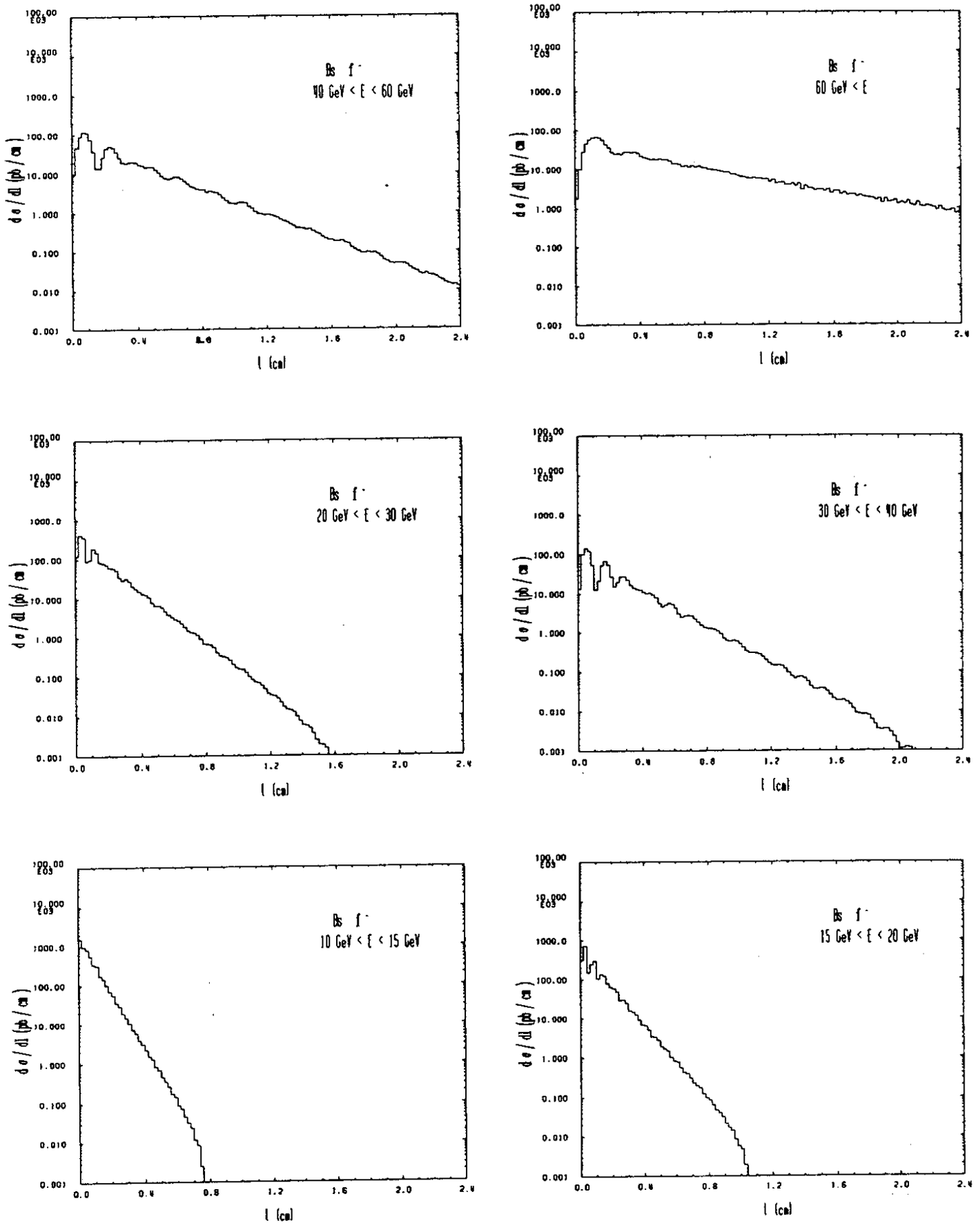

Figure 4.28 Same as Fig. 4.26 for $B_s^0 \to \bar{B}_s^0$ but with $x_s = 10.0$.

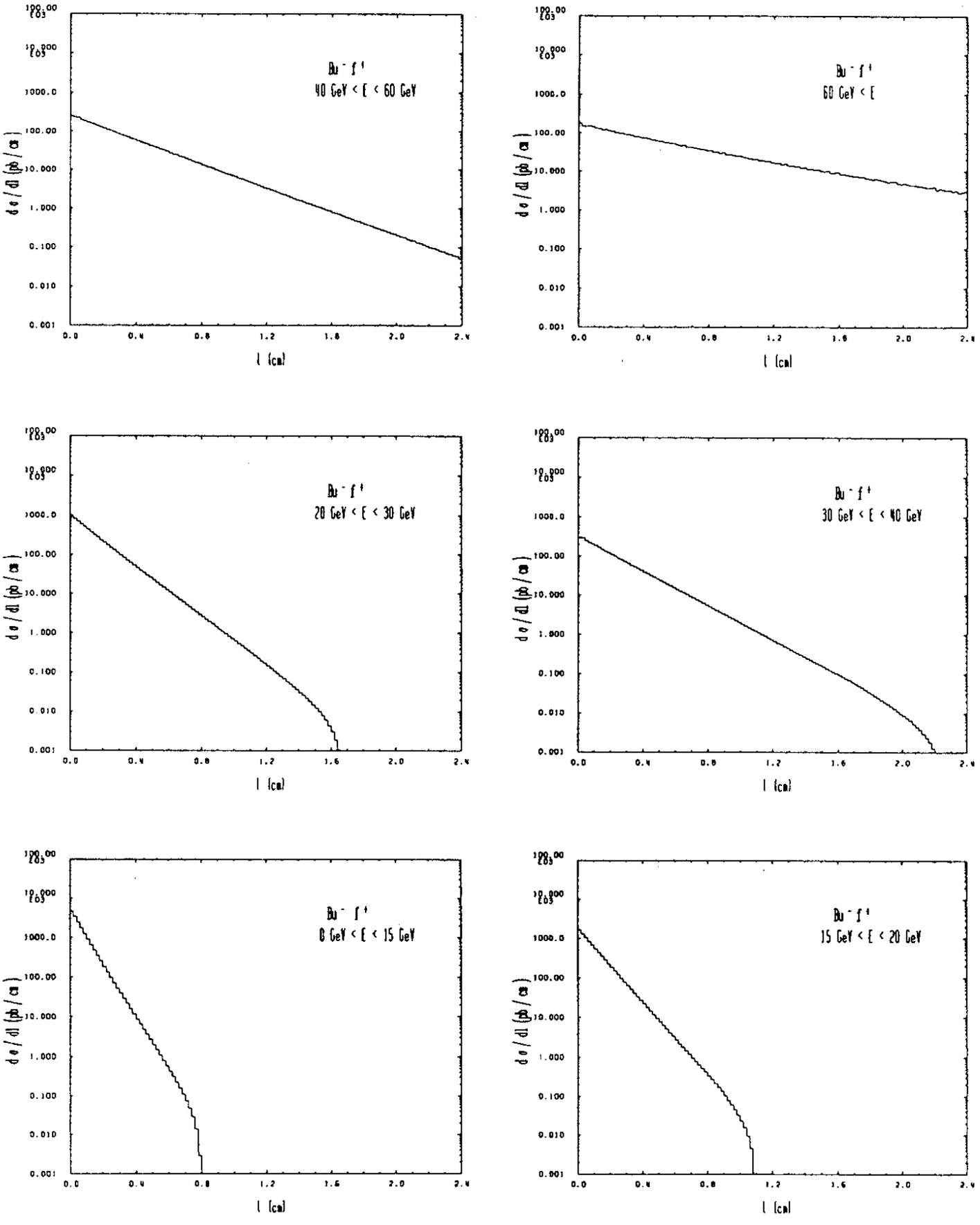

Figure 4.29 Distribution in decay length $\frac{d\sigma}{dl}$ for the process $ep \to eb\bar{b}X \to B_u^- X$ at HERA energy $\sqrt{s} = 314\ GeV$, for the various indicated bins in E_{B_u}. (From ref. [60])

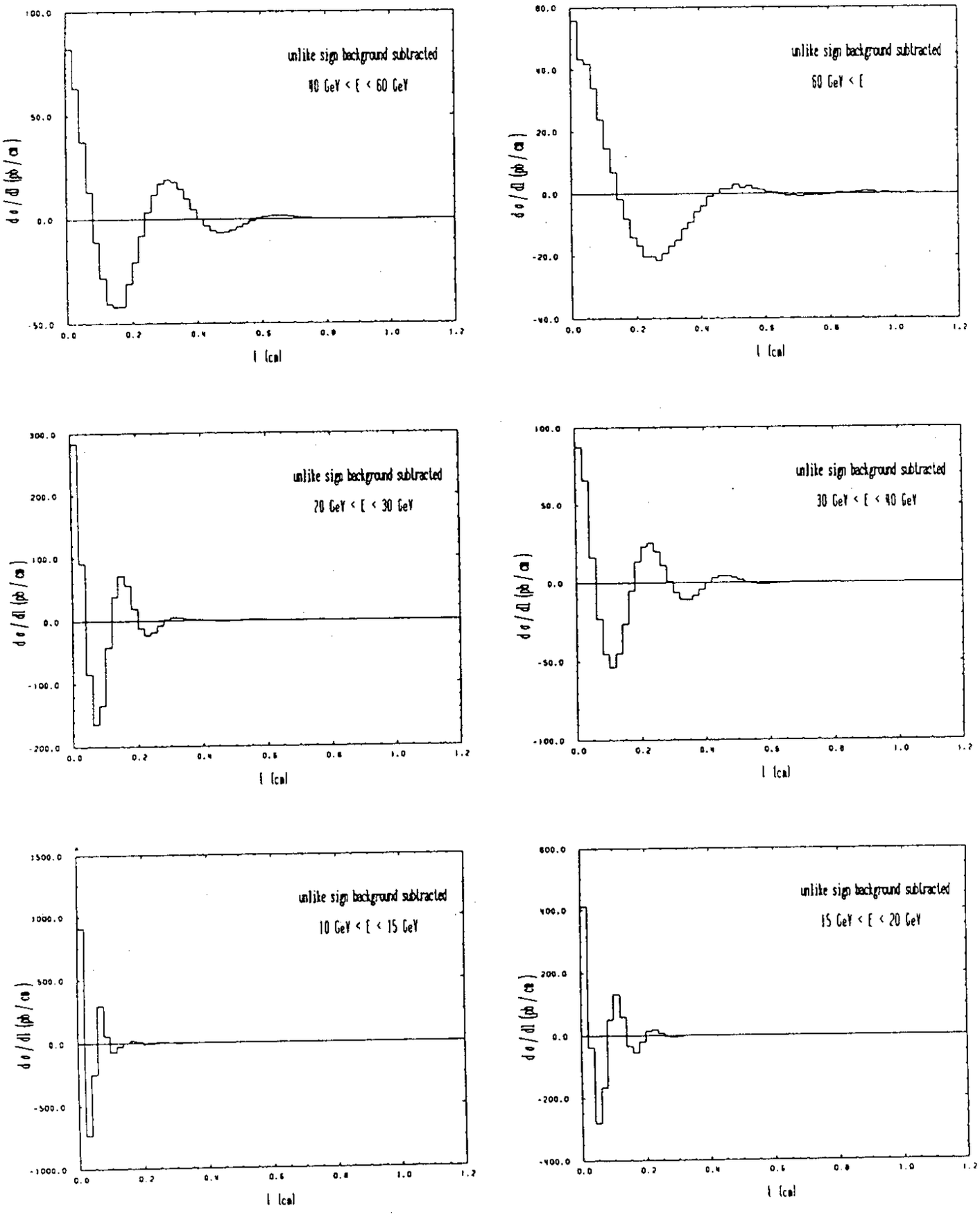

Figure 4.30 Distribution in decay length $\frac{d\sigma}{dl}$ for the process $ep \to eb\bar{b}X \to BX$ for the "right sign meson" after substracting an exponential background at HERA energy $\sqrt{s} = 314$ GeV and assuming $x_s = 5$. The oscillation pattern in $B_s \to B_s$ is clearly visible. (From ref. [60])

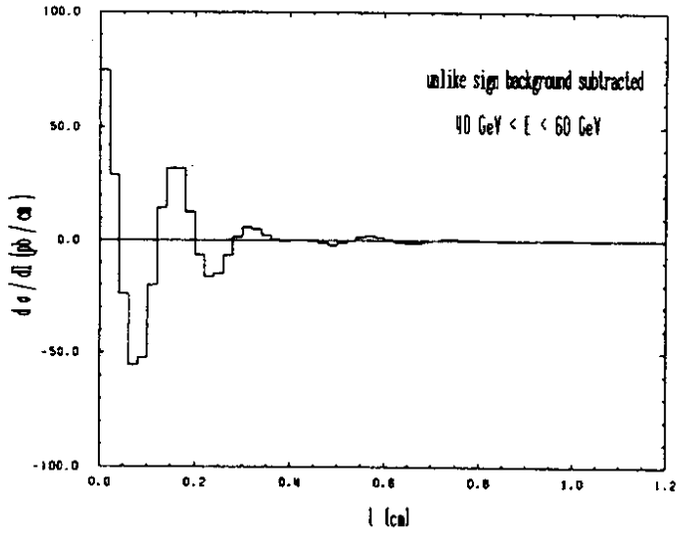

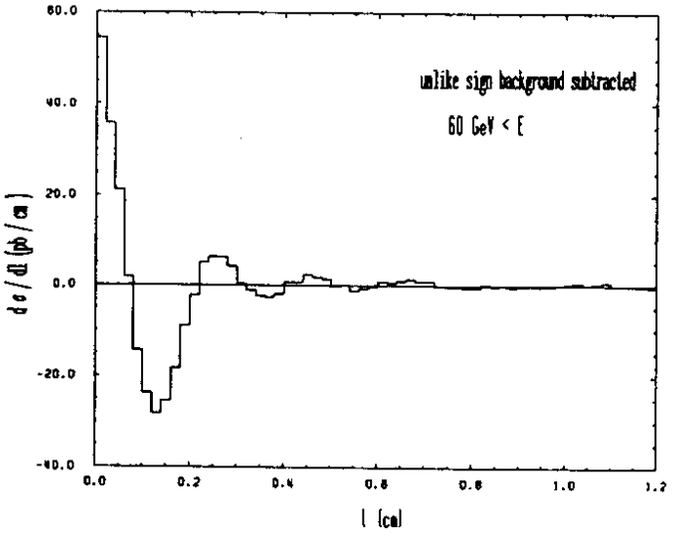

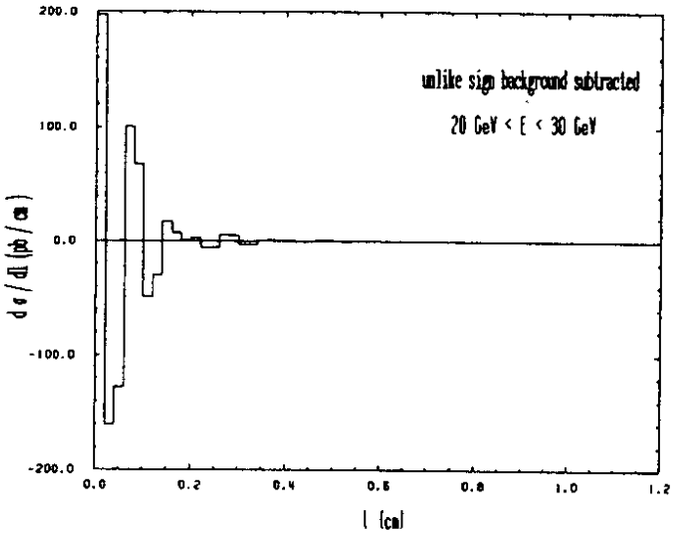

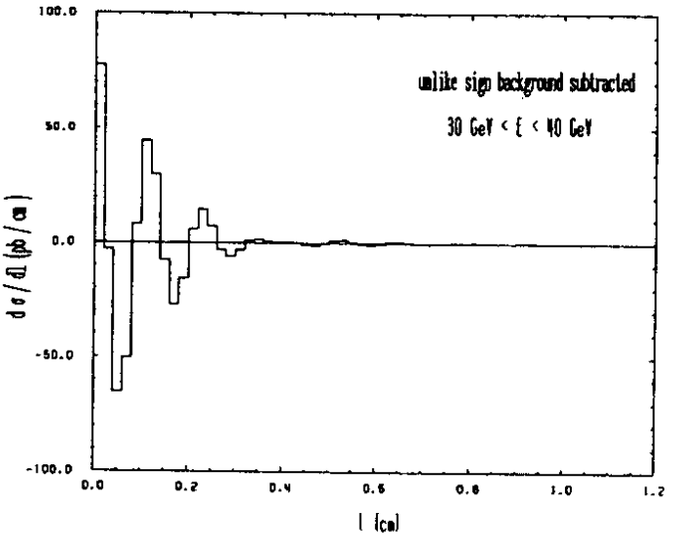

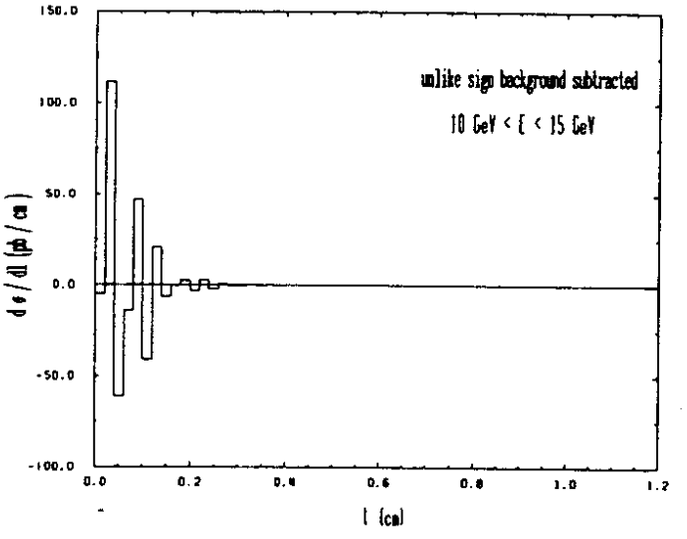

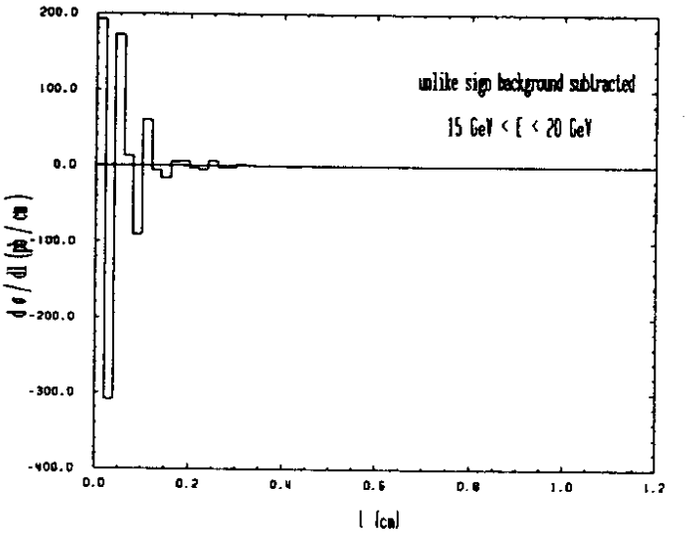

Figure 4.31 Same as Fig. 4.30 but with $x_s = 10$.

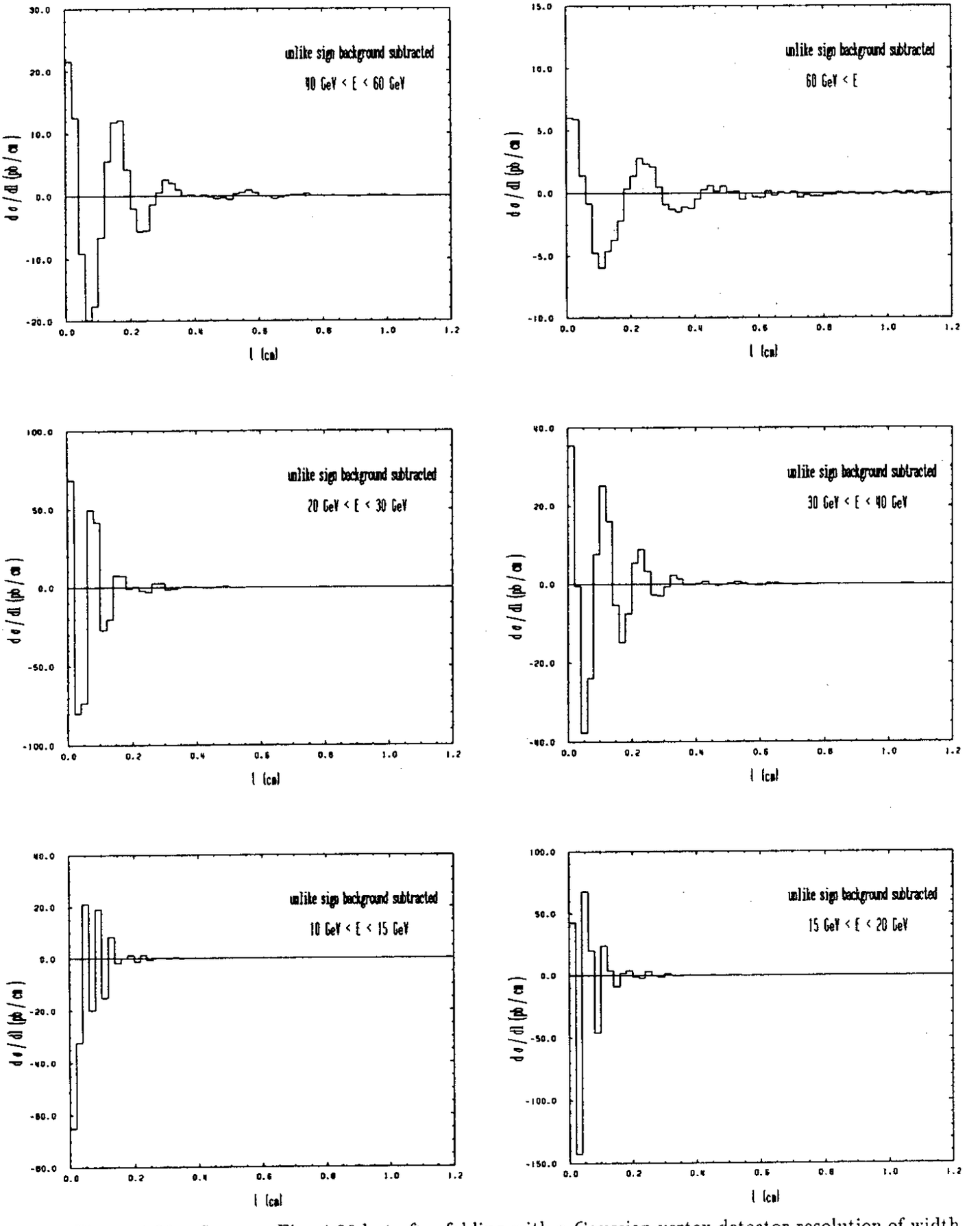

Figure 4.32 Same as Fig. 4.30 but after folding with a Gaussian vertex detector resolution of width $\sigma_V = 100\ \mu m$ and beam acceptance cut of 100 mrad at $x_s = 10$. (From ref. [60]).

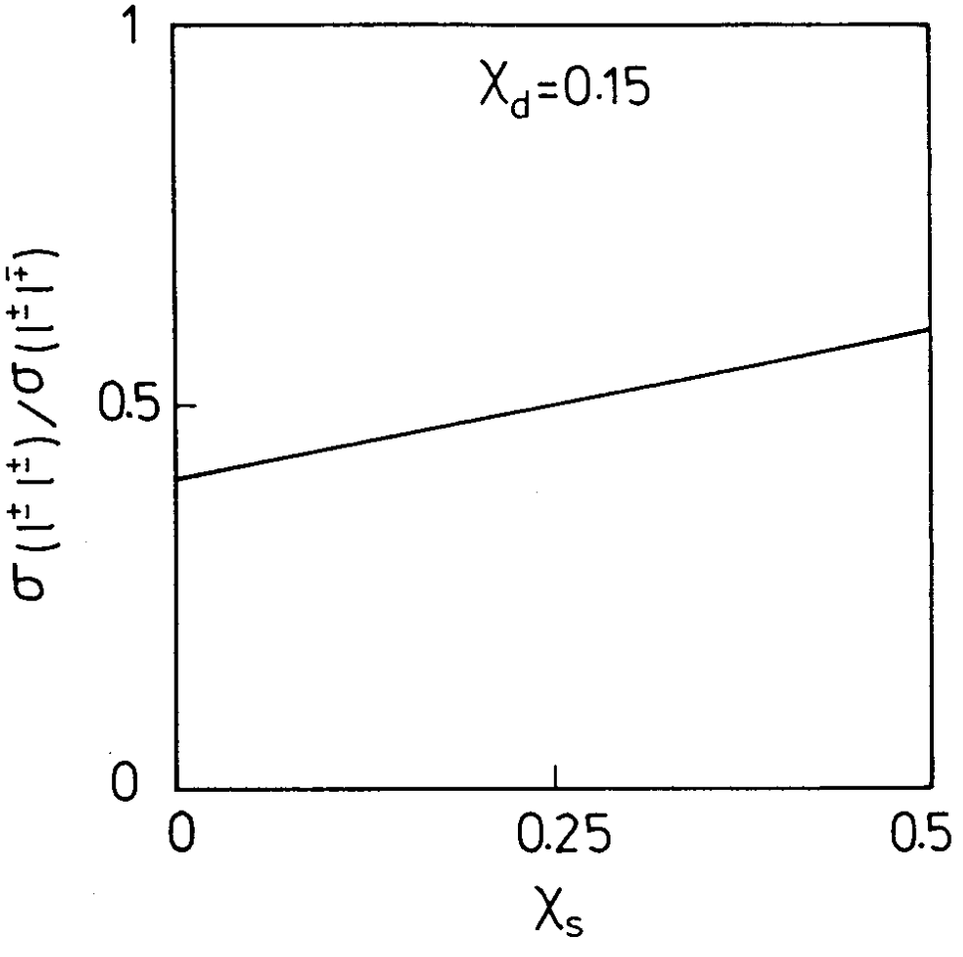

Figure 4.33 Time integrated dilepton ratio $R = \frac{\sigma(l^+l^+)+\sigma(l^-l^-)}{\sigma(l^+l^-)}$ at HERA energy $\sqrt{s} = 314 GeV$ as a function of χ_s, assuming $\chi_d = 0.15$, $P_d = 0.375$ and $P_s = 0.15$. (From ref. [65])